# EDGE EFFECTS AND SUBMICRON TRACKS IN MAGNETIC TAPE RECORDING

Graduation Committee

| | |
|---|---|
| Prof. dr. ir. J. van Amerongen | Univ. Twente (chairman) |
| Prof. dr. J.C. Lodder | Univ. Twente (promotor) |
| Dr. ir. J.P.J. Groenland | Univ. Twente (assistant promotor) |
| Prof. dr. ir. P.P.L. Regtien | Univ. Twente |
| Dr. ir. L. Abelmann | Univ. Twente |
| Prof. dr. P.R. Bissell | Univ. Central Lancashire, UK |
| Prof. dr. J.-P. Nozières | Spintec, CEA/CNRS Grenoble, FR |
| Prof. dr. S.B. Luitjens | Philips Research Laboratories |

The research described in this thesis was funded by the Dutch Technology Foundation STW, project TTF.5041 "High-density recording in magnetic tape". The work was performed in the Systems and Materials for Information storage group (SMI) of the MESA$^+$ Institute for Nanotechnology, University of Twente.

Printed by Wöhrmann Print Service, Zutphen


ISBN 90-365-2166-1

# EDGE EFFECTS AND SUBMICRON TRACKS IN MAGNETIC TAPE RECORDING

DISSERTATION

to obtain
the doctor's degree at the University of Twente,
on the authority of the rector magnificus,
prof. dr. W.H.M. Zijm,
on account of the decision of the graduation committee,
to be publicly defended
on Thursday 17 March 2005 at 15.00

by

**Adrian Hozoi**

born on 18 February 1977
in Iaşi, Romania

This dissertation is approved by

| | |
|---|---|
| promotor: | Prof. dr. J.C. Lodder |
| assistant promotor: | Dr. ir. J.P.J. Groenland |

# Contents

Chapter 1

# Introduction

Since the early stages of computing, magnetic tape has been the medium of choice for information storage due to its high volumetric capacity and competitive pricing. Steady advances in drive, media and automation robotics helped it to remain the most cost-effective and reliable solution for data backup and archiving. Most advanced tape technologies offer nowadays capacities between 200 and 500 GB per cartridge, and multi-terabyte recording is already envisaged. They will continue to evolve to meet the increasing demands for capacity, performance and functionality of data storage applications.

## 1.1 Brief Story of Magnetic Tape Storage

The basis of magnetic recording dates back to 1878 when Oberlin Smith established the principle to record electrical signals from a telephone onto a steel wire. He described his idea in the journal *Electrical World* of Sep. 8, 1888. It was in 1898 that the Danish engineer Valdemar Poulsen built the first working magnetic recorder, called the Telegraphone. The device used an electromagnetic head to record telephone messages on a steel wire wrapped around a drum (Fig. 1.1). Over the next few years Poulsen produced improved sound recorders employing steel wire or steel tape. During the 1920s and 1930s, important advances in magnetic recording were achieved in Germany with the introduction of electronic amplification and the transition to coated tapes. The steel wires and tapes were first replaced by paper tapes covered with iron powder. Then BASF developed the plastic tape coated with a magnetic oxide intended for an advanced recorder designed by AEG, called the Magnetophon. They were presented to the public during the 1935 Radio Fair in Berlin. The Magnetophon became a machine of excellent quality with the advent of high frequency bias-

**Figure 1.1:** *Early version of Poulsen's Telegraphone.*

ing.
After 1947, first American tape recorders were developed based on German expertise and designs. Originally intended for government use, they quickly spread onto the commercial market. The data was recorded in parallel tracks from the beginning of the tape to the end, method also known as *linear scan*. However, its performances were insufficient for video recording, and Ampex introduced in 1956 a professional video recorder using *rotary heads*. The recording heads, mounted onto a cylinder rotating at high speed, were scanning tracks perpendicular to the tape travel direction. This implementation was favorable to increase the relative head to tape velocity and reach higher track density. Toshiba introduced a superior rotary head configuration in 1959, known as *helical scan* recording. In this case the tracks were recorded diagonally to the tape, at a relatively small angle to its travel direction. Due to high performance and capacity, rotary heads systems became the standard for professional video applications. The operating principles of linear and helical scan recording are schematically described in Fig. 1.2.

In the late 40s IBM understood that punched cards would not be enough to solve the increasing need of data storage and processing, and was searching for alternative technologies. Magnetic tape was just coming into audio systems and offered great potential to become the primary storage medium for computers. Eckert and Mauchly were probably the firsts to use magnetic tape to record data with their Binary Automatic Computer (BINAC), completed in 1949. The unit used steel tape, and an improved version was integrated with the Universal Automatic Computer (UNIVAC), released in 1951. The first IBM magnetic tape storage system, the IBM 726, was announced in 1952 together with the IBM 701 Defense Calculator. It was a reel-to-reel drive using half-inch

magnetic tape, with a plastic substrate coated with iron oxide. The diameter of the reel was 270 mm, and the data was recorded in 7 parallel tracks at 4 b/mm (100 b/in) linear density. The IBM 726 reached a capacity over 0.25 MB at a data rate of 6.6 kB/s, and became the industry standard. Throughout the 60s and the 70s more advanced media formulations became available and the open-reel systems evolved by mainly increasing the bit density and the tape speed.
The Quarter-Inch Cartridge (QIC) was introduced in 1972 by 3M Corporation as a storage format for telecommunications and data acquisition applications. QIC data cartridges stored the tape onto two reels driven by a built-in belt, and were available with capacities of few megabytes. The QIC minicartridge appeared in 1975, and many QIC-based recording formats started to develop in the following years. Capacity gains were achieved by upgrading the media, increasing bit densities, and adding more parallel tracks. Due to its relative low cost, QIC became in the 80s a popular data storage system for entry-level applications.
The latest IBM open-reels tape unit by early 80s, the IBM 3420, could store 180 MB of data in a 9-track configuration. In 1984 IBM introduced a completely new system, the 3480, featuring a closed cartridge including a single reel with half-inch $CrO_2$ tape. A take-up reel was located in the drive itself. Single reel cartridges could contain more tape length in a given volume than dual reel cassettes, increasing the tape area available for recording and thus the data capacity. The 3480 was the first drive to use thin-film, magnetoresistive (MR) heads, which were grouped in a 18 channel configuration to provide a data rate of 3 MB/s. It was a high performance tape platform with increased reliability, that could hold 200 MB of data in a 120 mm square cartridge. About the same time, Digital Equipment Corporation (DEC) released a proprietary linear scan system also using a single reel, half-inch tape cartridge. Ten years later the technology was sold to Quantum Corporation where it evolved into the Digital Linear Tape (DLT) format.

The audio and video recording industry achieved significant advances during the 60s and the 70s, and a multitude of formats were released for professional and commercial use. In the 70s the costs of helical scan technology started to drop significantly and entered the consumer market in the form of home video systems. Higher track densities became possible using azimuth recording to reduce cross-track interference, first demonstrated by Matsushita in 1968. The helical scan technology was derived by Sony to launch the Digital Audio Tape (DAT) in 1987, using tiny cassettes with 4 mm metal particulate (MP) tape. It was intended to replace the venerable Compact Cassette introduced by Phillips in 1963, but never gained the expected popularity. In the mid-80s Exabyte perceived the opportunity to adapt helical scan technology from Sony to build high capacity storage platforms using compact cartridges of 8 mm tape. Their first drive was launched in 1987 and had a capacity of 2.4 GB. A

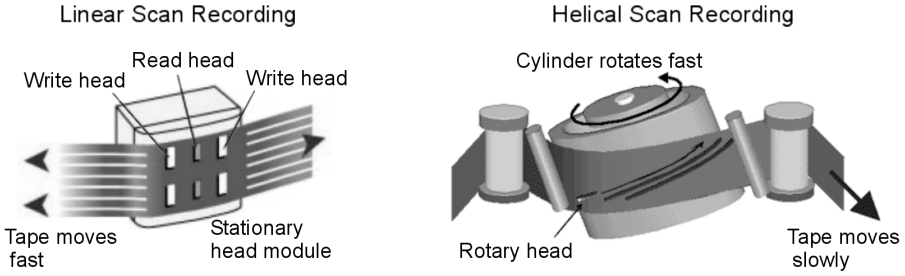


**Figure 1.2:** *Operation principles of linear and helical scan recording. The head module for linear recording may have different configurations, depending on each specific system.*

few years later, HP and Sony adapted the DAT format to introduce the Digital Data Storage (DDS) tape platform, intended for low-end applications. The first DDS system was released in 1991 with a capacity of 2 GB, and its success increased over the years with millions of units shipped worldwide.
In the early 90s, metal evaporated (ME) tape appeared in compact video systems with high recording density. Its reliability improved by evolving into advanced metal evaporated (AME) tape, which became the media of choice for new data storage platforms with rotary heads. Sony's Advanced Intelligent Tape (AIT) and Exabyte's Mammoth drives were launched in 1996, both using 8 mm AME tape in tiny cartridges, with dual reels. Their areal recording density was more than five times higher than that of the linear scan drives of the time. Therefore, they could offer capacities up to 25 GB, in the same range as half-inch tape, linear technologies.

During the 1980's QIC tapes were available in a variety of formats and a wide range of capacities, leading sometimes to compatibility problems. Higher capacities were achieved by increasing the areal recording density and by widening and lengthening the tape. Still, the QIC standards failed to keep up with the storage media explosion of the 90s. The Scalable Linear Recording (SLR) platform developed by Tandberg Data became the sole successor of the QIC data cartridge to support the growing market needs. 3M Corporation introduced the Travan technology in 1994 as a superior replacement for the QIC minicartridge, to better suit the increase of capacity and performance.
Meanwhile, half-inch linear tape drives were evolving by improving capacity and performances. The use of MP tapes and progresses in coding allowed for higher bit densities. The tape length was increased and the precision of the transport mechanisms was improved to support more tracks. IBM introduced the factory-written servo pattern for proper track following with the 3590 platform, released in 1995. Servo tracks pre-written onto the media were then

adopted in different forms by most linear systems with high track densities. However, for its Super DLTtape (SDLT) line introduced in 2001, Quantum developed an optical based servo system, known as Pivoting Optical Servo (POS). The backside of the media is embedded with optical targets that are read by a laser coupled to the magnetic head, providing the servo information. The Linear Tape-Open (LTO) is an open tape format developed jointly by IBM, Hewlett-Packard and Seagate RSS (currently known as Certance) to provide enhanced reliability, scalability, and interchangeability. The first generation of LTO Ultrium drives was introduced in 2000, supporting a capacity of 100 GB in a single reel cartridge, using half-inch wide MP tape.

## 1.2 Magnetic Tape Storage Nowadays

### 1.2.1 A Multitude of Formats

During the last decade a multitude of improved tape storage formats were brought to the market, in a wide range of capacities and performances. The high-end server market have been dominated by IBM and StorageTek (STK) with tape drives offering high level of performance, reliability, and functionality. Their latest products, the IBM 3592 and the STK T9940B continue to lead this segment. They use linear recording technology and advanced MP tapes to reach capacities of 300 GB and 200 GB respectively, high data rates, and fast access times.

A number of linear and helical scan formats are available for workstations and low-end servers, including Travan, SLR, DLT VS, DDS, VXA, and AIT. Most of them offer capacities currently comprised between 70 GB and 100 GB, except Travan and DDS reaching only 20 GB and respectively 36 GB. The DDS's modest capacity is limited by the very small dimensions of the cartridge, as the format has been featuring some of the highest areal recording densities achieved in magnetic tape (Fig. 1.4). DDS is leading the low-cost tape market due to a large base of drives installed, reduced prices, and multi-vendor support. According to Gartner Dataquest, over 2.2 million tape drives were shipped worldwide in 2003, out of which DDS represented more than 1 million units [1].

However, low-end tape systems are under increasing pressure from alternative storage technologies. Tape solutions are migrating away from the desktop to the data center, with a trend toward storage consolidation, increased use of automation, and enhanced backup strategies such as disk-to-disk-to-tape (D2D2T). The centralization of tape is driving the need for high-performance drives suited for mid-range server environments, like LTO, SDLT, SAIT, and AIT. Also known as super-drives, they feature high data capacities and low cost per gigabyte. The progress of storage capacity in mid-range tape formats is pictured in Fig. 1.3, covering the last decade as well as predictions for the

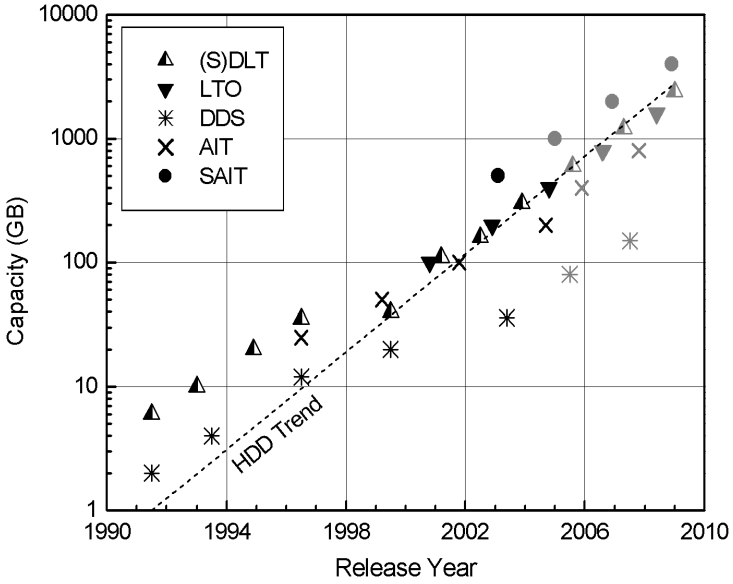


**Figure 1.3:** *Evolution of storage capacities in magnetic tape versus the trend in hard disk drives (dashed line). Following the year 2004, predictions are plotted based on roadmaps published by manufacturers.*

coming four years. The DDS format and the trend in hard disk drives are also included. It can be noted that SAIT is the most comfortable positioned tape format against HDDs in term of capacity. SAIT was introduced by Sony and Matsushita in early 2003 with a capacity rated at 500 GB, which was about triple than in linear scan formats. This was realized by combining a single reel, half-inch tape cartridge with helical scan technology derived from AIT platforms, which allows for high areal recording density. SAIT is expected to be the first half-inch tape format to reach the terabyte target in 2005 (Fig. 1.3). Super-drives' shipments have been increasing significantly during the last years and their growth is expected to continue [2]. They comprised 14% of unit shipments and 45% of revenues in 2002, and will probably represent 50% of unit shipments and 83% of revenue in 2008. It is forecasted that over 2.8 million compact tape drives of all types will be shipped worldwide in 2008, totalling for a revenue of $3.25 billions.

### 1.2.2 Areal Density Trends

In 1973, the IBM 3340 revolutionized the hard disk drive (HDD) industry by introducing low-mass heads flying on lubricated disks in a sealed assembly. The

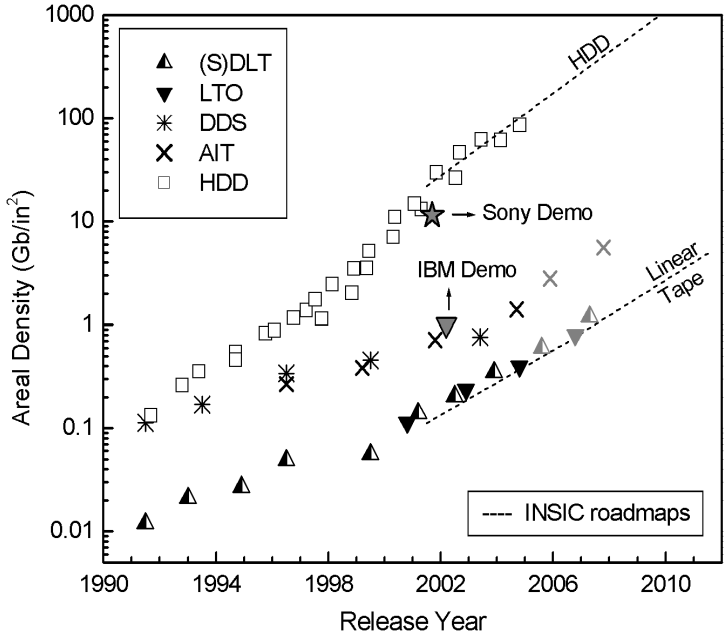


**Figure 1.4:** *Progress of the areal density in tape and hard disks. Tape recording demonstrations by Sony and IBM are also included. HDD releases consist of IBM / Hitachi GST products, with form factors of 3.5 in and 2.5 in.*

technology, also known as *Winchester*, allowed to store nearly 2.6 kb per mm$^2$ (1.7 Mb/in$^2$). The consumer video systems of the mid 70s, Betamax and VHS, were reaching areal densities around 20 kb/mm$^2$ (13 Mb/in$^2$), if we assume that the shortest wavelength recorded in the analog format corresponds to one digital bit. At that time, the helical tape recording technology was reaching higher densities than the hard disk. The track width varied around 50 $\mu$m, almost two times narrower than in HDDs, while the track pitch in linear formats was much larger, close to the millimeter. The bit densities both in helical and linear recording were superior to hard disks.

IBM developed the first thin-film inductive head and a superior slider design in 1979, with the 3370 disk drive. The growth of the track and linear densities in helical scan tape systems slowed down during the 80s, and they were caught up by HDDs in the early 90s. The IBM's demonstration of 1.6 Mb/mm$^2$ (1 Gb/in$^2$) in 1990, using anisotropic magnetoresistive (AMR) read heads and thin-film media [3, 4], marked the beginning of a spectacular growth of the areal density in HDDs. This was possible by increasing the track density more

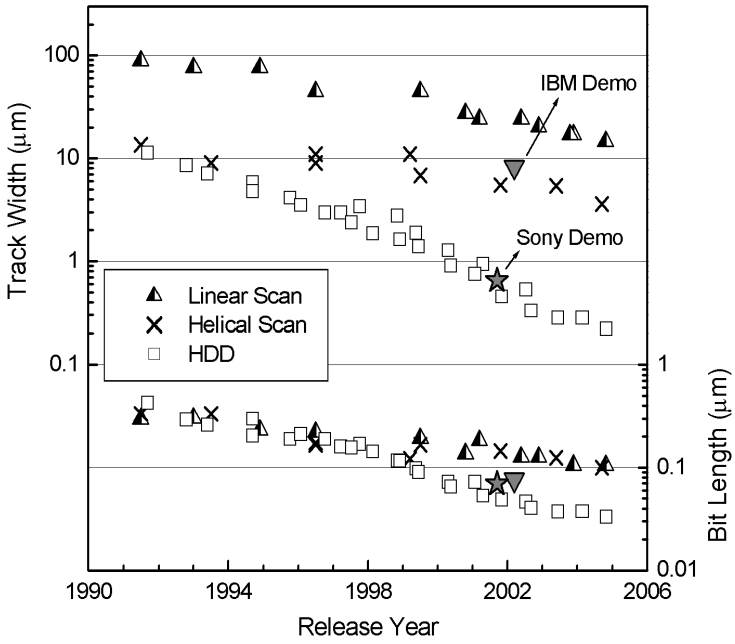


**Figure 1.5:** *Reduction of the track width and of the minimum bit length in magnetic tape and hard disk during recent years.*

aggressively than the linear density. The progress of areal densities in magnetic tape and disk drives since 1991 is plotted in Fig. 1.4. The evolution of the track width and minimum bit length is depicted in Fig. 1.5. It can be noted that the progress of the hard disk's areal density during the last decade has been mainly driven by reducing the track pitch. Decreasing the track width rather than the bit length leads to better signal-to-noise ratio (SNR) [5, 6, 7, 8, 9]. The bit aspect ratio (BAR), which is the track width over the minimum bit length, is often used to describe the bit cell in a recording system. The areal density is plotted versus BAR values in Fig. 1.6, for magnetic tape and hard disk systems released since 1991. The trend to increase more drastically the track density reflects in lower BAR.

While the areal density of hard disks was booming in the 90s, the progress in magnetic tape recording was relatively slow, as reflected by Fig. 1.4. The track width in helical scan systems got stuck around 10 $\mu$m for many years while a slow progress was achieved in linear formats, reducing the gap between the two tape technologies (Fig. 1.5). The linear density in tape recording and hard disk evolved closely up to the end of the 90s, when the latter evolved to giant magnetoresistive (GMR) read heads, improved media, and reduced magnetic

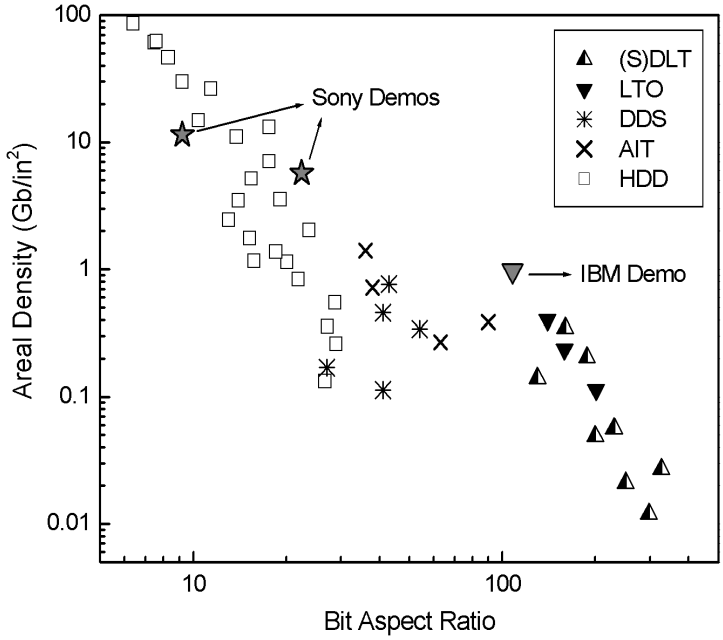


**Figure 1.6:** *Decreasing the bit aspect ratio (BAR) allows for higher areal densities in hard disk and tape recording. Sony and IBM demonstrated higher recording densities in magnetic tape at reduced BARs.*

spacing. The areal density of HDDs became so large by early 2000, so that their capacity was approaching the mid-range tape formats, while the low-end tape drives were already behind (Fig. 1.3). The hermetically-sealed operating environment and a coordinated design of head and media helped to achieve a fast progress in HDDs. Tape systems must deal with additional issues such as interchangeable media, backward compatibility, multi-vendor compliance, durability, and low cost. Moreover, the head-to-tape contact engender harsh operating conditions where problems due to wear, corrosion, and electrostatic discharge (ESD) need to be addressed. The flexible, thin polymer substrates implies specific requirements for media fabrication, and also affect the tracking performance of the drives.

However, increased efforts from the tape industry became recently necessary in order to keep the pace with the growth of HDDs and to remain cost competitive. This triggered the introduction of the super-drive formats like LTO, SDLT, and SAIT, with new levels of performance and capacity. In 2001, the Information Storage Industry Consortium (INSIC) established a roadmap that should secure the role of linear tape recording as a viable and competitive solution for backup

and archiving [10]. The scope of this roadmap was to maintain a fix ratio between the capacity and performance of tape versus hard disk. The trend suggested by INSIC have been accomplished to date by the LTO and SDLT formats (Fig. 1.4), as well as by the high-end drives from IBM and StorageTek. They all use thin-film AMR heads, advanced MP tapes, and efficient active track following schemes. IBM proved in 2002 the possibility to increase the capacity of linear drives at a faster rate, by demonstrating an areal density allowing to store 1 TB of data in a LTO cartridge [11, 12]. This was achieved on an experimental set-up similar in many ways to a commercial IBM LTO drive, indicating the feasibility to extend the current technology. An experimental MP tape with small particles' size of 60 nm, thin magnetic layer of 100 nm, and low roughness was used. The BAR employed in IBM's demonstration to reach 1.5 Mb/mm$^2$ (1 Gb/in$^2$) was equal to 108, almost half than in the first generation LTO format.
Similar areal densities are already available in commercial helical scan systems, at BAR values below 40 (Fig. 1.6). The helical scan technology is still achieving significant narrower track widths than the linear formats while the bit density is in the same range, as visible in Fig. 1.5. In order to maintain this advantage over linear systems, rotary head platforms are also accelerating the growth of their areal density (Fig. 1.4). Significant progress has been achieved in ME tape and Sony already demonstrated densities of 18 Mb/mm$^2$ (11.5 Gb/in$^2$) and 8.8 Mb/mm$^2$ (5.7 Gb/in$^2$) [13, 14]. The latter corresponds to what should be accomplished by the 6th generation AIT format, expected in 2007. GMR read heads and advanced ME tapes with the magnetic layer's thickness of 28 nm and respectively 40 nm were used for the demonstrations. The corresponding BAR values were 9 and 22, which are close to operating points typical for hard disks (Fig. 1.6). These results prove that magnetic tape recording is not near any fundamental limitation, however, substantial technological issues still have to be addressed. Reliability of AMR and GMR heads in helical scan systems is still a subject of intensive work [15, 16, 17, 18], and other system aspects like precise track positioning should also be mentioned. The narrow track widths achieved in rotary head platforms also require an increasingly better control of the track edge effects [19, 20].

### 1.2.3 Technology Status

Advanced MP tapes with high coercivity ($H_c \approx 200$ kA/m), thin magnetic layers ($\delta \leq 100$ nm), small particles' length around 60 nm and lower roughness became recently available [21, 22, 23]. Decreasing the length of metal particles below $\approx 40$ nm may lead to poor thermal stability [24, 25] and new types of particles with enhanced crystalline anisotropy may be needed. Barium ferrite particles are a potential candidate for high density tape recording due to their small dimensions down to 20 nm and high coercivity ($H_c > 200$ kA/m) [26, 27,

28]. The ME tape technology is in good shape and significant progresses have been achieved by improving its morphology and crystallographic orientation, and decreasing the thickness of the magnetic layer [29, 30, 31, 32]. ME tape with a thin layer $\delta = 50$ nm and coercivity $H_c = 135$ kA/m is already available in a commercial video format, the MICROMV [20]. Much higher coercivity, up to 240 kA/m, has just been obtained in development samples [32]. Thin-film tapes have been studied during the last years by sputtering of Co or Co alloys, using diverse underlayers and deposition configurations. It had been shown that very thin magnetic layers down to 20 nm can be obtained with high coercivity up to 300 kA/m and fine grain size [33, 34, 35, 36]. Metal sputtered (MS) tapes have been receiving recently an increasing interest, and are believed to be a good candidate for very high density recording.

A true progress potential exists for the magnetic tapes, both over the short and long time range. They will evolve toward thinner magnetic layers with lower $M_r\delta$, higher coercivity, and improved tribological properties. The thin-film and MR heads technology for tape recording is generally well developed. AMR read heads have been successfully employed in linear scan tape drives [37, 38, 39] and GMR structures show good promise [40, 41]. GMR heads have been intensively studied for application in helical scan systems as well [13, 14, 42], likewise AMR [15, 43] and even tunneling magnetoresistive (TMR) devices [44]. The tribological properties of the heads, tapes, and drives are also being researched for improved reliability and recording performances [18, 45, 46, 47, 48]. For example, the magnetic spacing is affected by the tape roughness and wear effects such as pole tip recession [49, 50, 51, 52], debris and stain formation [53, 54, 55]. The magnetic spacing is limiting the linear density via an exponential read loss factor (Section 2.4.2), but also through the efficiency of the write process [56, 57, 58].

### 1.2.4 Toward Higher Track Densities

Nowadays hard disk drives feature much higher areal density than magnetic tape systems, mainly achieved through very narrow tracks. The track width in HDDs is nearly 15 times lower than in helical scan tape formats, and about 40 times than in linear scan systems (Fig. 1.5). The minimum bit length in hard disks is lower than in magnetic tape by approximately a factor of 3, supported by advanced thin-film media, sensitive GMR heads, low flying heights close to 10 nm, and a sealed environment free of impurities. Due to higher magnetic spacing and media limitations, it is improbable that the bit density could be drastically increased in tape recording. However, there is much space available to decrease the track width (Fig. 1.5). Indeed, both areal density demonstrations of Sony [13] and IBM [12] were based on reducing the track pitch more than the bit length. For the incisive demonstration of 18 Mb/mm$^2$ (11.5 Gb/in$^2$), Sony narrowed the track width by a factor of

9 compared to the time being helical scan technology, while the bit length was just dropped by half. It was therefore proved that tape recording has great potential to increase the areal density, which will probably be achieved mainly through the reduction of the track pitch. Such approach demonstrated its effectiveness in the spectacular capacity growth of hard disk drives during the last decade. According to the INSIC roadmap, a track pitch close to 2.5 $\mu$m should be reached by 2011 in linear recording [10]. Track widths below 3 $\mu$m are expected in helical scan systems in less than two years, and they should approach 1 $\mu$m by 2010. Research for enabling the linear scan technology to reach very narrow tracks below the micrometer range is being conducted [59, 60].

A number of technical issues like accurate track following need to be solved in order to support very high track densities. The inability to keep the recording heads perfectly centered on the data tracks give rise to track misregistration. Other critical aspects are intrinsic to the recording process and are related to the cross-track resolution of the write and read heads. The write head generates a maximum magnetic field in the track center, while its amplitude is gradually decreasing at the edges and the gradient is deteriorating [61]. The side fringing fields write data with distorted geometries at the track edges, and partially erase previously written information in adjacent tracks, causing *side write* and *side erase* effects [62, 63, 64, 65, 66, 67]. This generates an area between neighboring tracks that does not contain well defined magnetic transitions and does not contribute to the useful read signal, known as *side erase band*. Moreover, the track edges usually exhibit higher noise levels than on-track [68, 69, 70, 71, 72]. Consequently, side writing affects the SNR of a recording system by decreasing the effective write track width and by generating noise. Good control of edge effects is therefore extremely important for narrow track recording [5].

The cross-track resolution is also of concern for the read heads, which can sense magnetic flux from adjacent tracks, known as *side reading* [62]. Side read effects are usually less severe than side write, partly due to the shorter gap lengths. Moreover, established techniques exist to compensate for side reading and track misregistration. Disk drives employ a guard band between the tracks as well as a "write wide read narrow" scheme. The latter consists in designing the read track width to be smaller than the write track width [73]. The same approach has been widely used in linear tape recording systems. However, track misregistration and side reading are dealt with very differently in helical scan systems. Inter-track interference during playback is avoided by writing the bits in adjacent tracks at opposite azimuth angles. The method allows a read head wider than the track pitch as well as large read tracking margins, extremely useful in tape recording. A guardband is not needed in such systems and minimum erase bands are preferable for maximizing the playback signal [74]. It is possible that guardband-less azimuth recording will be adopted in

future linear tape formats to reach very high track density, with an eventual pitch below 1 $\mu$m [59, 60].

## 1.3 This Thesis

In 1990, the track pitch in rigid disks was close to 15 $\mu$m and the erase bands were around 2-3 $\mu$m [64, 75]. Track widths narrower than 0.25 $\mu$m are currently achieved in commercial hard disks, and around 0.1 $\mu$m in laboratory demonstrations [76, 77]. The off-track capability in these demonstrations suggests that the erase bands are relatively small compared to the track pitch. The thinnest erase bands reported to date in magnetic tape recording systems are around 0.4 $\mu$m, evaluated at moderate linear densities [19, 20]. As track widths are getting closer to the micrometer, increasingly better control of side writing and erasing is required. Sony demonstrated the feasibility of an areal density of 18 Mb/mm$^2$ (11.5 Gb/in$^2$) using a GMR read head with the physical width of 0.45 $\mu$m [13]. Nevertheless, the offtrack capability of the system was not addressed in this demonstration. The experiment was performed with a write track much wider than the read head, and it was assumed that a track pitch of 0.64 $\mu$m would be achievable. A tight margin around 0.2 $\mu$m was therefore implied for the write track reduction caused by erase bands and tracking errors together. Still, both issues are far from being sufficiently controlled in nowadays tape recording systems. Erase bands, noise, and transitions' distortion at the track edges need to be much better confined than they are presently, in order to reach submicron tracks in tape recording. Such issues have been sporadically explored and extended studies are not yet available in the literature.

The scope of the work presented in this thesis was to investigate the recording phenomena at very high track density and understand the requirements for reaching submicron tracks in magnetic tape. A broad study of edge effects is presented with a focus on side writing and erasing, which are critical factors for reaching narrow tracks. Different types of recording heads and magnetic tapes were investigated. They comprise advanced HSS (Helical Scan Silicon) and MIG heads with pole widths ranging between 1.3 $\mu$m and 6.2 $\mu$m. ME and MP tapes were employed, featuring various magnetic properties and thickness of the magnetic layers between 50 and 300 nm. The edge effects were studied using common approaches based on track profiling techniques or magnetic force microscope (MFM) imaging, while novel methodologies are proposed as well. Detailed analyzes were performed up to very high linear recording densities around 10 kfc/mm (254 kfc/in).

The principles of digital magnetic recording are introduced in Chapter 2. The write and read processes are presented and narrow track recording is then discussed with emphasis on edge effects. Chapter 3 provides an overview of modern recording tape and head technologies. The HSS and MIG heads and

the ME and MP tapes analyzed in this work are also described.

Chapter 4 deals with test equipment for tape recording experiments. The requirements and design guidelines for a high precision tape-drum tester aimed at track widths down to 200 nm are discussed. However, the redesign of an existing tester was preferred for our recording investigations. A tracking accuracy below 0.1 $\mu$m was reached, suitable for track widths close to 1 $\mu$m.

Chapter 5 begins with an overview of common techniques to study edge effects, including track profiling and magnetic imaging such as MFM. Track profiles of HSS heads with pole widths down to 1.3 $\mu$m are presented. An *imbalanced overwrite* method suitable for qualitative studies of side writing is then described. The method is applied to analyze the side write asymmetry of an early stage prototype HSS head, with the recording poles misaligned at one edge.

In Chapter 6, a novel interpretation model of *triple-track profiles* is proposed, allowing precise estimations of the erase bands and side read widths. The method is extensively applied to investigate the edge effects of HSS and MIG heads in combination with different ME and MP tapes. It is shown that the erase bands are strongly reduced at good alignment of the recording poles and short write gap. They are also decreased at high tape coercivity and thin recording layers. Triple-track profiling, *erase profiles* and MFM imaging are applied to analyze the erase bands of a HSS head with gap length of 0.11 $\mu$m, using ME tape with thin recording layer of 50 nm and coercivity of 164 kA/m. We find values below 0.25 $\mu$m down to short recording wavelengths of 0.2 $\mu$m, at the edge with optimum pole alignment.

Chapter 7 provides a study of submicron tracks in tape recording based on *microtrack* measurements. It is shown that the investigation of microtracks is a meaningful method to predict the recording performances of future narrow track tape systems. Complex side write effects are addressed from their frequency and/or current responses. We evidence the influence of the asymmetric trailing poles of a MIG head on side write performances.

The results presented in this work are finally synthesized in Chapter 8. The requirements for reaching submicron tracks in tape recording are outlined, from a side writing point of view. Suitable recording test equipment and investigation methods of edge effects are also reviewed.

Chapter 2

# High Density Magnetic Tape Recording

In this chapter the principles of digital magnetic recording are briefly reviewed. The basic magnetic properties of the recording medium are introduced in relation to its hysteresis loop. The write process in thin recording layers is described using the William-Comstock analytical model, followed by a discussion on thick tape media. Further, the reciprocity principle is employed to explain the read process and it is applied to derive the voltage pulse generated by a single arctangent transition. The spectrum of square wave recording is further analyzed. A discussion on narrow track recording and related issues is included at the end of the chapter. Great emphasis is given to edge effects, side write and erase being strong limiting factors for increasing the track density in magnetic tape recording.

## 2.1 Digital Magnetic Recording

Magnetic data storage employs a digital type of recording, where two magnetization states with opposite directions are preferred. During the write process, the magnetization of the medium is more or less saturated in alternating directions which are separated by *magnetic transitions*. In the read process, the transitions induce voltage pulses which are detected for reconstructing the digital information. In *longitudinal recording*, the medium's magnetization is oriented in plane, parallel to the head moving direction. This scheme has been adopted in all commercial hard disks and tape recording systems to date. *Perpendicular recording*, where the magnetization is perpendicular to the medium's plane, is a serious candidate for achieving very high densities in future hard

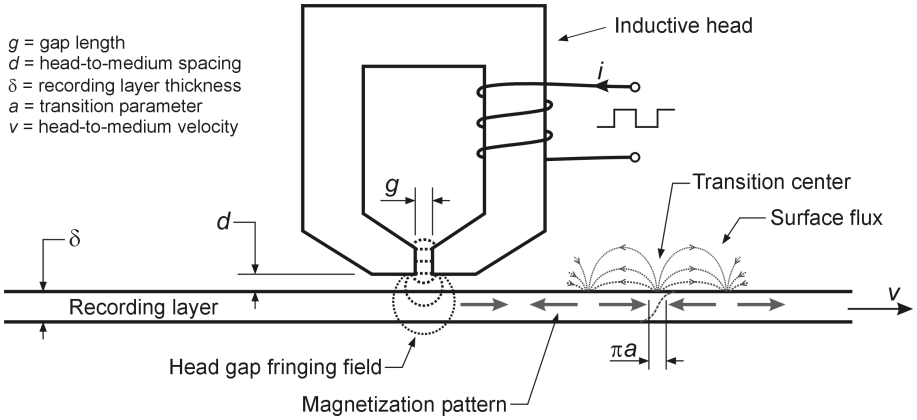


**Figure 2.1:** *Schematic representation of digital magnetic recording.*

disk drives. It presents a number of advantages like stronger write field capability, lower demagnetization effects, and improved thermal stability. Current magneto-optical storage systems employ a perpendicular recording method. *Transverse* and *tilted recording* schemes could also be mentioned, the latter receiving increased interest recently.

Longitudinal recording is a well established technique which is far from reaching its limits in magnetic tape storage. A representative recording configuration is schematically drawn in Fig. 2.1. The inductive recording head consists of a soft magnetic yoke with a gap of length $g$ and an electrical winding around the core. A magnetic field is generated in the gap region and its proximity when a current is passed through the coil. The head is closely spaced to the medium at distance $d$, and there is a relative motion between them with high velocity $v$. The gap fringing field has to exceed the switching field of the medium in order to magnetize it. Magnetization transitions are recorded by reversing the direction of the write field/current. The length of the transitions is finite and it determines the maximum linear density that can be achieved in a system, in terms of write resolution. The written transitions generate magnetic flux that can be sensed at the surface of the medium using the same inductive recording head as for writing, or a dedicated read head. Using distinct heads for writing and for reading allows to optimize them for each specific operation, and significantly enhance the performances of the system. The use of magnetoresistive (MR) heads greatly increases the signal output and the read resolution in thin media.

## 2.2 Medium Magnetization

The recording medium consists of a thin magnetic layer, with hard magnetic properties. That is, it can be magnetized by a relatively large applied field and retain a substantial fraction of the saturation magnetization after the field is removed. Modern media have a granular structure ensuring reduced interference between recorded patterns and good signal-to-noise ratio (SNR). The magnetization of such media is a complicated process influenced by a large number of factors such as field history, anisotropy, and microstructure.
A very common way to characterize magnetic materials is by measuring the *hysteresis loop*, which is a plot of magnetization, $M$, versus applied field, $H$. The magnetization is measured along the same direction as the external field. The field is incrementally increased up to reaching saturation, then is reduced to zero, reversed and brought to saturation in the opposite direction. A typical hysteresis curve of a recording medium is shown in Fig. 2.2. The magnetization is maximum when the medium is fully saturated, and is called the *saturation magnetization*, $M_s$. If the external field is dropped to zero, the magnetization relaxes to a lower value known as *remanent magnetization*, $M_r$. The ratio $S = M_r/M_s$ is called the *remanence squareness*. The magnetization is reduced to zero when the applied field reaches the *coercive field*, $H_c$. The *coercive squareness*, $S^*$, is defined by the slope of the hysteresis curve at the coercive state:

$$\left.\frac{dM}{dH}\right|_{H=H_c} = \frac{M_r}{H_c(1-S^*)} \ . \tag{2.1}$$

The shape of the hysteresis curve depends much on the composition, microstructure and inhomogeneities of the recording media. Even though it gives a basic picture of the magnetic properties of some material, it is not sufficient for understanding the magnetization reversal process and underlying interaction phenomena. Additional information may be obtained from the study of minor loops, such as initial remanence magnetization (IRM) and DC demagnetization (DCD) curves. The DCD curve differs from the major hysteresis measurement in that the magnetic sample is brought to saturation each time before applying a new field. The *remanent coercive field*, $H_{cr}$, can be extracted from the DCD curve and represents the field needed to be applied to the saturated medium for reducing its magnetization to zero. The remanent coercive field $H_{cr}$ differs from $H_c$ by the fact that switching is achieved only through irreversible magnetization changes, and therefore is more representative for the recording process. If the external field is applied along the easy axis of the magnetic medium, $H_{cr}$ is just slightly stronger than $H_c$. However, for arbitrary directions of the applied field, $H_{cr}$ and $H_c$ may present well different angular dependencies [78]. Magnetic torque measurements, where the direction of the applied field is varied rather than its amplitude, are used to analyze the switching mechanisms and the anisotropic energy.

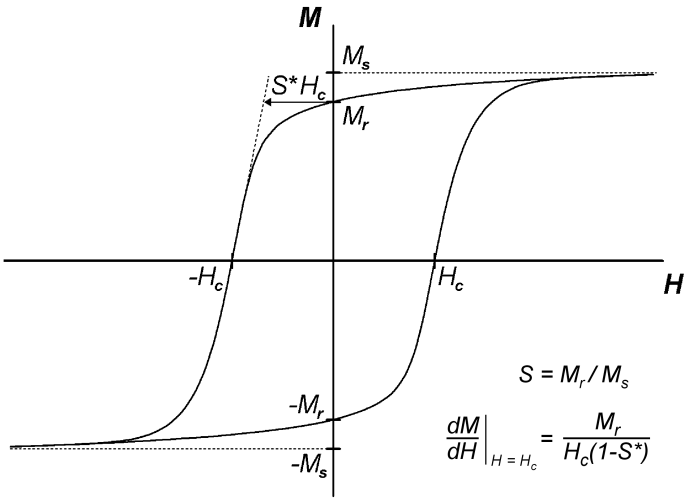


**Figure 2.2:** *Typical hysteresis loop of magnetic recording media, with characteristic parameters. The remanence squareness, $S$, and the coercive squareness, $S^*$, are also expressed.*

## 2.3 Write Process

The magnetic field applied to each position in the medium passing the write head is a rotating vector of varying amplitude. The distribution of the magnetization in the recording layer depends on the complex history of head fields and internal demagnetizing fields. The intricate hysteretic and vectorial nature of the process is difficult to be accurately modeled. Rigorous modeling of the write process implies self-consistent computer calculations where only the head field is considered to be known, while the other vectors are calculated iteratively until convergence is reached. Simplified analytical formulations can, however, provide significant insights into the write process, allowing useful qualitative analysis of recording systems. Most analytical models of the write process neglect the vector aspect of the phenomena, and only longitudinal components are considered. The assumption is justified for thin media with strong in-plane orientation. A popular model introduced by Williams and Comstock in 1971 [56] provides a simple analytic formula for the magnetic transition length, making surprisingly successful predictions.

### 2.3.1 Williams-Comstock Model

The Williams-Comstock model considers a recording head that interacts with a very thin medium magnetized in its remanent state, $+M_r$, to reverse the mag-

netization toward $-M_r$. A magnetic transition is formed underneath the head, its length being determined by the influence of the write and demagnetizing fields on the medium. The transition broadens when it moves away from the recording head, as the write field has vanished and the demagnetizing field is still present. The demagnetizing field causes most often a weak broadening, known as relaxation. The model assumes that writing takes place along the major hysteresis loop of the medium (as the one plotted in Fig. 2.2), while relaxation is described by a straight line minor loop. The write process is expressed in terms of magnetization slopes and field gradients at the center of the transition, $x_0$, by the following equation:

$$\left.\frac{dM}{dx}\right|_{x=x_0} = \left.\frac{dM}{dH}\right|_{H=-H_{cr}} \left( \left.\frac{dH_x}{dx}\right|_{x=x_0} + \left.\frac{dH_d}{dx}\right|_{x=x_0} \right), \tag{2.2}$$

where $H_x$ is the longitudinal head field and $H_d$ is the demagnetizing field [56]. The derivative $(dM/dH)_{H=-H_{cr}}$ is the slope of the hysteresis loop of the recording medium at the remanence coercive point. In order that the magnetization in the transition center is null after the head field is vanished, writing is assumed to occur at the field $-H_{cr}$, which is just slightly stronger than the medium's coercivity ($H_{cr} \approx H_c$). Therefore, the slope of the hysteresis loop in the middle of the transition can be approximated using Eq. (2.1):

$$\left.\frac{dM}{dH}\right|_{H=-H_{cr}} \approx \left.\frac{dM}{dH}\right|_{H=H_c} = \frac{M_r}{H_c(1-S^*)} \ . \tag{2.3}$$

The magnetic field from a recording head with infinite poles can be expressed along the longitudinal and vertical directions using the Karlqvist approximations [79]:

$$\begin{aligned} H_x(x,y) &= \frac{H_g}{\pi}\left[\arctan\left(\frac{x+g/2}{y}\right) - \arctan\left(\frac{x-g/2}{y}\right)\right], \\ H_y(x,y) &= -\frac{H_g}{2\pi}\ln\left[\frac{(x+g/2)^2+y^2}{(x-g/2)^2+y^2}\right]. \end{aligned} \tag{2.4}$$

where $H_g$ is the field achieved in the gap region of the head.

The shape of the magnetic transition was assumed to be defined by an arctangent function:

$$M(x) = -\frac{2M_r}{\pi}\arctan\left(\frac{x-x_0}{a}\right), \tag{2.5}$$

where $a$ is known as the *transition parameter*. The transition length is approximated by $l_a = \pi a$ and it reflects the shortest bit that can be effectively written. The parameter $a$ must therefore be minimized for achieving high linear density.

The gradient of the demagnetizing field produced at the center of an arctangent transition and in the middle plane of the recording layer is [80]

$$\left.\frac{dH_d}{dx}\right|_{x=x_0} = \frac{M_r\delta}{\pi}\frac{1}{a(a+\delta/2)} \ , \tag{2.6}$$

which can be approximated for a very thin medium ($\delta \ll 2a$) by

$$\left.\frac{dH_d}{dx}\right|_{x=x_0} \approx \frac{M_r\delta}{\pi a^2} \ . \tag{2.7}$$

The demagnetizing field is null at the transition center, and the longitudinal component of the write field, $H_x$, has to overcome the remanence coercivity ($H_{cr} \approx H_c$), yielding

$$\frac{\pi H_c}{H_g} = \arctan\left(\frac{x_0/g + 1/2}{y/g}\right) - \arctan\left(\frac{x_0/g - 1/2}{y/g}\right). \tag{2.8}$$

where $y$ is the spacing between the head surface and the middle of the medium ($y = d + \delta/2$). The equation above can be solved to get the relative position of the transition ($x_0/g$):

$$\frac{x_0}{g} = \sqrt{\frac{1}{4} - \left(\frac{y}{g}\right)^2 + \frac{y}{g}\cot\left[\pi\left(\frac{H_c}{H_g} - k\right)\right]} \ , \qquad \text{for} \quad k = \begin{cases} 0 & \text{if } H_g \geq 2H_c \\ 1 & \text{if } H_g < 2H_c \ . \end{cases} \tag{2.9}$$

For optimum recording performances, the deep-gap field usually needs to be larger than the coercivity by at least a factor of 3 ($H_g \geq 3H_c$), which implies $k = 0$ in Eq. (2.9). The transition location, $x_0$, is constant across the recording depth if the medium's thickness is small compared to the gap length ($\delta \ll g$). The write field gradient can be expressed as

$$\left.\frac{dH_x}{dx}\right|_{x=x_0} = -Q\frac{H_c}{y} \ , \tag{2.10}$$

where $Q$ depends on the deep-gap field relative to the coercivity ($H_g/H_c$), and the relative spacing ($y/g$) [81, page 215]:

$$Q = 2\frac{x_0}{g}\frac{H_g}{\pi H_c}\sin^2\left[\pi\left(\frac{H_c}{H_g} - k\right)\right]. \tag{2.11}$$

We note that the relative distance ($x_0/g$) can be replaced in Eq. (2.11) as a function of ($H_g/H_c$) and ($y/g$), from Eq. (2.9).

The Williams-Comstock model assumes that the write field gradient at the center of the transition is maximized, which would result in a minimum transition length. The optimum value of $H_g$ to get the highest field gradient could be calculated for a given system by numerically solving

$$\frac{dQ}{dH_g} = 0 \ . \tag{2.12}$$

This approach to find the optimum deep-gap field is similar to those presented in [81, pages 215-216] and [82], leading to more precise estimates than in the original Williams-Comstock model. Typical values calculated for $Q$ range between 0.8 and 0.9 for deep gap fields around 3 to 4 times higher than the coercivity.

Substituting Eqs. (2.3), (2.5), (2.7), and (2.10) into Eq. (2.2) yields to a good approximation of the transition parameter for thin media:

$$a = \frac{(1-S^*)y}{\pi Q} + \sqrt{\left[\frac{(1-S^*)y}{\pi Q}\right]^2 + \frac{M_r \delta y}{\pi H_c Q}} \ , \qquad y = d + \delta/2 \ . \tag{2.13}$$

After the transition moves away from the recording head, the magnetization in the medium relaxes under the influence of demagnetizing fields. This causes the written transition to broaden, but the effect is often negligible and therefore it is not treated here.

Short transitions are usually obtained at reduced magnetic spacing $d$, large medium coercivity $H_c$, low $M_r\delta$ product, and high coercive squareness $S^*$. Typical values of $S^*$ for in-plane oriented, modern magnetic media range between 0.7 to 0.9. The coercivity has to be increased without detriment to the capability of an inductive head to write the medium. That is, the deep-gap field needs to be sufficiently strong to ensure a high $Q$, as given by Eq. (2.11). It is therefore necessary to use write heads with high saturation magnetic flux density ($B_s$). Usual values of $(M_r/H_c)$ are currently around 1 for advanced metal particulate (MP) tapes and between 1.5 and 3.5 for metal evaporated (ME) ones.

The last term in Eq. (2.13) typically tends to dominate, yielding

$$a \approx \sqrt{\frac{M_r \delta y}{\pi H_c Q}} \ . \tag{2.14}$$

Eqs. (2.13) and (2.14) apply for very thin media where $\delta \ll 2a$ and $\delta \ll g$. Lifting the condition $\delta \ll 2a$, by using Eq. (2.6) instead of Eq. (2.7) to solve Eq. (2.2), leads to a less restrictive approximation of the transition parameter [80, page 2.38]:

$$a \approx -\frac{\delta}{4} + \sqrt{\left(\frac{\delta}{4}\right)^2 + \frac{M_r \delta y}{\pi H_c Q}} \ . \tag{2.15}$$

### 2.3.2 Thick Tape Media

The Williams-Comstock model can be used to estimate transition lengths in very thin media, whose thickness is considerably narrower than the write gap ($\delta \ll g$). For example, at a gap length of 200 nm, one may approximate as thin a recording layer with $\delta$ around 50 nm or below. The applicability of the model to thick media is just qualitative. That is, the same requirements to reach short transitions apply in either case but their precise influences would be different. In thick media, both the position and the length of the transition vary with the recording depth, and so does the peak magnetization [83]. The vector aspect of the write process becomes essential. Even in MP tapes with good longitudinal orientation, the vertical component of the magnetization may be significant in the transition region. The complexity of the recording process is further increased in ME tapes, as their easy axis is tilted out of plane.
A number of attempts to extend the Williams-Comstock model to thick media have been performed, featuring different levels of complexity. In simple approaches, the recording medium is divided into thin sublayers and the transition length varies with the depth while the position of the transition stays unchanged [84, 85]. More sophisticated models include the variation of the position location with the recording depth and make use of vector fields [86, 87, 88]. In [87] and [88], arbitrary orientation of the easy axis is supported and the peak magnetization is determined specifically for each sublayer. The latter also considers the effect of the degree of particle orientation and angular dependence of the switching field. However, these models for thick media do not lead to simple analytical solutions and need to be solved numerically.

Development tapes with the thickness of the recording layer below 50 nm have been recently reported, both in MP [21] and ME [13, 32] technologies. Experimental metal sputtered (MS) tapes with magnetic layers as thin as 20 nm were also produced [34, 89]. ME tape with a thin magnetic layer of 50 nm is already employed in a commercial digital video system [20]. Thin media approximations become usable at such thicknesses and the transition parameter could be estimated for a longitudinally oriented medium using Eq. (2.15). However, the Williams-Comstock model is not applicable to tilted media like ME and some MS tapes.
The thickness of the magnetic layer in current data tapes is usually comprised between 100 and 200 nm, making thin media approximations inappropriate. In thick media, recording is approximated to occur up to a maximum depth where the head field equals the coercivity. The write limit at long wavelengths can be estimated using the Karlqvist expression from Eq. (2.4) and without considering demagnetization effects, to yield [90]

$$\delta_w^{max} = \frac{g}{2\tan\left(\frac{\pi H_c}{2H_g}\right)} - d \ . \tag{2.16}$$

The approximation above should be reconsidered for ME tapes, where the easy axis is oriented out of the film plane. In some tape systems, the thickness of the magnetic layer may be lower than $\delta_w^{max}$ (i.e. $\delta < \delta_w^{max}$), and the maximum recording depth is given then by $\delta$. For the thin media approximation $\delta \ll g$, it can be deduced that $\delta \ll \delta_w^{max}$.
A thick medium is not saturated across the full depth $\delta_w^{max}$ given by Eq. (2.16), and the peak magnetization toward the recordable limit is lower than $M_r$. In fact, $\delta_w^{max}$ would rather correspond to the erase depth. The effective recording depth may be significantly reduced at short wavelengths depending on the head field gradient, magnetic interactions within the medium and switching mechanisms. Their interplay also influences the shift of the transition center position with the recording depth. These phase shifts were shown to be considerably increased by the demagnetizing fields [83]. At a given depth into a thick medium, the demagnetizing field vector at the transition center is not zero due to the influence of other sublayers and of the vertical magnetization. The net write field, given by the head field and the demagnetizing field, is therefore decreased. The influence of demagnetizing fields from the other sublayers is more pronounced in the deeper regions causing higher phase shifts of the transition center. These shifts give rise to broadening and asymmetry of the read pulse [83, 91]. It has been observed in thick longitudinal media that the read pulse is sharper at short wavelengths than at long ones [92, 93]. The deep regions within the medium, which typically present highest transition lengths and shifts, are mainly recorded only at long wavelength. At short wavelength, writing takes place to a lower extent within the medium and the contribution of the deep sublayers to the read signal is strongly decreased. Moreover, the lower recording depth has the effect to reduce the demagnetizing fields and consequently to narrow the transition length as well as its phase shift. They are further reduced by the magnetostatic interaction between very closed transitions [83, 86]. The combined effect of decreasing the transition length and the depth dependent phase shift leads to sharper read pulses at short wavelengths.

Reversal of a magnetic entity (or particle) within the medium occurs when the net write field vector overtakes the switching field. The switching field amplitude varies with the angle formed between the applied field and the particle's easy axis. It is generally flat up to an angle around 45°, followed by an increase that is steeper for ME than for MP tapes. The Williams-Comstock model implicitly assumes an inverse cosine angular dependence of the switching field ($H_s = H_c/\cos(\theta_s)$), which is relatively steep. The switching field variation affects the recording position $x_0$ and the $Q$ factor, which could be recalculated for other angle functions. The angular dependence of the switching field causes particles with different orientations of their easy axis to reverse at distinct $x$ locations [94]. This makes the transition to broaden in a medium with non-uniform orientation of the particles [90].
In tilted media like ME tapes, the angular variation of the switching field is

not symmetric with respect to the plane normal. This causes the transitions to be written at different locations (or field angles) depending on the head-to-tape moving direction. Best recording results are achieved when the write field at the trailing pole of the head is oriented close to perpendicular to the easy axis of the medium. A high field magnitude is then needed to switch the magnetization, available at a longitudinal position close to the write gap. The field gradient is considerable stronger near the gap corner resulting in shorter transition length, according to the Williams-Comstock model. Moreover, the position shift of the transitions with the recording depth is also reduced. It is generally admitted that ME tapes recorded in the "good" direction present superior performance than MP tapes. However, the recording properties of ME media deteriorate considerably when moved in the reverse direction. In this case, the write field at the trailing pole is oriented close to the easy axis of the medium and switching is achieved at low magnitude. The transitions are written at certain distance from the gap at low field gradient. Their length is therefore increased as well as the position shift with the recording depth.

## 2.4 Read Process

### 2.4.1 Reciprocity Principle and Readback from Single Transition

The magnetic transitions written in a recording medium generate magnetic flux that can be sensed by a read head. In the simplest approach to quantify the reproducing process an inductive read head is considered. As long as frequency effects are neglected, reading with an inductive head is a fairly linear process which is possible to describe conveniently using the reciprocity principle. Accordingly, the sensed flux can be expressed as a convolution between the recorded magnetization and the field from the read head. The playback voltage can then be estimated analytically using the reciprocity integral, which for wide track recording is given by

$$V(\bar{x}) = -NWEv\mu_0 \int_{-\infty}^{\infty} \int_{d}^{d+\delta} \frac{\partial \mathbf{M}(x-\bar{x},y)}{\partial x} \cdot \mathbf{h}(x,y)\, dy\, dx \ , \tag{2.17}$$

where $\bar{x} = vt$, $v$ is the relative velocity, $W$ is the track width, $N$ is the number of turns, and $E$ is the efficiency of the head. $\mathbf{M}$ is the magnetization vector in the medium and $\mathbf{h}$ is the head field normalized to the magnetomotive force:

$$\mathbf{h}(x,y) = \frac{\mathbf{H}(x,y)}{NIE} \ . \tag{2.18}$$

In the case of a thin medium ($\delta \ll d + g_r$) with strong in-plane orientation, Eq. (2.17) can be approximated by a simplified scalar expression:

$$V(\bar{x}) = -NWEv\mu_0\delta \int_{-\infty}^{\infty} \frac{\partial M_x(x-\bar{x})}{\partial x}\, h_x(x, d+\delta/2)\, dx \ . \tag{2.19}$$

The magnetization pattern was assumed to be constant across the depth of the medium, while a first order approximation was used for the longitudinal component of the head field. It is convenient to express the head field using the Karlqvist approximations from Eq. (2.4). The replay voltage from a single transition described by an arctangent variation of the magnetization is then readily calculated involving a mathematical formalism as presented in [80]:

$$V_{sp}(\bar{x}) = \frac{2}{\pi g_r} NWEv\mu_0 M_r \delta \left[ \arctan\left( \frac{\bar{x} + g_r/2}{d + a + \delta/2} \right) - \arctan\left( \frac{\bar{x} - g_r/2}{d + a + \delta/2} \right) \right], \tag{2.20}$$

where $g_r$ is the gap length of the read head. The read pulse is commonly characterized by its peak value and the width at half amplitude, which are deduced from Eq. (2.20) to be:

$$V_{sp}^{peak} = \frac{4}{\pi g_r} NWEv\mu_0 M_r \delta \arctan\left[ \frac{g_r}{2(d + a + \delta/2)} \right], \tag{2.21}$$

$$PW_{50} = \sqrt{g_r^2 + 4(d + a + \delta/2)^2} \ . \tag{2.22}$$

The above expression of the half pulse width $PW_{50}$ is very close to the better known approximation proposed in [95]:

$$PW_{50} = \sqrt{g_r^2 + 4(d + a)(d + a + \delta)} \ . \tag{2.23}$$

It can be deduced from Eqs. (2.21) and (2.22) that short read gap, reduced spacing, and small transition length are suitable to obtain narrow pulses with high amplitude. Sharp read pulses are necessary in order to solve closely spaced transitions and achieve high data density. The replay voltage of an inductive head is proportional to the track width, relative velocity, head efficiency and number of turns. The effect of the $M_r\delta$ product on the read performance is not direct. On the one hand it increases the voltage amplitude, but on the other hand it broadens the transition parameter (see Section 2.3.1) and the $PW_{50}$. The read resolution is therefore improved at low $M_r\delta$. The trend in high density recording is to reduce the $M_r\delta$ and use sensitive MR heads to cope with the weaker read flux.

MR devices generate much stronger read signals than inductive heads and their frequency bandwidth is also superior. MR heads operate in linear regime if the magnetic field from the recorded transitions is sufficiently small and are suitable for media with low $M_r\delta$. The reciprocity principle can then be adapted to analyze the playback voltage of MR heads [81, pages 177-194]. A similar expression as for inductive read heads is obtainable for the pulse voltage of a shielded MR device reading an arctangent transition. However, the pulse amplitude of MR heads is about one order of magnitude higher than achievable

with inductive heads, and does not depend on the relative velocity. The pulse width at half amplitude can be approximated as

$$PW_{50}^{MR} = \sqrt{(g_s/2)^2 + 4(d + a + \delta/2)^2} \,, \tag{2.24}$$

where $g_s$ is the gap between the shields of the MR element. That is, a MR head with a shield-to-shield distance $g_s$ feature a read pulse width equivalent to that of an inductive head with a gap length $g_r = g_s/2$.

### 2.4.2 Spectrum of Square Wave Recording

When multiple transitions are written at constant spacing using step changes of the write current, it is referred to as *square wave recording*. The variation of the peak voltage versus transition density is commonly known as *roll-off curve*. The other usual technique is to study the *spectrum* of the fundamental component over a wide range of recording wavelengths. The spectrum can be calculated assuming linear superposition of the read pulses, which implies that the transition shape must not vary over the density range considered. Using the approximations of arctangent transitions and Karlqvist read head, the fundamental of the replay signal at the recording wavelength $\lambda$ is given by [81, pages 148-156]

$$V_{rms}^{Fund}(k) = \frac{4}{\pi\sqrt{2}} NWEv\mu_0 M_r (1 - \mathrm{e}^{-k\delta}) \mathrm{e}^{-k(d+a)} \left| \frac{\sin(kg_r/2)}{kg_r/2} \right| , \tag{2.25}$$

where $k$ is the wavenumber $k = 2\pi/\lambda$. A similar expression is obtained for higher order odd harmonics:

$$V_{rms}^{m}(k) = \frac{4}{m\pi\sqrt{2}} NWEv\mu_0 M_r (1 - \mathrm{e}^{-mk\delta}) \mathrm{e}^{-mk(d+a)} \left| \frac{\sin(mkg_r/2)}{mkg_r/2} \right| , \tag{2.26}$$

for $m = 3, 5, 7, \ldots$ . The above voltages are expressed as root mean square (rms) values, as they correspond to what is normally measured by a spectrum analyzer. The magnetization pattern was considered to be invariant within the depth of the medium.
For studying the wavelength dependence of the fundamental voltage, it is convenient to write Eq. (2.25) as

$$V_{rms}^{Fund}(k) = Ck\delta \, \frac{1 - \mathrm{e}^{-k\delta}}{k\delta} \, \mathrm{e}^{-k(d+a)} \, |\mathrm{sinc}(kg_r/2)| \,, \tag{2.27}$$

where $C = \frac{4}{\sqrt{2}\pi} NWEv\mu_0 M_r$ is constant, and "sinc" is the sinus cardinal function defined as $\mathrm{sinc}(x) = \sin(x)/x$. The fundamental signal normalized to $C$ is plotted in Fig. 2.3 versus the inverse of the wavelength relative to $g$, for the case when $g = 2(d+a)$. The thickness of the recording layer is taken to be $\delta = d+a$.

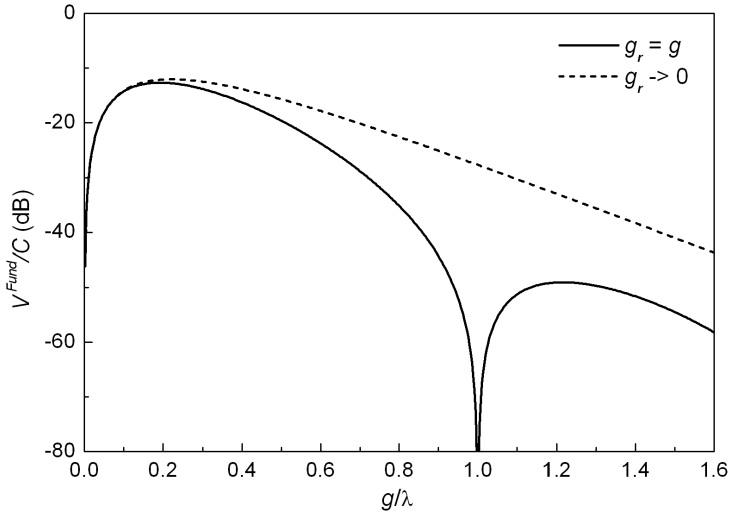


**Figure 2.3:** *Spectrum of the fundamental component at square wave recording, for finite read gap length and infinitely small gap length.*

The curve in solid line corresponds to a finite read gap length $g_r = g$, while the dashed one is representative for an infinitely small gap. At high recording density, the playback performance with a very short gap is largely superior. This is related to the better read resolution at short gap length, as also given by the $PW_{50}$ expression from Eq. (2.22). The signal from the infinitely small gap shows an almost exponential decay at short wavelengths, being dominated by the *spacing and transition loss*, $\mathrm{e}^{-k(d+a)}$. For the finite gap, the output is further reduced by the *gap loss* term, $|\mathrm{sinc}(kg_r/2)|$. It also causes the signal to vanish each time the gap length is equal to a multiple of the wavelength, known as *gap null* points. The first null point occurring at $\lambda_1 = g$ is visible in Fig. 2.3. However, the above gap loss is quite a rough estimation due to the approximate precision of the Karlqvist field equations. More accurate expressions are given in [96], where the first gap null occurs at $g/\lambda_1 = 0.8795$ (for an infinite pole head). The gap loss depends on the geometry of the head poles [96] but also on the medium permeability and magnetic spacing [97].
At recording wavelengths much larger than the thickness of the medium, the fundamental component of the output voltage increases almost proportionally to $k\delta$. However, at reduced wavelengths, the contribution of the deep sublayers to the read signal is decreased due to spacing losses. This effect is reflected in Eq. (2.27) by the *thickness loss* term, $(1 - \mathrm{e}^{-k\delta})/k\delta$.

The three distinct loss terms are plotted in Fig. 2.4. The spacing and transition loss factor has a drastic attenuation effect at high recording density.

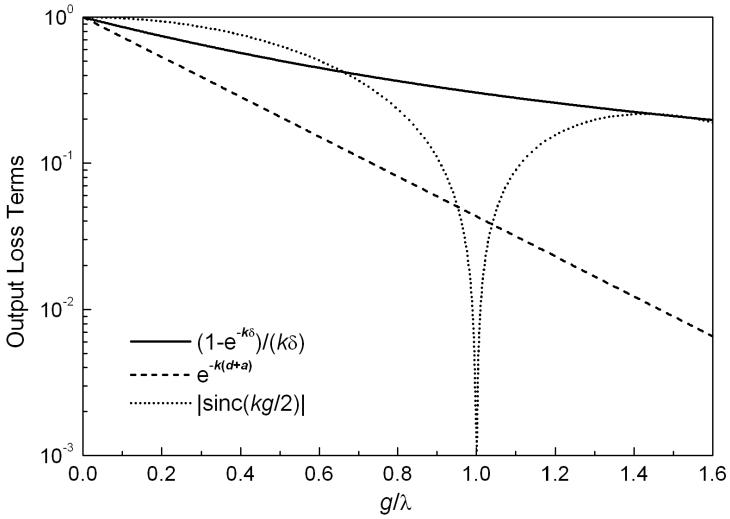


**Figure 2.4:** *Plot of wavelength dependent terms affecting the square wave spectrum of a recording system.*

It is therefore desirable to keep the magnetic spacing and the transition length as short as possible. The thickness loss also presents considerable decay at increasing density, resulting in a reduction of the effective read thickness. It can be shown that at wavelengths shorter than the medium's thickness, the read depth contributing to the output voltage in proportion higher than 95% is given by

$$\delta_r^{95\%} = 0.48\lambda \ . \tag{2.28}$$

This means that thicker media enhance the replay signal only at long wavelength, worsening the frequency roll-off. Note that $\delta_r^{95\%}$ is even lower than in Eq. (2.28) if the transitions are phase shifted with the recording depth. This is likely to happen in thick media as described in Section 2.3.2. It is suitable that the recording layer is thinner than the readable depth at the minimum wavelength for which it is designed:

$$\delta < \lambda_{min}/2 \ . \tag{2.29}$$

Thin media are therefore necessary for reduced thickness loss as well as for achieving short transition lengths during writing, according to Eq. (2.15). As recording wavelengths in tape recording are getting below 200 nm (Fig. 1.5), magnetic layers thinner than 100 nm should be made available. Read heads with short gaps are necessary to reach good resolution and to operate far enough

from the first gap null point. Similar square wave spectra are obtainable for shielded MR heads, which also present spacing and transition loss, thickness loss, and gap nulls.

## 2.5 Narrow Track Recording and Edge Effects

The write and read operations were presented in the previous sections as two dimensional processes, assuming that they are uniform along the cross-track direction. Nevertheless, both head and medium fields are different at the edges of the track than in the center, and there is magnetic interaction between adjacent tracks. In the case of wide tracks the non-uniformities caused by the edges could be neglected. Up to recent years, this used to be a valid approximation in magnetic tape recording as the track widths were not yet below the ten micrometers. However, concerns related to finite track widths are getting increasing importance as shrinking the track pitch in tape systems has been accelerated, as shown in Fig. 1.5. The lowest track pitch achieved in helical scan recording is currently around 3.6 $\mu$m, being expected to get close to 1 $\mu$m within few years.
The magnetic fields generated by three dimensional inductive heads can be computed with a high degree of accuracy using finite element modeling. Commercial packages like OPERA-3d and Flux3D allow simulating complex head structures. Analytical approximations for the side fringing fields of heads with infinite poles length and semi-infinite track widths have been derived in several works [62, 98]. Lindholm extended the calculations to finite track heads, using superposition [61]. It was generally found that the side fringing field is not considerable reduced up to a distance from the magnetic poles which is few times the gap length. Short gap lengths are therefore suited for confined side fringing fields. Moreover, the side field contains an important component oriented in the cross-track (transverse) direction. The components of the field are affected even underneath the poles, in regions close to their edges.

### 2.5.1 Side Write and Erase

Optimum recording occurs if the write field amplitude is superior to the switching field of the medium and its gradient is maximum around this value (Section 2.3.1). For reaching a suitable gradient, the on-track write field is typically few times higher than the medium's coercivity. In cross-track direction, the write field vanishes at the head edges over a finite distance causing a side fringing field. This can exceed the switching field of the medium over a certain range resulting in *side write* and *side erase* effects. The side field can write magnetic transitions as long as it overcomes the switching field of the medium and is sustained by a suitable gradient. This is known as side writing. At

increased distance from the poles, the side field may still be able to switch the medium but the gradient becomes too low for efficiently writing information. Distorted magnetization patterns are typically recorded over this area or, at short wavelength, just erasure occurs. The track edge region that does not contribute to the useful signal is referred to as *side erase band*. The extent to which side erasure occurs is typically given by the location where the head side field equals the medium's switching field. Side erasure is therefore reduced at high coercivity. It should not depend on the write wavelength as long as frequency losses do not occur within the write head. The width of the erase band determines how close adjacent tracks can be recorded. It largely depends on the ability of the side field gradient to write a transition shorter than the length of the bit under recording. This is treated in [99] as an effective enlargement of the transition parameter at the track edges. The erase bands are therefore increased at high bit densities, as it has also been observed experimentally in hard disk [64, 100] and tape recording [101, 102].

At the track edges, the medium experiences a complex write field sequence of in-plane rotations and switchings. The amplitude and the direction of the write field are degraded toward the head margins, frequently causing distortions of the recorded transitions. Bending of the transitions at the track edges is often observed [99, 103, 104, 105, 106]. Moreover, magnetization oriented in transverse direction may be present, especially in the case of isotropic media [65, 66, 107]. The distorted regions of the transitions have a nonlinear contribution to the replay signal and can appear as an increase of the effective erase bands.

When two data tracks are recorded very close together, especially with partial overlap, side writing is affected by interactions with the abutting magnetization pattern. It is often referred to as *edge overwrite*. In such cases, the intricate side write process is further complicated by the influence of the adjacent track. The magnetization texture at the edge depends on the patterns in both the overwriting track and the side erased track. A typical example is the dependence of the erase band on the phase difference between the transitions in the overlapping tracks [108, 109, 110]. The effect is most pronounced at long recording wavelengths. If they are in-phase, the transitions in the two tracks join at the common edge without an erase band being formed. However, in the out-of-phase case, there is a clear erase band generated between the tracks. At small phase differences, bending of the transitions edges in the overwriting track often occurs tending to bridge the transitions in the two tracks [67, 108]. Side writing is clearly affected by magnetic interactions with the pattern in the overlapped track. The effect is observed in both thin-film and particulate media and could be due to a complex sequence of magnetostatic interactions. The phase dependence is attenuating at bit lengths close to the write gap, up to completely vanishing. At high recording densities, the width of the erase band is dominated by the gradient of the side write field.

Edge effects have been mainly intensively investigated in hard disks, however, the principles can be extended to magnetic recording in general. Side writing and erasing are influenced by a multitude of factors related to the head, medium, and recording system. The head geometry plays a crucial role, most important being the alignment of the magnetic poles. Good alignment of the poles is required to contain the side write field and achieve minimum erase bands [5, 75, 111, 112, 113]. The side erase distance increases with the gap length $g$, being approximately direct proportional to it at small magnetic spacing ($d \ll g$) [62]. High saturation magnetic flux of the head poles, $B_s$, not only improves its writability, but also reduces the erase bands [114].
As expected from the theory [62, 98], it was also shown experimentally that side writing increases with the write current [63, 64, 115, 116]. More of concern is probably the increase of the erase band with the linear density. At short wavelengths, the side field gradient becomes insufficient to write well-defined transitions leading to the expansion of the erase bands [63, 64, 100, 101, 109]. That is, edge effects may limit the combination of very high track and linear densities, as it was also suggested by micromagnetic modeling [117]. The magnetic spacing was reported to have little direct influence on the width of the erase bands, as long as the writability is not affected [116]. This seems to have an almost proportional effect on the side erase distance and on the side write distance. However, it is important to keep the magnetic spacing as low as possible for superior writability. Apart from improved on-track performances, this would allow using shorter gap length and/or lower recording current resulting in reduced erase bands [5].
The medium's properties determining the on-track transition length, discussed in Section 2.3.1, impact as well on the side writing. Higher coercivity, $H_c$, typically results in reduced side erase distance and narrower erase bands [100, 118, 119]. Low $M_r\delta$ product is suitable to decrease the erase bands by enabling shorter transitions at the track edges [19]. It equally helps to reduce the magnetostatic interaction between the side field and the adjacent track, which may cause magnetization distortions especially if edge overwrite occurs. The side field contains both longitudinal and transverse in-plane components. The magnetization pattern recorded by the side field depends therefore on the medium's anisotropy. The track edges are better defined in oriented than in isotropic media resulting in narrower erase bands [65, 107].

### 2.5.2 Side Read

According to the reciprocity principle (Section 2.4.1), the side fringing field of inductive heads could be related to a side sense field in playback mode. That is, the read head can sense magnetic flux from areas in the medium located outside its edges, causing *side reading* [62, 64, 98]. The side read voltage can be estimated using a three dimensional extension of the reciprocity principle.

The profile of the read sensitivity function at the edge of a semi-infinite head was calculated in [98], for different wavelengths. The signal from a magnetic charge at a cross-track distance $z$, much higher than the magnetic spacing $d$ or the read gap length $g_r$, decays exponentially:

$$V_{SR}(k, z) \propto \mathrm{e}^{-kz} \ . \tag{2.30}$$

It can be readily observed that side reading is stronger at long wavelengths than at short ones. The head was considered perfectly aligned, with no azimuth angle. The effective read width for a head of physical width $w$ reading over an infinitely wide track was approximated in [62] as

$$w_r(\lambda) = w + \frac{\lambda}{\pi} \ , \tag{2.31}$$

which is valid for $\lambda \gg \pi g_r$.

Side read also occurs in MR heads and depends much on their construction and biasing schemes [5, 120, 121, 122]. Their shielding helps to reduce side reading at low recording density [123, 124]. However, such aspects are beyond the scope of this thesis. Side write effects are usually more severe than side read due to larger head gaps, high magnitude of the write fields, and magnetic interactions at the track edges. Moreover, side reading is more effectively dealt with using schemes such as "write wide read narrow" and azimuth recording. In azimuth recording tape systems, the read sensitivity function does not have to be confined to the track width. It allows for large tracking margins and is suited for very high track density tape recording [59, 60, 74]. Such systems do not need guardbands between tracks and it is therefore most important to keep the erase bands as low as possible.

## 2.6 Conclusion

The requirements for reaching high linear density in digital magnetic recording were treated from analytical models of the write and read processes. Short magnetization transitions are achievable in media with low $M_r\delta$ product, high coercivity, and high squareness. The recording layer must also present fine granular structure with minimum exchange coupling. Reduced magnetic spacing is also necessary, implying very smooth surface of the medium. The write head must be able to generate strong fields and should therefore employ soft magnetic materials with high saturation flux density ($B_s$). The longitudinal field gradient is sharper at short gap length, however, its amplitude is reduced (at finite distance $y$ from the poles). In relative thick media, as most current recording tapes, the recording nonlinearities caused by depth distortions are better tailored at long write gap. At the same time, long gap length causes excessive side writing and erasing, which are critical for achieving high track

density. The current trend in tape recording systems to accelerate the decrease of the track pitch imposes better control of the edge effects. Write heads must be designed to ensure confined side fields through well aligned poles, high $B_s$, and small gap length. Reducing the thickness of the recording layer $\delta$ is therefore needed to support shorter transitions but also to cope with shorter write gaps. Low $\delta$ is also required for improved read resolution, together with small read gap and magnetic spacing. Read heads with improved sensitivity are necessary to deal with decreasing $M_r\delta$, the use of MR devices becoming widespread. Moreover, they feature superior resolution and frequency bandwidth.

Chapter 3

# Magnetic Tapes and Heads

An overview of the current status of recording tape and head technologies is given in this chapter. Tape recording heads are briefly treated in the beginning of the chapter, followed by the introduction of Helical Scan Silicon (HSS) heads. They feature significant technological advances and were designed for very high track density, having well aligned, narrow recording poles. The HSS samples studied in this thesis are presented, their pole widths being comprised between 1.3 $\mu$m and 6.2 $\mu$m. Metal-in-gap (MIG) ferrite heads with track widths down to 3.6 $\mu$m are also included. The magnetic poles of one MIG sample were trimmed by Focused Ion Beam (FIB) in order to improve their alignment at the gap corners.
Magnetic recording tapes are treated in the last half of the chapter, the samples employed in this thesis being as well presented. Metal particulate (MP) and metal evaporated (ME) media are then discussed with an outline of most recent developments and future perspectives. Metal sputtered (MS) tapes are also described as promising candidates for very high density tape recording. They can be produced with thin magnetic layers around 20 nm and high crystalline anisotropy.

## 3.1 Tape Recording Heads

Inductive heads have been traditionally employed for writing and/or reading magnetic information. They consist of an electric circuit wound around a soft magnetic yoke, which is opened by a short gap exposed toward the media (Fig. 2.1). There are typically two categories of inductive heads: ring heads and thin-film heads. Ring heads such as MIG devices are usually fabricated by micro-mechanical machining and are not well suited for miniaturization. The

thin-film technology allows to produce heads with small and precise dimensions, achieving better frequency response. Also, multiple heads can be fabricated on the same chip at close spacing which is particularly interesting for tape recording applications.

The requirements for magnetic heads to optimally perform the writing and the reading operations are distinct, many of them being deduced in Chapter 2. Writing is always performed using inductive heads. Their coil is energized with a write current to spread intense magnetic flux out of the gap forming the so-called *write bubble*. The fringing field must be strong enough to efficiently magnetize media with high coercivity. Moreover, its gradient at the trailing pole of the head needs to be sharp in order to write narrow transitions and consequently short bits. The strength of the field is usually limited by the saturation magnetic flux density ($B_s$) of the head poles' material, which is preferably to be as high as possible. Soft magnetic materials commonly employed in the construction of thin-film tape heads feature the $B_s$ in a range from 1 T to 1.6 T (e.g. $Ni_{80}Fe_{20}$ and $Ni_{45}Fe_{55}$), while the maximum achievable limit should be around 2.4 T (e.g. FeCo alloys). Similar values apply for the metal-in-gap (MIG) films of ferrite ring heads. The length of the write gap has to be chosen as a trade-off between media writability and spatial resolution. It is around 0.2 $\mu$m in high track density helical scan systems and often above 0.5 $\mu$m in linear scan drives.
Read heads should offer high sensitivity, efficiency, linearity, and good resolution. Inductive replay heads feature fairly linear response with the sensed flux, but are susceptible to be affected by losses at high frequency. Their permeability has to be very large for good efficiency and laminations are often used to prevent Eddy currents. The signal amplitude is proportional to the head-to-medium relative velocity, which has to be elevated for achieving good signal-to-noise ratio (SNR). Magnetoresistive (MR) read heads feature much higher sensitivity and their output is roughly independent on the relative velocity, allowing for variable speed operation. Their resolution and frequency response are also better than for inductive heads. However, their output is linear for a restricted flux range and media with low $M_r\delta$ is suitable to avoid head saturation at long wavelengths. Reduced $M_r\delta$ is also required to write sharper transitions through lower demagnetizing fields, making MR heads particularly attractive for high density recording. The system noise is dominated by medium noise when sensitive MR heads are used.

In linear scan tape systems, the inductive ring heads have been widely replaced by thin film, MR heads. Anisotropic magnetoresistive (AMR) elements are currently employed and the application of giant magnetoresistive (GMR) devices has been investigated [40, 41]. The sustained contact between head and media cause a harsh environment for MR heads in magnetic tape recording. Mechanical wear, electrostatic discharge, corrosion, and thermal asperity noise are likely to affect the performance and the lifetime of MR elements. This is

still an issue in helical scan systems, however, significant progresses have been reported recently [18, 20, 42, 47].

### 3.1.1 Helical Scan Silicon Heads

*Helical Scan Silicon* (HSS) heads were developed by CEA-LETI and Alditech using advanced thin-film technology [125]. They feature unique construction with technological breakthroughs such as integrated solenoid coil and azimuth angle. A schematic drawing of the head structure is shown in Fig. 3.1. The azimuth angle of the gap is obtained in the batch process using anisotropic chemical etching, being determined by the (111) plane orientation of the silicon substrate [126]. The gap length is defined by thermal oxidation of silicon before the deposition of the magnetic poles (e.g. $Ni_{82}Fe_{18}$). A planarization process ensures very good alignment of the magnetic poles. The fabrication method is suitable for producing narrow poles, and widths down to 1 $\mu$m were already demonstrated. Short gap lengths of 0.1 $\mu$m and 0.2 $\mu$m were typically produced.
The solenoid copper coil is closely wound around the magnetic core to achieve low static resistance below 8 $\Omega$ for 40 turns, and good efficiency. The magnetic circuit is build in permalloy ($Ni_{82}Fe_{18}$) and it is multilayered for reducing Eddy currents. Recently, the laminations were also optimized to suppress permeability losses due to the formation of closure domains at the boundary of the magnetic core [42]. The recording poles also contain laminations, which are interrupted near the recording gap.
First generations of HSS heads were designed for performing both write and read operations. Specific devices were also developed recently, such as HSS read heads with a GMR element placed on a flux guide optimized for high efficiency [42]. A hard bearing structure was employed to reduce the head wear caused by tape friction, resulting in improved head life above 5000 hours. Write optimized HSS heads were also fabricated using materials with high saturation flux density for the recording poles (e.g. $Co_{88}Fe_{10}Cr_2$). The HSS heads treated in this work are inductive and have permalloy magnetic poles.

Scanning electron microscope (SEM) images of three HSS heads, corresponding to different prototyping series, are shown in Fig. 3.2. The orientation of the images corresponds to the position of the heads on our recording tester, and is reversed with respect to the structure in Fig. 3.1. That is, the silicon substrate of the heads in Fig. 3.2 is at the top of the images. It is observed that very good alignment of the magnetic poles is achieved for the HSS2 and HSS3 head types. In early stage prototypes like HSS1, accurate alignment is achieved at one side of the poles while it is not optimized at the other side. A misalignment around 0.25 $\mu$m was typically observed. However, in helical scan tape systems, the tracks are recorded with partial overlap always at the same side of the head, the erase bands being defined by one single edge. Good align-

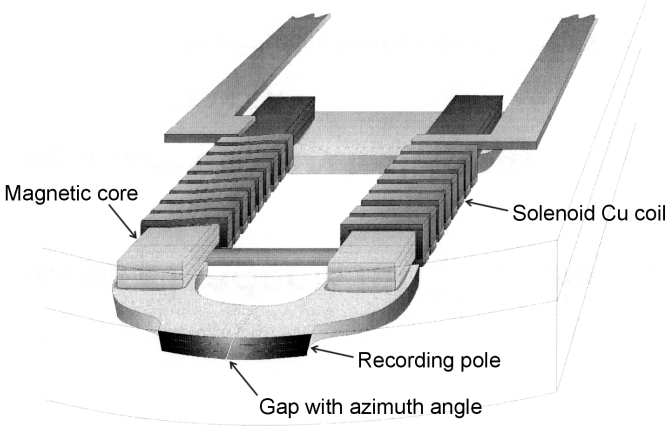


**Figure 3.1:** *Schematic structure of inductive HSS heads.*

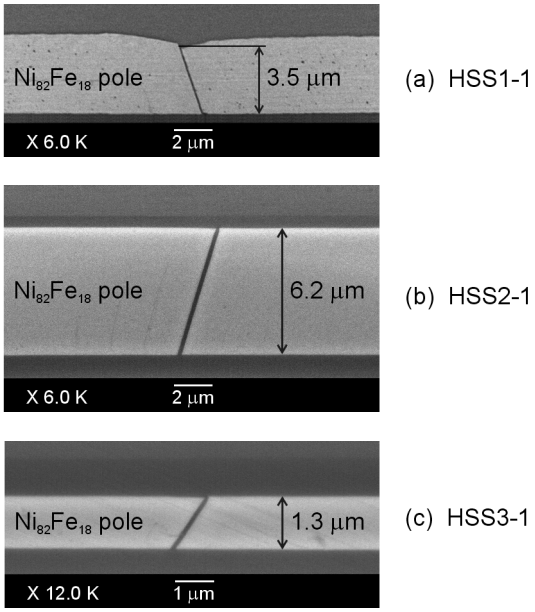


**Figure 3.2:** *View of the tape bearing surface of three types of HSS heads, with pole widths from 1.3 μm to 6.2 μm (see also Table 3.1).*

**Table 3.1:** *Recording poles' dimensions of selected HSS heads.*

| Head sample | Pole width ($\mu$m) | Gap length ($\mu$m) | Azimuth angle (deg) |
|---|---|---|---|
| HSS1-1 | 3.5 | 0.11 | $-20$ |
| HSS2-1 | 6.2 | 0.20 | $+15$ |
| HSS3-1 | 1.3 | 0.10 | $+35$ |

ment of the poles only at that specific edge is therefore sufficient to minimize the erase bands of the system.
The three HSS head types in Fig. 3.2 share most technological bases, however, a number of details are distinct. They feature different pole width, gap length, and azimuth angle. The HSS3 heads have very low pole width around 1.3 $\mu$m and large azimuth angle of 35°. Large azimuth angles are believed to enable very high track densities in future tape recording systems [60]. The accurate pole alignment of the HSS3 prototypes should moreover ensure good control of the side writing and erase bands. Their interest for studying the recording process at very narrow track width and large azimuth angle is evident. However, these prototypes suffered from some fabrication problems and their performances were below expectations. A rigorous study of diverse recording issues and edge effects was therefore not possible. More efforts were concentrated in this thesis on the HSS1 and HSS2 head types. They were intensively used for studying narrow track recording phenomena and the influence of pole alignment and gap length on edge effects.

The dimensions of the magnetic poles of the HSS heads from Fig. 3.2 are given in Table 3.1. The pole width of the HSS1-1 head was measured from the well aligned edge to the middle of the misalignment at the other edge. The gap length was measured perpendicular to the gap lines. The heads feature solenoid coils with 40 turns, dc resistance around 6 $\Omega$, and inductance of approximately 0.5 $\mu H$ (at 20 MHz). Their optimum recording current was found at 10 mA (zero-to-peak), being negligibly influenced by the magnetic tapes employed. However, the optimum recording current may be different for other HSS heads. The procedure to determine the optimum write current was based on maximizing the output signal at short recording wavelength ($\lambda = 0.35$ $\mu$m). The overwrite performance was also checked; increasing the current by 1.5 times should result in marginal improvement of the overwrite ratio by less than 4 dB (at a frequency ratio of 6). For more details about overwrite measurements one can refer to [127, pages 273-286].

**Table 3.2:** *Poles' dimensions of the MIG-1 and MIG-2T samples.*

| Head sample | Pole width ($\mu$m) | Gap length ($\mu$m) | Azimuth angle (deg) |
|---|---|---|---|
| MIG-1 | 5.5 | 0.20 | $-10$ |
| MIG-2T | 3.6 | 0.22 | $+10$ |

### 3.1.2 MIG Ferrite Heads

The recording performances of narrow track MIG ferrite heads were also investigated in this thesis, with special emphasis on their edge effects. Two samples, MIG-1 and MIG-2T, were employed featuring similar construction. Their coils have 15 turns and an inductance around 0.6 $\mu H$ (at 5 MHz). The optimum write current was 20 mA for both heads. The edges of the MIG-2T head were trimmed by Focused Ion Beam (FIB) milling to achieve very good alignment of the recording poles. This was performed in order to evidence the effect of the pole edges on the side write characteristics of MIG heads. The pole width of the MIG-2T head is therefore narrower, equal to 3.6 $\mu$m, while that of the MIG-1 head is around 5.5 $\mu$m. Evaluating the physical pole width of the MIG-1 sample is somewhat arbitrary because the edges are poorly defined, as visible in Fig. 3.3. The pole edges were estimated for this head at the points where the gap length becomes double. The pole width, gap length, and azimuth angle of the MIG-1 and MIG-2T samples are given in Table 3.2. They have opposite azimuth angles, however, their influence on the results was controlled by performing the recording measurements in both tape moving directions. Also, the MIG-1 head features a gap length slightly smaller than MIG-2T, being probably related to the limited reproducibility of the manufacturing process.

The edges of the MIG-2T sample were etched to a depth around 1.5 $\mu$m and over a longitudinal distance of 21 $\mu$m, which is much longer than the gap length. The trimmed poles can therefore be assumed as being infinite. Etching was performed in a FEI 200 FIB workstation with 30 kV $Ga^+$ ions. Using FIB milling for sensitive applications requires judicious selection of the ion beam current $I_b$ or mean diameter $\phi_b$ (we note that they are interconnected). Large beam diameter is suitable for etching a high volume of material in a reasonable short time. However, it would cause damage to the surrounding area and high local energy dissipation by heating. Milling with a narrow ion beam is necessary in order to obtain abrupt, well defined flanks. The MIG-2T head was etched in three steps, starting with large beam diameter of $\phi_b = 120$ nm ($I_b = 2700$ pA) and reducing it successively close to the recording poles, up to $\phi_b = 25$ nm ($I_b = 70$ pA). Sharp edges were therefore obtained near the head gap as

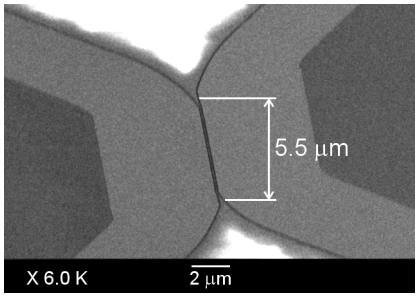


**Figure 3.3:** *SEM image of the recording gap and magnetic poles of the MIG-1 head.*

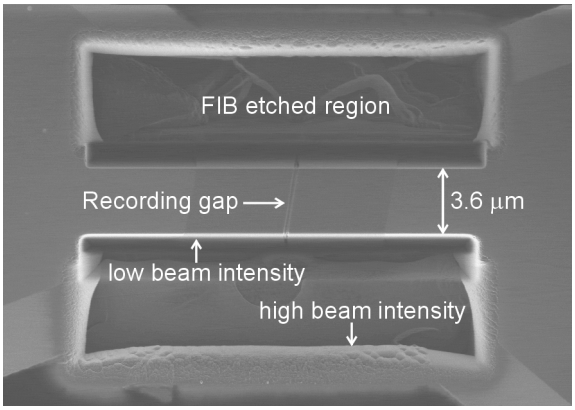


**Figure 3.4:** *The magnetic poles of the MIG-2T head were trimmed by FIB in order to achieve very good alignment.*

shown in Fig. 3.4, which is a second electron image acquired just after FIB milling. The outer flanks of the trimmed trenches are considerable affected by the high beam intensity and damage to the surface material occurred over a large area. Such effects would not be tolerable at the recording poles. After FIB trimming, the head was slightly polished by operating it with abrasive tape in order to ensure a clean contact surface. The magnetic properties and the efficiency of the resulting head structure were not altered, as deduced from recording measurements.

**Table 3.3:** *Parameters of tape samples representative of three different technologies: MP, ME, and MS.*

| Tape Sample | Magnetic Technology | $\delta$ (nm) | $H_c$ (kA/m) | $M_r\delta$ (mA) | $S$ | $S^*$ | $OR$ |
|---|---|---|---|---|---|---|---|
| MP-1 | Fe-Co particles | 300 | 145 | 72 | 0.79 | 0.68 | 1.9 |
| MP-2 | Fe-Co particles | 200 | 195 | 60 | 0.85 | 0.75 | 2.5 |
| MP-3 | Fe-Co particles | 70 | 200 | 20 | 0.84 | 0.72 | 2.6 |
| MP-4 | Fe-Co particles | 150 | 203 | 33 | 0.85 | 0.76 | 2.4 |
| MP-5 | Fe-Co particles | 150 | 209 | 29 | 0.86 | 0.69 | 2.7 |
| ME-1 | Co-CoO | 200 | 124 | 80 | 0.77 | 0.35 | 3.8 |
| ME-2 | Co-CoO | 50 | 164 | 15 | 0.67 | 0.52 | 4.1 |
| MS-1 | Co / Cr | 20 | 208 | 4.3 | 0.77 | 0.67 | 4.0 |
| MS-2 | CoCrPt / CoCrMn | 30 | 287 | 8.7 | 0.67 | 0.76 | 2.3 |

## 3.2 Magnetic Tapes for High Density Recording

The analyzes of the write and read processes in Chapter 2 suggested that the recording layer should feature high coercivity, low thickness, and high squareness. Well isolated magnetic entities and low noise are also required. It is moreover necessary to achieve smooth surface of the tapes with low roughness and abrasivity. High density tape recording systems are currently based on metal particulate (MP) and metal evaporated (ME) tapes. Metal sputtered (MS) tapes are receiving increased interest for future applications due to very thin magnetic layer ($\delta < 50$ nm) and high coercivity ($H_c > 200$ kA/m).
Several significant magnetic and physical parameters of the recording tapes of interest for this thesis are resumed in Table 3.3. Two MS samples recently developed in a concurrent work [128] are also included. The magnetic measurements were performed in the longitudinal direction using a vibrating sample magnetometer (VSM), applying a maximum field equal to 1000 kA/m. The thickness of the samples is approximate and the orientation ratio ($OR$) is calculated as the ratio between the remanent magnetizations in longitudinal and transverse directions.

### 3.2.1 Particulate Tapes

MP tapes are made of acicular magnetic particles dispersed in an organic binder, which is coated on a polymer base substrate. The particles used in current data storage tapes have a composition of Fe with some amount of Co,

and are covered by a thin oxide shell around 2-3 nm for passivation. They feature an aspect ratio typically between 4:1 and 6:1 (length over diameter), their magnetic properties being dominated by shape anisotropy. For high density recording, the size of the particles needs to be small and uniform. They are nowadays produced with lengths down to 60 nm for commercial applications, and around 40 nm in the laboratory. The trend in modern MP tapes is to further decrease the particles' size, improve their anisotropy, and reduce the thickness of the recording layer. It is moreover necessary to minimize non-uniformities such as particle size distribution, concentration fluctuations, medium thickness variations, and surface roughness. These factors are considered to represent significant sources of medium noise [129, 130, 131, 132]. Double coating techniques are typically used in order to apply thin magnetic layers with good uniformity and low roughness [133, 134]. The underlayer contains non-magnetic particles. MP tapes with the thickness of the recording layer around 150 nm are currently commercial, and magnetic coatings down to 50 nm were achieved in the laboratory [21]. Achieving uniform layers with such low thickness is one of the major challenges to be faced. The average surface roughness $R_a$ of current MP tapes is around 4-5 nm, and it was reduced below 2 nm in development samples [12].

A transmission electron microscope (TEM) image of a cross-section in the longitudinal direction of the MP-5 tape sample (Table 3.3) is shown in Fig. 3.6. The thickness of the magnetic layer is around 150 nm, however, the interface formed with the underlayer is hardly distinguishable in the figure. The hysteresis curves of the same sample measured in longitudinal and transverse direction are given in Fig. 3.5. In longitudinal direction, the squareness is reasonable high and the remanent magnetization is slightly lower than the coercivity, resulting in reduced demagnetization effects. In fact, most of the modern MP tapes have low remanent magnetization close to the coercivity, around 200 kA/m. Their orientation ratio is usually comprised between 2 and 3.5. The metal particles in the sample MP-5 have a mean length around 60 nm, corresponding to an approximate volume of $7 \cdot 10^{-15}$ mm$^3$. Smaller Fe-Co particles with adequate magnetic properties are difficult to produce and may present poor thermal stability at volumes below $3 \cdot 10^{-15}$ mm$^3$ [24, 25]. The corresponding particle length is around 40 nm.

Barium ferrite particles are potential candidates to develop particulate tapes for very high density recording [26, 27, 28]. The Ba ferrite particles have platelet shape and can be obtained with diameters as low as 20 nm and coercivity well in excess of 200 kA/m [135]. However, the thermal stability of such media is also a matter of concern as well as the inter-particle interaction [27, 28, 135]. Ba ferrite tapes feature weak remanent magnetization around 100 kA/m resulting in very low demagnetization and reduced read flux, suitable to avoid saturation of sensitive MR heads. The requirement for very thin magnetic layer to achieve high density is therefore less critical.

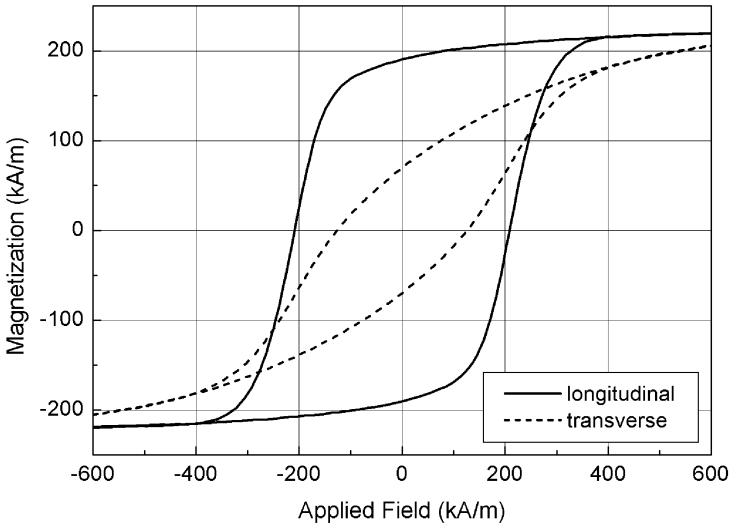


**Figure 3.5:** *Hysteresis curves of the MP-5 tape sample measured in longitudinal and transverse directions.*

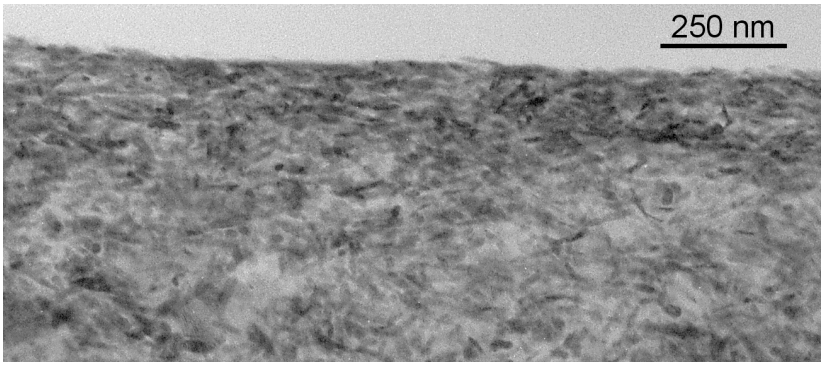


**Figure 3.6:** *Cross-sectional TEM image of the MP-5 tape sample. The magnetic layer of thickness $\delta \approx 150$ nm is coated on top of a much thicker non-magnetic underlayer.*

### 3.2.2 Thin-Film Tapes

Thin-film technology allows to grow uniform magnetic layers with very low thickness, which is hard to achieve in particulate tapes. The magnetic properties and microstructure can be controlled through the choice of magnetic alloys, underlayers, and deposition conditions. Oblique deposition is an efficient technique to achieve decoupling between magnetic entities [136] and is applied in ME tapes to produce a columnar structure with high shape anisotropy. Oblique evaporation of Co or Co-Ni has been successfully employed to fabricate ME tapes, however, the use of more complex alloys is restricted. A wide range of magnetic materials and alloys can be deposited on hard disk substrates by sputtering to achieve very high quality recording media. Similar processes are hardly applicable to magnetic tapes due to strict temperature limitations of the polymer substrates. Nevertheless, significant progress has been achieved recently and MS tapes with thin magnetic layers and high coercivity were produced [34, 35, 36].

#### ME Tapes

Modern ME tapes are produced by oblique evaporation of Co on a polymer substrate under a varying incidence angle, in presence of an oxygen atmosphere. The magnetic film is protected by a thin hard coating layer of diamond-like carbon (DLC), on top of which an organic lubricant is further applied. The recording layer presents a tilted columnar structure with rich content of Co, decoupled by CoO crystallites [137]. The surface roughness $R_a$ of modern ME tapes is around 3 nm. The magnetic interaction is therefore low between the Co columns and high within the columns. Narrow, well decoupled columns are suitable for good magnetic segregation and high shape anisotropy. The shape anisotropy of a single column may be supplemented by a certain amount of crystalline anisotropy, depending on the content and orientation of Co crystalized in hexagonal closed pack (hcp) phase. The easy axis of ME tapes is oriented out of the film plane at a lower angle than that formed by the columns, due to demagnetization effects. Typical Co-CoO tapes have the in-plane coercivity comprised between 100 and 160 kA/m. They can be produced with very low thickness down to 30 nm, and have been demonstrated to achieve very high recording densities up to 18 Mb/mm$^2$ (11.5 Gb/in$^2$) in combination with GMR read heads [13, 14].

The recording properties of ME tapes are asymmetric with respect to the relative moving direction of the write head due to the oblique columns and easy axis. That is, they present a good and a bad recording direction as described in Section 2.3.2. This limits their interest for linear scan recording systems which employ bidirectional recording. It was recently shown from SNR measurements that the linear density loss caused by recording in the bad direction is around 14%, despite a $PW_{50}$ degradation of 28% [138].

The two ME samples included in Table 3.3 feature different magnetic properties and thickness of the recording layer. The ME-2 sample has a thin magnetic layer of 50 nm and higher coercivity of 164 kA/m, which could be due to improved columnar structure. Its hysteresis curves measured in the film plane along longitudinal and transverse directions are given in Fig. 3.7. The sample has a high degree of orientation in longitudinal direction, which is typical for ME tapes. The shape of the loop is influenced by the out of plane orientation of the easy axis. Therefore, $S$ and $S^*$ are not directly comparable between ME and MP tapes. The columnar structure of the ME-2 sample is clearly visible in the TEM cross-section from Fig. 3.8. The columns make an angle of approximately 50° with the film plane, and their diameter is close to 15 nm. Their tilt angle is slightly higher at the top of the medium than at the base, this feature being more pronounced in thicker tapes like the ME-1 [30, 137]. In such cases, the diameter of the columns is also increasing toward the surface, being usually comprised between 20 and 40 nm.
It has been reported that the magnetic properties of thin ME tapes can be improved by introducing a non-magnetic underlayer. A $SiO_2$ underlayer of 6 nm was shown to improve the coercivity of a Co-CoO thin magnetic film ($\delta = 33$ nm), by reducing the initial growth layer [31]. Superior results were obtained using a 50 nm CoO underlayer to deposit a Co-CoO magnetic layer ($\delta = 50$ nm), leading to high coercivity up to 240 kA/m [32]. The CoO underlayer is believed to improve the columnar structure of the Co-CoO film and therefore the shape anisotropy. It may also help to promote uniaxial orientation of hcp-Co grains along the columns direction [29, 139, 140].

### MS Tapes

Application of sputtering methods to the fabrication of magnetic tapes has been receiving an increasing interest during recent years. Such deposition techniques allow the use of complex magnetic alloys and underlayers, and have been already proven in magnetic hard disks. Longitudinal recording hard disks usually employ Co alloys for the recording layer. They are sputtered at high temperature close to 300 °C in order to achieve hcp structured Co alloys with in-plane orientation of the c-axis, as well as segregation of the magnetic grains. In recording tapes, magnetic films have to be deposited at room temperature without causing degradation by heating of the polymer substrates. Convenient hcp texture $(10\bar{1}0)$ with in-plane orientation was recently obtained by sputtering of a CoCrPt magnetic alloy and a stack of underlayers on a polymer substrate [33, 141]. High coercivities up to 300 kA/m were reached, however, large intergranular coupling was present in the films due to the low temperature deposition. Voltage biasing of the underlayers was then introduced during sputtering of the magnetic film in order to achieve better grain segregation [142]. Such media with a thin $Co_{62}Cr_{15}Pt_{23}$ recording layer of 25 nm and coercivity

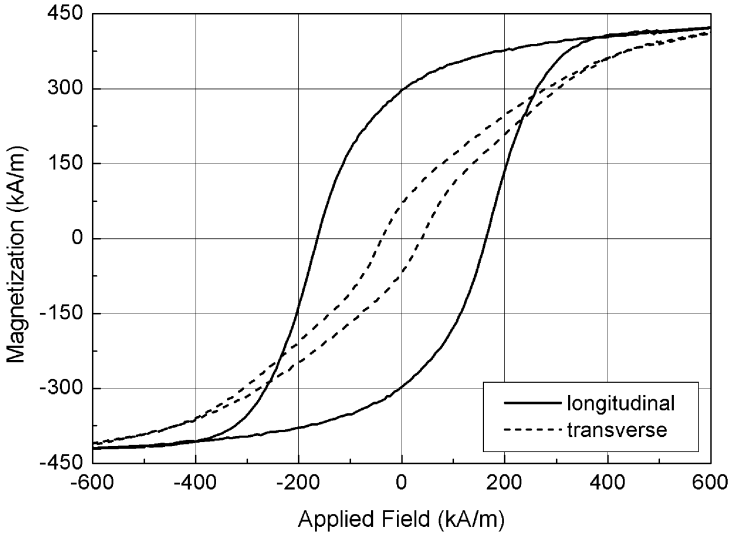


**Figure 3.7:** *Hysteresis curves of the ME-2 tape sample measured in the film plane, in longitudinal and transverse directions.*

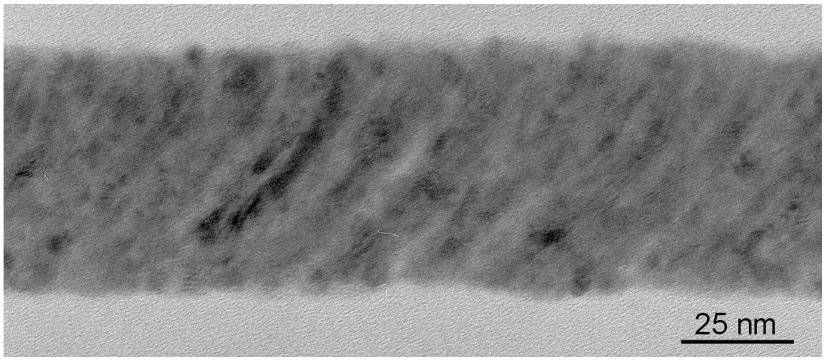


**Figure 3.8:** *Cross-sectional TEM image of the ME-2 tape sample, having a thin magnetic layer of* 50 *nm. The Co columns have a diameter around* 15 *nm and are tilted out of the film plane by approximately* $50^{\circ}$.

around 200 kA/m was shown in [34] to possess promising recording properties. A seed layer of NiAl and two underlayers of $Cr_{92}Mn_8$ and $Co_{69}Cr_{29}Ta_2$ were employed.

A different approach to achieve decoupling between magnetic grains in thin films sputtered on polymer substrates is by using oblique deposition [136]. MS tapes with high crystalline anisotropy were recently produced by oblique sputtering of Co on Cr underlayer [89]. The Cr underlayer promotes the growth of Co with dominant hcp texture $(10\bar{1}1)$, having the c-axis oriented out of the film plane at an angle about 28°. Also, the tilt plane of the c-axis is orthogonal to the tilt plane of the columns. The crystalline anisotropy is dominant in the Co films thinner than 50 nm and the orientation of the easy axis follows the c-axis, but with less deviation from the film plane [128, pages 69-78]. The longitudinal direction for recording is therefore perpendicular to the tilt plane of the columns. High coercivities around 200 kA/m were obtained for thin Co layers of 20 nm, using Cr underlayers between 120 nm and 180 nm. In such tapes, the easy axis was found to be slanted from the film plane by an angle close to 20°. The MS-1 tape sample from Table 3.3 feature high orientation ratio of 4 and very low $M_r\delta$, suitable for high density recording. Decoupling between magnetic grains is achieved due to the oblique deposition process, and they seem to switch by incoherent rotation [89]. The size of the grains can be reduced by using a NiAl seedlayer. Experimental MS tapes of Co/Cr and Co/Cr/NiAl that were deposited at continuous movement of the polymer substrate gave promising recording results [35].

Using appropriate magnetic alloys may help to improve the properties of recording thin films, such as granular structure and anisotropy. Impressive results were obtained by oblique sputtering of $Co_{68}Cr_{13}Pt_{19}$ with an underlayer of $Co_{67}Cr_{30}Mn_3$ on polymer substrate [36], [128, pages 93-98]. The CoCrPt film was found to present two hcp textures, $(10\bar{1}1)$ and (0002). Very fine columnar structure of the layers was obtained, as shown by the TEM image of the MS-2 sample in Fig. 3.10. The thickness of the CoCrMn underlayer is 50 nm and the CoCrPt magnetic layer is 30 nm. The columns are uniform and well separated, with a low diameter close to 6 nm. The contribution of both crystalline anisotropy and shape anisotropy of the columns enhance the hard magnetic properties of the recording layer. The easy axis was found to be slanted out of plane by an angle close to 32°. The in-plane hysteresis curves show a double switching behavior, as seen in Fig. 3.9. The bimodal switching field distribution is probably related to the presence of the two hcp textures, or the growth of CoCrPt in the pores of the CoCrMn underlayer [36]. Strong coercivity of 287 kA/m is observed in longitudinal direction, as well as high coercive squareness $S^* = 0.76$. The low $M_r\delta$ of 8.7 mA is suitable for low demagnetizing effects and operation with GMR heads without causing saturation. It is believed that this type of MS tapes could support very high recording densities due to enhanced magnetic properties and fine microstructure. Oblique sputtering allows growth

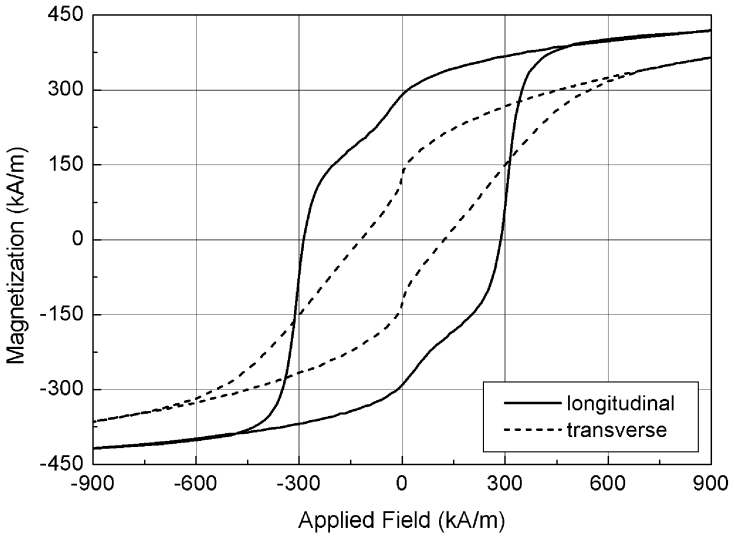


**Figure 3.9:** *Hysteresis curves of the MS-2 tape sample measured in the film plane, in longitudinal and transverse directions.*

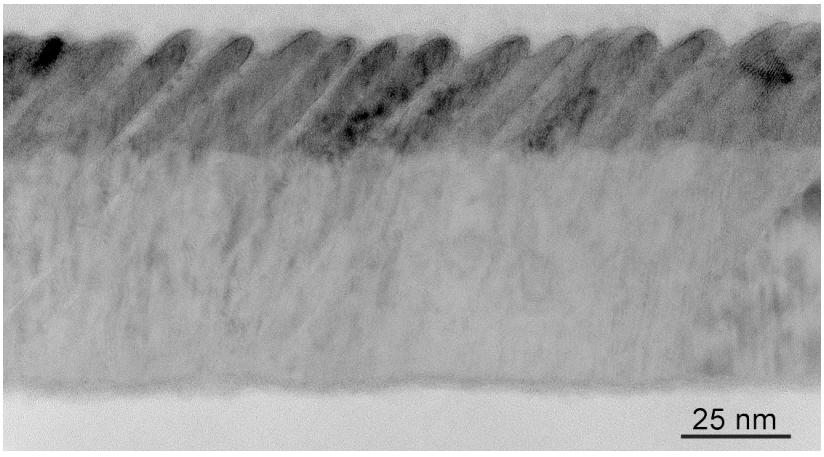


**Figure 3.10:** *Cross-sectional TEM image of the MS-2 tape sample produced by oblique sputtering of* $Co_{68}Cr_{13}Pt_{19}$ *on a non-magnetic underlayer of* $Co_{67}Cr_{30}Mn_3$*. The magnetic layer is as thin as 30 nm and exhibits very narrow, well separated columns.*

of recording thin films on polymer substrates with good magnetic anisotropy and decoupling, while keeping the deposition process relatively simple. Moreover, orientation of the medium is achieved.

## 3.3 Conclusion

Recording tapes and heads have been achieving steady progress during recent years and still present significant growth potential. Thin film write heads and AMR read elements have been widely adopted, while GMR devices with enhanced wear and corrosion properties are being developed. Write heads with smaller, better controlled dimensions and higher $B_s$ are expected. MP and ME magnetic tapes evolve toward thinner magnetic layers with $\delta < 100$ nm, fine morphology, and coercivity $H_c$ around 200 kA/m and above. The control of the tapes' tribological properties is also improved. MS tapes, with $\delta \approx 30$ nm and $H_c > 250$ kA/m, are believed to be promising candidates for achieving very high recording density in future systems.

The recording heads and tapes employed in this thesis for the study of edge effects were also introduced. The HSS heads present many interesting features such as solenoid coil, integrated azimuth angle, short gap length, and well aligned, narrow poles. They are suitable for narrow track recording, and heads with pole widths comprised between 1.3 $\mu$m and 6.2 $\mu$m were employed here. MIG ferrite heads with narrow pole widths were also included, one having the gap corners aligned by FIB trimming. MP and ME tapes were used featuring various thickness of the recording layer from 50 nm to 300 nm, and coercivity between 120 kA/m and 200 kA/m.

Chapter 4

# Test Equipment for Tape Recording Experiments

The common approach to improve the performances of magnetic recording systems is based on a *scaling principle*. That is, the increase of the areal density is supported by the reduction of relevant dimensions such as medium thickness, grain size, head gap, track width, and magnetic spacing. A subsequent improvement of the medium's magnetic properties and of the read head's sensitivity is usually implied. The data rate per recording channel scales with the linear density and the relative velocity between head and medium. Advanced channels need therefore to deal with lower signals and higher frequencies. In magnetic tape recording it is typical to increase the recording capacity per volume by shrinking the thickness of the polymer base, which can be as low as 5 $\mu$m in some systems. Narrower tracks, thinner tapes, and higher relative velocities require enhanced mechanical accuracy and stability of tape storage drives. Detailed investigations of the recording process and characterization of development tapes and heads are usually performed on high-precision experimental setups. They feature superior mechanical and electronic performances, however, studying the recording process at submicron track width is hardly achievable.

Recording experiments with write heads having the track width down to the micrometer were performed in this thesis. The cross-track accuracy suited to investigate the edge effects of modern heads and media was estimated here to be around 50 nm. A very precise and stable tester was needed for that purpose. The technical issues to achieve an experimental setup with ultimate performances were studied, considering advanced capabilities to support current and future developments in very high density tape recording. The construction of

a tape-drum tester supporting track widths down to 200 nm was investigated leading to the design guidelines formulated in Section 4.2. Very stable head-to-tape contact and high relative velocity up to 30 m/s were aimed at. However, such tester could not be built mainly due to time constraints and subcontracting difficulties. Instead, an existing setup with moderate performances was redesigned focusing on cross-track stability and quality of the head-to-tape contact. The upgraded tester proved to adequately operate at narrow track widths down to 1 $\mu$m, and is described in Section 4.3.

## 4.1 Testers for Linear and Helical Scan Recording

Evaluating the recording properties of future generations magnetic tapes and heads becomes more and more challenging, especially at very narrow track widths. As submicron tracks are already envisaged, the cross-track resolution and stability of tape recording testers is increasingly important. Good contact between head and tape has to be ensured while the relative speed can be accurately varied within a relatively wide range. The instrumentation electronics should offer low noise and high bandwidth, allowing for various time domain and frequency domain measurements.

Recording testers for linear tape scan resemble the commercial drives to a certain extent. They may be constructed using open tape reels or a closed loop path. The tape transport path is improved using advanced roller guides [12] or porous ceramic air bearings for ultimate performance [143]. These bearings produce an uniform thin film of air underneath the tape to guide it smoothly and precisely, achieving a lateral tape motion (LTM) in the order of 1 $\mu$m. Cross-track accuracy may be further improved using closed loop tracking. However, servo tracking is limited by the mass of the relatively bulky heads and their friction with the tapes. That is, moving the head may engender fluctuations of the tape position, due to important contact surface and pressure. The relative velocity is typically comprised between 1 and 12 m/s. At higher velocities the tape is likely to get damaged and system stability may be affected.

In helical scan recording, rotating tape-drum testers are commonly employed for research and development of heads and media, as well as for mass production tests. In such systems the tape is wound around a drum which can rotate at very high speed. The diameter of the drum is usually around 10 cm, making the tester suitable for operation with short tapes down to almost 45 cm, such as experimental samples. The drum is machined with very high precision and presents a pattern of tiny holes to generate an air film underneath the tape. A very smooth surface of the tape is therefore achieved. While the drum turns at high speed, one or more heads can be brought in contact with the tape for accurate recording measurements. As the tape is stationary fixed to the rotating drum, the relative velocity and the LTM are not limited by

the tape transport mechanism, in contrast to linear scan testers. For a well designed drum, the LTM mainly depends on the spindle accuracy. Air bearing spindles offer very low run-outs, allowing to achieve LTM values in the order of 10 nm. Still, the cross-track accuracy of the tester is normally worst than the LTM as the contact between head and tape may cause local perturbations. This is most susceptible to happen when the head is moved in cross-track direction. Such instabilities are diminished if the contact pressure is low, which can be achieved on high quality drums.
The position of the head can be precisely tuned to optimize the spacing between the magnetic gap and the medium. Because the tape does not wrap around the head, contact is achieved over a limited surface. The use of such testers is therefore restricted to heads designed for very small contact area, like those used in helical scan recording. However, heads with very small mass and dimensions may appear in future linear recording systems to support a drastic increase of the track density. Using flying head technology inspired from hard disk drives was proposed in [59]. Low inertia heads and reduced contact pressure would enable fast and accurate track following. It is conceivable that the recording performances of such devices could be initially investigated using advanced tape-drum testers. This would allow to characterize diverse heads and media prior to the development of new, complex systems. We note that various head fixtures and actuators can generally be easily adapted on a tape-drum tester.

## 4.2 Considerations for High Precision Tape-Drum Testers

Rotating tape-drum testers are probably the only tape recording systems allowing nowadays accurate measurements at submicron track width. An example of such experimental setup is schematically drawn in Fig. 4.1. It mainly consists of a tape-drum, an air bearing spindle, two head positioning mechanisms, and the read/write (R/W) instrumentation. The tape is wound around the drum and its ends are attached at the interior of the cylinder. The drum is mounted on an air spindle with very stable operation, its air supply unit not being shown in the drawing. Low pressure air also has to be fed into the drum for achieving smooth head-to-tape contact. Modern testers can usually accommodate two heads of which one is optimized for writing and the other for reading. Magnetoresistive (MR) heads are becoming the standard read devices due to their good sensitivity and high intrinsic bandwidth. The heads are mounted on precise positioning mechanisms allowing optimum contact to be achieved with the tape, as well as accurate tracking. About five freedom degrees are usually supported, some of which are manually actuated and others are motorized. The positioning stages and the spindle must be mounted on a very stable support, such as a granite table. For maximum performance, the

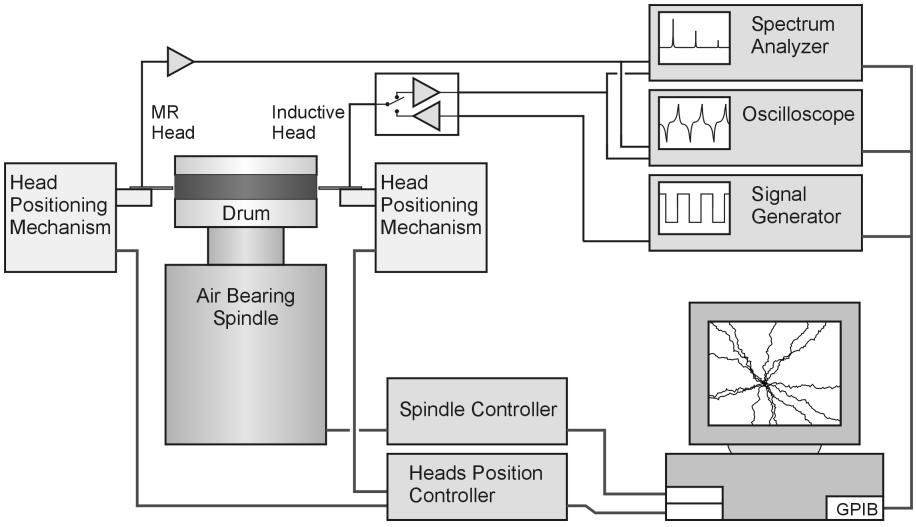


**Figure 4.1:** *Schematic representation of a tape-drum tester using an inductive write head and MR read head. The measurement apparatus may vary for different implementations.*

tester should be installed in a clean bench with air and temperature control. The external vibrations should also be limited.

The R/W instrumentation comprises signal generation and acquisition equipment connected to R/W modules. The R/W modules are mounted very close to the heads and can either drive a high current for writing magnetic data, or amplify the replay signal with very low noise level. In principle, inductive heads can perform both in write or read mode, even though they are generally optimized for one single task. The R/W module can switch between the two operation modes synchronized with the spindle rotation. For inductive heads aimed just at writing, the ability to read may help to optimize their contact with the tape. However, inductive read heads are becoming obsolete as MR devices offer largely superior performances. MR heads need dedicated preamplifiers with very low noise and biasing capabilities. The read preamplifiers are connected to measurement apparatus such as a digital oscilloscope and a spectrum analyzer. The oscilloscope or a fast digitizer are used for time domain measurements, while the spectrum analyzer offers excellent performance in the frequency domain. The write driver is coupled to a pattern generator. A hardware channel may be included with the instrumentation to allow for bit errors analysis. Some manufacturers of recording test equipment propose read/write analyzers specifically designed for digital magnetic recording. They comprise the pattern generator, the data acquisition and processing module, plus the

hardware channel. The measurement instruments plus the control units for the heads position and the spindle rotation are all connected to a computer managing the complete setup.

The requirements and design issues for constructing a tape-drum tester suited for read and write track widths below one micrometer were studied. It was aimed to reach head-to-tape positioning errors in the cross-track direction below 35 nm, without employing servo tracking and assuming that good temperature stability is ensured. The errors are mainly caused by instabilities of the tape path and of the air spindle, attempted here at less than 20 nm and 15 nm respectively. They are expressed as $3\sigma$ values. The non-repeatable tracking errors of the read head could probably be reduced under 20 nm using servo tracking. However, narrow track write heads would not be able to read the servo data. If separate read and write chips are used, servo tracking is then applicable just during reading. Generally, the tracking margin should account for both positioning errors of the read and write heads relative to the tape. Optimum results would be obtained with merged read/write heads, allowing servo tracking to be applied in both operating modes. It is believed that track widths close to 200 nm could then be achieved.

### 4.2.1 Tape-Drum Construction

The tape-drum is a critical component of the tester. The design and fabrication of the drum is crucial for achieving a very smooth surface of the tape and a highly concentric path. The radial deviations of the tape path should be as low as possible in order to ensure uniform head-to-tape contact. These properties are favorable to obtain fine recording contact under low pressure, resulting in increased stability of the system. The situation is particularly suitable for submicron track recording as well as for testing sensitive experimental media and heads. The common approach to finely control the tape tension and surface is by forming an uniform air film underneath it. This has been traditionally implemented by feeding low pressure air through a pattern of holes, as shown in Fig. 4.2 (a). The reference surface holding the tape contains a groove with holes for flowing the air. The concentricity of the reference surface and the uniformity of the air pressure along the groove determine the accuracy of the tape path. The tape forms a circular path with an interruption to guide its ends inside the drum where they are fixed. The opening into the drum walls create a discontinuity of the reference surface and of the groove. They have to be carefully shaped around this region to avoid inducing stress or deviations to the tape, but guide it gently toward the drum center. The air holes communicate with a supply channel where very uniform pressure must be ensured, further complicating the design of the drum. Even then, the discrete nature of the holes still may cause slight variations of the air pressure along the groove beneath the tape. Note that a small air volume continuously moves from the groove toward

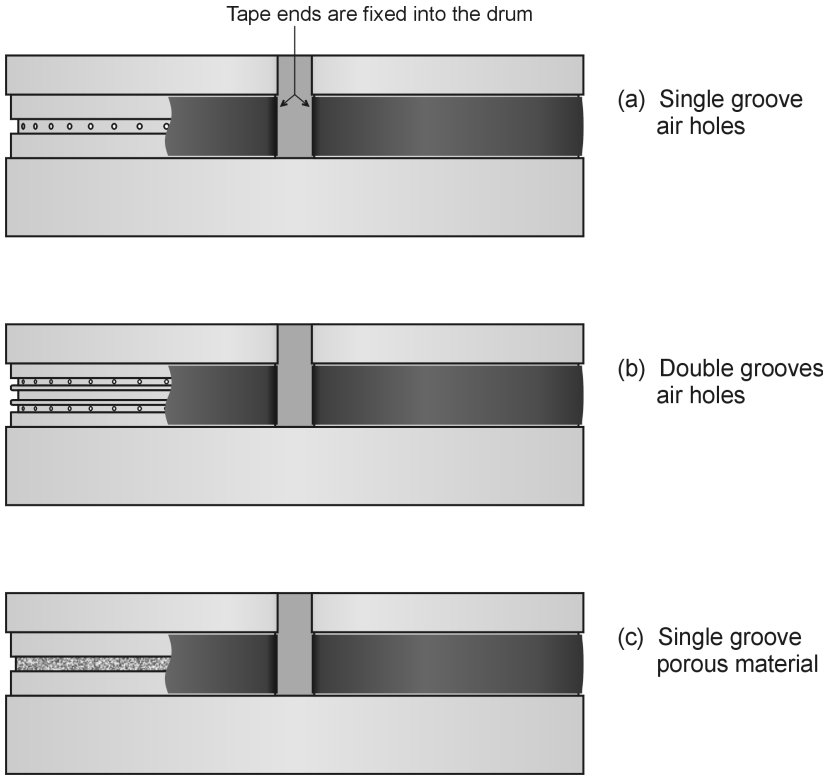


**Figure 4.2:** *Simplified drawing of three tape-drums with different approaches for air feeding. Single or double grooves with air holes are nowadays employed.*

the tape edges were it escapes. The usable recording range across the width of the tape is restricted to the region of the depression, where safe head-to-tape contact is realized. The width of the groove is typically comprised between 1.2 mm and 2.5 mm.

In some tape-drums with more advanced design, the depression intended for recording measurements is exempted of air holes. Instead, they are contained in two flanking grooves, as illustrated in Fig. 4.2 (b). The air pressure propagates from the lateral grooves to the central region with enhanced damping. Due to the symmetry of the configuration, the air volume moving to the central depression is minimum and good pressure uniformity is achieved. The virtual lack of air transfer through the measurement depression should improve the stability of the head-to-tape contact.

Tape drum designs using single or dual grooves with air holes were ana-

lyzed in this research for being employed on a stable and precise tester. During tracking motions a certain friction is performed between the head and the tape in transverse direction, still at very low contact pressure. Even slight frictions may induce minor displacements of the tape, which have to be minimized in an optimum tape-drum. In fact, modern tapes may have polymer bases as thin as 5 $\mu$m, while instabilities below 20 nm were aimed at. The transverse tape displacements are expected to be minimum if this has a flat profile, the contact with the head is gentle, and sufficient friction with the drum is achieved. Therefore, a smooth air film underneath the tape is suited near the head contact area but also some adhesion to the drum surface. Better adhesion is obtainable using a drum with a single air groove while dual grooves are favorable to smoother air film. A superior design based on a single groove and a porous material was analyzed for reaching the above targets. Porous materials are known to have very good properties for damping the pressure of fluids. They show thus great potential for use in tape-drum constructions to achieve homogenous air distribution underneath the tape. Actually, porous ceramics have been successfully employed in linear tape transport paths [143]. Nevertheless, the application of porous materials in tape drum designs has not been proposed before, at our knowledge. Preliminary studies were performed here, resulting in few design schemes employing either porous metal or plastic. They employ a single groove both for the air dispense and for the recording measurements, as suggested in Fig. 4.2 (c). A porous material component is embedded into the groove while leaving a buffer air channel at the back. Very uniform pressure should be attainable along the buffer channel even with a simple air supply configuration. This would result in smooth air flow through the porous material, achieving highly homogeneous pressure along the groove. The groove could therefore provide well suited stability for recording measurements. It is believed that using porous materials can increase the performances of the tape-drum while simplifying the manufacturing. However, such designs were not implemented or tested in this thesis, mainly due to lack of time and other priorities.

For optimum operation, tape-drums are usually designed specifically for each tape width. Most common widths used in recording systems are 12.7 mm (1/2 in), 6.35 mm (1/4 in), and 8 mm. The tape-drum is rigidly fixed on the shaft of a high precision spindle, as previously shown in Fig. 4.1. In modern testers, the drum is supplied with air directly via the shaft of the spindle. If the tester is intended for use with tapes of different widths, which is often the case, changing the drums should not affect its performance. That is, the concentricity and the balancing of the drums should not degrade after multiple replacements. The mass of the drum has to be precisely balanced with respect to the rotation axis in order to avoid a perturbing centrifugal force on the spindle shaft. Such unbalance force would engender radial and tilt error motions. The effect of tilt errors on the tracking accuracy is reduced at low drum diameter (see Section 4.2.2), still, this has to be large enough for convenient

construction and manipulation. A diameter around 80 mm was judged here as a good compromise. The drums are generally constructed of stainless steel for achieving high hardness and stability. According to the author's investigations, a state-of-the-art tape-drum should fulfill the following requirements:

- Radial deviation of the reference surface: $< 2.5$ $\mu$m
  (measured statically with the drum mounted on the spindle)
- Radial deviation of the tape path: $< 4$ $\mu$m
  (measured from dynamic recording experiments)
- Width of the measurement groove: $\approx 1.5$ mm
- Unbalance force (at 30 m/s): $< 1$ N
- Diameter of the drum: $\approx 80$ mm
- Mass of the drum: $< 0.8$ kg

### 4.2.2 Air Bearing Spindle

The drum needs to be accurately rotated at high tape velocities comprised between 1 m/s and 30 m/s, with extremely low vibration. Very good stability is typically offered by spindles with air bearings, which feature low error motions around ten(s) nanometers. The error motions are called synchronous when they occur in a repeatable manner at every rotation of the shaft. That is, they cause a deviation from the ideal movement, but do not introduce relative errors between revolutions. Asynchronous errors, or non-repeatable, appear randomly or at frequencies that are not multiples of the rotation frequency. They cause deviations from the ideal movement and also between different revolutions. It is therefore desirable to keep the asynchronous errors to a minimum, while synchronous errors can often be tolerated to a higher extent. For example, the asynchronous radial error (also known as non-repeatable runout or NRR) can considerably affect the tracking performances in hard disk testers, whereas the influence of the synchronous radial error is marginal. In tape-drum testers the cross-track stability is mainly affected by the axial and tilt errors, according to:

$$\varepsilon_{ct} = \varepsilon_{axial} + r \cdot \varepsilon_{tilt} \ , \tag{4.1}$$

where $r$ is the radius of the drum (here around 40 mm). The cross-track error $\varepsilon_{ct}$ may be synchronous or asynchronous. Synchronous errors are an issue if the phase difference between the write and read heads is not negligible compared to the time constants of the fluctuations. This is normally the case in tape-drum testers, where separate write and read chips are employed mounted at large phase difference, generally of 180 degrees. The positioning of the read head relative to the write track is then affected both by synchronous and asynchronous errors, causing a maximum deviation equal to $2\varepsilon_{ct}$ (plus those caused by tape instabilities). The tracking of a single head chip with respect to the tape is preponderantly affected just by the asynchronous error, $\varepsilon_{ct}^{A}$.

The velocity of the tape should be very stable in order to ensure good time and frequency resolution for the recording measurements. A feedback loop is used to control the rotation speed of the spindle. However, speed jitter occurs due to a number of factors including encoder errors, disturbance torques on the shaft, control loop efficiency, and inertia of the system. Most air bearing spindles comprise an incremental optical encoder with digital output to monitor the speed. They usually consist of a transparent disk with opaque fringes, placed between a light emitter and a detector as sketched in Fig. 4.3. The disk is mounted on the shaft of the spindle and voltage pulses are generated as the optical marks pass by the light stream. The frequency of the pulses is processed by the controller to calculate the rotation speed of the spindle. The optical pattern on the disk may suffer from inaccuracies, which can be reasonable counteracted by averaging the signal over few consecutive pulses. It is less trivial to deal with eccentricity errors caused by imperfect alignment of the grating pattern to the shaft. They cause modulation of the encoder output and introduce errors into the feedback signal. A tight control loop would follow closely the erroneous feedback signal, reverberating the encoder modulation on the rotation speed. A loose control loop may in fact result in better speed jitter. This was observed experimentally in this work, as the speed jitter of the available tape-drum tester was reduced by decreasing the proportional gain of the controller. Encoder modulation mainly affects the speed jitter within one revolution in a repeatable way, and could be seen as a synchronous speed jitter. An encoder with very low modulation is suitable for fine control of the velocity. The asynchronous speed jitter depends to a large extent on external disturbances and on the respective response of the control loop. It is normally easier to be tailored and very low values below 10 ppm can be achieved for unloaded spindles.

For optimum reliability, the speed error of an air spindle and corresponding controller should be checked by measurements with an external detector, featuring adequate accuracy (e.g. total error lower than 50 ppm). However, the speed jitter is most often specified based on readings from the encoder integrated to the spindle and do not account for sensor errors. The optimum choice of the spindle and of the control loop is therefore not straightforward and special attention should be paid to the encoder accuracy. The tape-drum user could evaluate the speed jitter also from recording measurements, usually known as Wow-Flutter. Therefore, the control loop may be further tuned for the specific load applied on the spindle by the user. The tape-drum and an eventual chuck would produce a load mass close to one kilogram. On the one hand, low inertia of the system makes the control loop more responsive and capable of correcting rapidly for the external disturbances. On the other hand, higher inertia results in less sensitivity of the velocity to small perturbations and encoder errors. Moreover, the error motions of the spindle (axial, radial, and tilt) may increase considerable in loaded conditions. It is therefore desirable that the air bearing

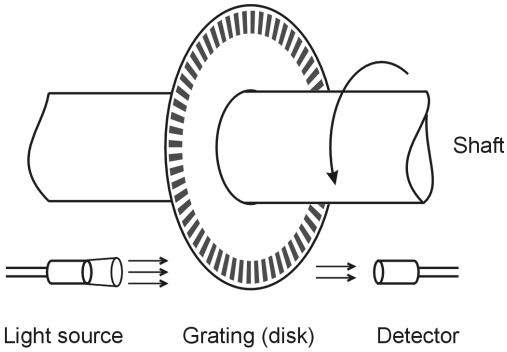


**Figure 4.3:** *Operation principle of an incremental optical encoder. In practice, a mask may be placed between the grating and the detector in order to increase the resolution.*

features great stiffness and a load capacity considerable higher than the weight of the tape-drum. The drum must be very well balanced and engender low air friction forces (a top lid is generally useful to reduce them).

According to the above discussions, the main requirements for a suitable air bearing spindle are expressed as:

- Rotation Speed Range: 150 to 10000 rpm
- Total Speed Jitter: $< 0.02\%$
  (measured externally, not from the feedback encoder)
- Axial Load Capacity: $> 250$ N
- Asynchronous Axial Error: $< 10$ nm
- Total Axial Error: $< 25$ nm
- Asynchronous Tilt Error: $< 0.1$ $\mu$rad
- Total Tilt Error: $< 0.2$ $\mu$rad
- Radial Stiffness: $> 50$ N/$\mu$m ($3 \cdot 10^5$ lb/in)
- Angular Stiffness: $> 0.25$ N·m/$\mu$rad ($2.2 \cdot 10^6$ lb·in/rad)

The axial and tilt errors given here would produce a total cross-track error $\varepsilon_{ct} < 33$ nm according to Eq. (4.1), and an asynchronous error $\varepsilon_{ct}^{A} < 14$ nm. This would result in non-repeatable tracking errors below 34 nm (at $3\sigma$), for tape instabilities lower than 20 nm. The track alignment errors for distantly separated write and read heads are estimated at less than 106 nm. Submicron track widths should therefore be attainable without servo tracking, but at very good temperature stability. Operation at widths approaching 200 nm is conceivable using servo tracking.

For proper operation, air bearings require clean and dry air at adequate pressure. Inadequate air supply may result in permanent damage of the bearing. The operating pressure for each specific spindle is quoted by the manufac-

turer and is usually comprised between 6 bar and 10 bar. The air supply unit usually comprises an oil-free compressor, a dryer, multiple filters (e.g. particulate, coalescing, and charcoal filters), plus a regulator. A buffer tank can be used as a precaution against fluctuations or loss of air pressure.

### 4.2.3 Head Positioning Mechanism

The recording heads have to be positioned accurately in contact with the tape to achieve low magnetic spacing and precise tracking. They are mounted on stable positioning mechanisms which support multiple translation and angular adjustments. The positioning mechanism described here is aimed for narrow track widths down to 100 nm. It comprises a number of motion stages as well as a head fixing jig. The jig should offer precise mounting of the head and easy replacement with high reproducibility. In a production test environment, easy and fast head interchange is usually favored and vacuum clamping devices may be used. For development or research applications, the precision of mounting is most important. The possibility to place the R/W module very close to the head is also of consideration. Moreover, the tester should be able to use heads of diverse formats, which have different base plates. Specific jigs are usually designed for each type of head plate in order to ensure accurate mounting. On a tester for recording experiments, it is often necessary to change between different format heads. An adequate restrain system must therefore allow to replace the head jig with simple manipulation and high precision. For top performance, the jig and the restraint must be conceived to ensure small mounting errors and low mass, as listed below:

- Head-to-Jig Mount Error: $< 20$ $\mu$m
- Jig-to-Restraint Mount Error: $< 20$ $\mu$m
- Jig + Restraint Mass: $< 50$ g

The errors apply to each orthogonal axis and can take either positive or negative values. They mainly account for the mechanical tolerances of the parts and the accuracy of the fastening system.

Most positioning mechanisms support five or six freedom degrees of the head. They are presented here with respect to the reference coordinate system drawn in Fig. 4.4. The *insertion* motion, along the $y$ axis, allows to fine tune the spacing between the head and the tape. A manual or a motorized stage could be used, with resolution around 1 $\mu$m or better. It is suitable that the insertion direction of the head gap intersects the rotation axis of the drum. This avoids the contact area to shift as the insertion is varied. A *balance* adjustment is therefore employed to translate the head along the $x$ axis. The *roll* rotation around the $x$ axis is necessary to accurately tune the perpendicularity between the head chip and the tape surface. Fine angular resolution is required in order to achieve small magnetic spacing and uniform contact at low pressure. The rotation should be performed precisely around

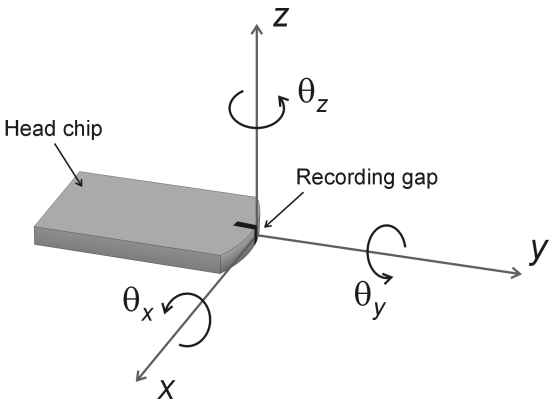


**Figure 4.4:** *Representation of the head's translation axes and rotation angles. The origin of the axes is in the gap center, which should be the rotation point for all angular movements.*

the head gap, such that its position does not move when adjusting the angle. It is therefore adequate to use a goniometer whose rotation axis passes through the gap of head. Goniometers allow to partially rotate an object about an axis located above the center of their top platform, at a fixed height. This height is known with a certain inaccuracy, which is called here the *goniometric error* (GE). Furthermore, assembling together the positioning stages and the head jig, as well as mounting the head, introduces additional deviations. The *total goniometric error* (TGE) accounts for all system and device imprecisions that contribute to shift the head gap from the rotation axis (in the height direction):

$$\mathrm{TGE} = \mathrm{GE} + \mathrm{SGE} \ , \tag{4.2}$$

where SGE is the system induced error. The TGE of the roll rotation mostly affects the cross-track accuracy, causing a displacement error $\varepsilon_{z,\mathrm{TGE}}$ depending on the adjustment angle, $\Delta\theta_x$:

$$\varepsilon_{z,\mathrm{TGE}} = \mathrm{TGE} \cdot \tan(\Delta\theta_x) \ . \tag{4.3}$$

For example, if the TGE is 150 $\mu$m, a roll angle modification of 0.1 degrees engenders a cross-track deviation $\varepsilon_{z,\mathrm{TGE}}$ equal to 0.26 $\mu$m. Such errors are particularly unsuitable at narrow track recording, when the contact positions of the read and write heads have to be adjusted while keeping good alignment. We note that the head-to-tape contact is usually fine tuned on a basis of optimizing the replay signal at short wavelengths. In order to minimize the SGE, the number of mechanical elements assembled between the goniometer and the head has to be reduced. An additional displacement error due to the *rotation center*

*runout* (RCR) is generated, relative to the adjustment angle. The RCR is the radial deviation of the rotation center from its mean position as the goniometer performs a full-range swivel. It is mainly caused by imperfect guiding and looseness of mechanical parts. The RCR component parallel to the platform of the goniometer is of main concern here as it affects the cross-track accuracy. The only mean of minimizing the RCR is by employing a goniometer featuring very high performance.

A second goniometer may be used to vary the *pitch* angle of the head, corresponding to a rotation around the $z$ axis. For typical helical scan heads' contours, such adjustments are not absolutely necessary. Small corrections could be performed using the balance motion, given the circular path of the tape. However, heads with different contours of the contact surface may require a consistent pitch angle adjustment. The TGE and RCR of the pitch rotation would have no effect on the cross-track accuracy of the head positioning mechanism. They mainly cause deviations of the head gap position along the $x$ any $y$ axis, being less critical for the recording measurements. They need, however, to be kept under control.
Tuning of the *azimuth* angle is supported as a rotation around the $y$ axis. It can serve to study azimuth losses or to match read and write heads with different azimuth angles. An azimuth misalignment of 500 $\mu$rad would cause a signal degradation around 0.1 dB for a bit aspect ratio (BAR) equal to 100. Narrow track recording implies smaller BAR and is less sensitive to azimuth misalignment. It is generally sufficient if just one of the two head positioning assemblies equipping the tester supports azimuth rotation. The eccentricity errors should be treated similarly to the goniometric errors of the roll rotation. The total eccentricity error also causes cross-tack displacements, however, azimuth adjustments are not performed frequently.

The *tracking* motion of the head is achieved by translating it along the $z$ axis. Motorized actuation is necessary in order to achieve fast and accurate travel. A precise linear or elevation stage driven electromagnetically (DC or pulse motor) could provide cross-track positioning with an accuracy down to 100 nm, or slightly better. However, for submicron track recording, better accuracy within few nanometers is needed. Such performances are typically achieved by piezoelectric positioning stages, known for great resolution down to the angstrom level. Moreover, they are not affected by backlash, stiction or friction like motor driven stages. Piezo stages have short travel range, usually comprised between 10 $\mu$m and 500 $\mu$m. Large travel range generally implies low resonant frequency and thus slow response time. Resonant frequencies vary from several kHz for piezo stages with total travel around 10 $\mu$m, to some hundreds Hz for travels of more than 100 $\mu$m. A piezo stage could reach its nominal displacement in about one third of the resonant period at best, but with strong overshoot and ringing. Leading motion controllers support advanced signal shaping techniques to considerable improve the positioning

stability and accuracy at high speed operation. Stable transient response with settling times (to 10%) close to the resonant period can therefore be achieved. A fast piezoelectric stage with the travel range around 25 $\mu$m may reach an unloaded resonant frequency up to 4 kHz. Loading it decreases the resonant frequency, which can be approximated by a function of the square root of the total mass (assuming an ideal spring-mass system):

$$f_r = \frac{1}{2\pi}\sqrt{\frac{k_T}{m_0 + m_{load}}}\ , \tag{4.4}$$

where $k_T$ is the actuator stiffness and $m_0$ is the effective moving mass of the stage. An indicative value for $m_0$ could be in the order of 50 g. The load mass should therefore be minimized in order to achieve fast and stable operation. The piezo stage must be placed as close as possible to the recording head in order to reduce the number of components that it has to carry. It can then achieve very accurate and fast cross-track positioning over short distances, from few nanometers to some tens of micrometers. Rapid response could serve to implement active track following, or to employ positioning strategies with superior stability. For example, the cross-track motion could be synchronized with the tape-drum rotation in order to move the head when this is not in contact with the tape (corresponding to the region where the tape is guided inside the drum). For course track positioning, the piezo has to be complemented by an electromagnetically driven stage. The latter would support long travels with lower resolution requirements while being less sensitive to load.

The motion capabilities of the head positioning mechanism that were discussed in this section are summarized in Table 4.1. A number of minimum requirements judged to be important for the good performance of the tester are also listed. They refer to each individual positioning stage independently of the other components, and should be met or surpassed by the manufacturer's specifications. The requirements were defined based on realistic calculations in order to guarantee precise and stable operation of the tester at submicron track width. The tilt error of linear stages refers to the angular deviation associated with an ideal straight line motion. It represents here the maximum of the three orthogonal components. The resolution represents the smallest increment that a motion system can be commanded to move and/or detect. In a motorized stage it normally corresponds to the resolution of the encoder. In order to reduce the amount of data, the minimum incremental motion of the devices is not specified here but should be taken very close to the resolution. However, in general, a system may or may not be able to consistently execute incremental moves equal to the resolution. The performances of the stages are susceptible to degrade as they are loaded and their load capacity should be considerably higher than the total charge intended to be carried. The effects of off-centered load and radial stiffens should also be considered. Stainless steel construction and guiding on crossed-roller bearings are usually preferred for very high pre-

**Table 4.1:** *Movements supported by an accurate head positioning mechanism, with descriptions and minimum requirements suggested for each specific stage.*

| Head Motion | Description | Actuator | Stage Main Requirements |
|---|---|---|---|
| Insertion | Translation $y$-axis | Manual or Motorized | Range: 5 mm<br>Resolution: 1 μm<br>Tilt Error: 150 μrad |
| Balance | Translation $x$-axis | Manual | Range: 5 mm<br>Resolution: 2 μm<br>Tilt Error: 150 μrad |
| Tracking | Coarse Translation $z$-axis | Electro-magnetic | Range: 5 mm<br>Resolution: 0.1 μm<br>Accuracy per 10 μm: 0.2 μm<br>Full-range Accuracy: 5 μm<br>Maximum Speed: 0.5 mm/s<br>Tilt Error: 100 μrad |
| | Fine Translation $z$-axis | Piezoelectric | Range: 25 μm<br>Resolution: 1 nm<br>Accuracy: 3 nm<br>Resonant Frequency: 3.5 kHz (unloaded)<br>Settling Time per 1 μm: 0.3 ms (to 10%, with 50 g load)<br>Tilt Error: 5 μrad |
| Azimuth | Rotation $\theta_y$ | Manual | Range: ±35°<br>Resolution: 250 μrad<br>Eccentricity: 25 μm |
| Pitch (optional) | Rotation $\theta_z$ (Goniometer) | Manual | Range: ±5°<br>Resolution: 100 μrad<br>Goniometric Error: 100 μm<br>RCR: 25 μm |
| Roll | Rotation $\theta_x$ (Goniometer) | Manual or Motorized | Range: ±2°<br>Resolution: 50 μrad<br>Goniometric Error: 50 μm<br>RCR (parallel component): 5 μm |

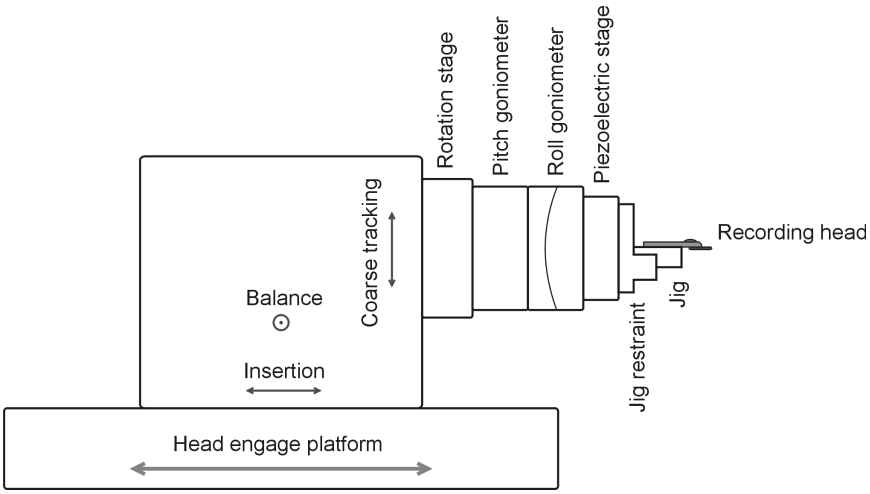


**Figure 4.5:** *Viable structure of a high precision head positioning mechanism. The insertion, balance, and coarse tracking motion stages are not explicitly shown.*

cision and stiffness. The choices for manual or motorized actuation, other than for the tracking motion, are indicative.

The assembly of the individual devices should result in minimum degradation of their inherent performances. We note that some components require special care to minimize the load or the alignment errors, like the piezo or the roll goniometer. Such considerations were accounted for in the build configuration presented in Fig. 4.5. Mounting the head jig restraint directly onto the piezo stage results in low mass to be carried and ensures short response times. The piezo is fixed to the roll goniometer with special attention to minimize the misalignment between the jig and the goniometer. Then follow the pitch goniometer and the azimuth rotation stage. The short travel range of the piezo would not affect considerable the alignment (eccentricity) errors between the head and the rotation stages. As discussed before, the use of a pitch goniometer is not strictly necessary. Moreover, it is generally sufficient if only one of the two head positioning mechanisms is equipped with an azimuth adjustment stage. The structure described in Fig. 4.5 may therefore be slightly reduced. The rotation devices are mounted on the translation stages which ensure the coarse tracking, balance, and insertion motions. Multiple choices for the configuration of the translation stages are possible, without sensitive issues to be addressed.

The insertion motion allows accurate traveling over a short distance range. However, in order to replace either the head, the jig or the tape, it is convenient

to carry the positioning mechanism further away from the tape-drum. A *head engage* platform allows to bring the head in close proximity to the tape-drum for recording measurements or place it at few centimeters away for easy access to the components. The platform should therefore operate between two stable positions: engage and withdraw. Manual, pneumatic or motorized actuation could be employed. In some cases, the insertion and the engage motion can be ensured by the same translation stage.

### 4.2.4 Read/Write Instrumentation

The read/write instrumentation of magnetic recording testers usually comprises a R/W module, a hardware channel, a pattern (signal) generator, and a read-back analyzer. The pattern generator could be a dedicated device for magnetic recording applications, integrating specific features like write precompensation. The read-back analyzer serves to perform a wide range of parametric measurements such as amplitude and pulse width. It may consist of a fast digitizer with a digital signal processor (DSP) for shaping the data. Additional processing is sometimes performed on the host computer controlling the tester. A digital oscilloscope could also be employed for analyzing the read signal, with the advantage of greater accuracy and versatility. Advanced oscilloscopes supporting extended functionalities for testing magnetic recording signals are nowadays available. It is more and more common that read-back analyzers and digital oscilloscopes are able to perform spectral signal manipulations by means of fast Fourier transforms (FFT). FFT can be employed to evaluate recording performances like overwrite ratio or noise power and signal spectra. Yet, if frequency domain measurements are of high interest, a stand-alone spectrum analyzer should be considered for ultimate performances.
The hardware channel usually accommodates a data channel circuit specific to some recording format of interest. It is generally employed for error rate measurements but may also support additional functionalities such as servo tracking control. The hardware channel should be customizable by the user for specific features and tests. It should be flexible enough to allow adapting diverse data channel chips. Partial response maximum likelihood (PRML) detection methods are becoming standard in high density magnetic tape storage.

The choice and the configuration of the measurement apparatus depends very much on the scope of the tester and preferences of the user. Multiple implementations are possible offering different levels of performance, flexibility, versatility, and cost. The requirements may therefore vary from case to case and only some dynamic features are discussed here. Modern tape-drum testers operate at high relative velocities up to 30 m/s and are suitable to investigate extreme recording densities due to their good stability. Linear densities up to 10 kfc/mm (254 kfc/in) are currently achieved in commercial tape drives and are expected to double in about half decade [10]. Actually, flux change densities

around 15 kfc/mm (380 kfc/in) and channel rates of 300 Mb/s were already demonstrated in a prototype helical scan tape recorder [14]. It is likely that densities around 20 kfc/mm (500 kfc/in) will become of increased interest during the next years, entailing channel data rates close to 500 Mb/s for a velocity of 25 m/s. It can be assumed that a tape-drum tester intended for research and development applications would have to perform at such elevated speeds. The electronic instrumentation should therefore enable accurate operation up to very high frequency and data rate, as suggested below:

- Maximum Channel Data Rate: $\geq 500$ Mb/s
- Analog Bandwidth ($-3$ dB): $\geq 350$ MHz
- Signal Acquisition Sampling Rate: $\geq 1$ GS/s
- Signal Generator Sampling Rate: $\geq 1$ GS/s
- Signal Generator Rise Time (10 to 90%): $< 1$ ns

The replay signals from magnetic read heads have wide bandwidth and very low magnitude, usually in the order of hundreds $\mu$V. Transmission of such signals requires appropriate amplification and conditioning in order to preserve their integrity. A read preamplifier is therefore placed as close as possible to the head to ensure low interference noise, large bandwidth, and weak attenuation. The same goes for the write current driver, which has to run high currents through the write head with minimum reversal times, down to 1 ns. It is therefore desirable to keep short the interconnect wires between the R/W module and the head, preferably below 5 cm. The interconnect comprises two balanced twin lines, one for the inductive head and other for the MR device. Optimum bandwidth is achieved if the lines are terminated at least at one end in order to avoid (multiple) signal reflections. It is generally easier to match the interconnect and the R/W circuits impedances.
Differential R/W circuits are preferred in order to suppress the common mode noise and reduce the electromagnetic interference. A balanced write driver also presents the advantage to increase the active voltage and achieve symmetric current reversal times. Multiple configurations are possible for the R/W modules, which may feature different properties. However, some typical features judged appropriate for a high performance tape-drum tester are resumed in Table 4.2. Attention must be paid that the R/W module and the head interconnects feature a well balanced differential configuration and parasitic impedances are minimized. The common mode and power supply rejection ratios should be better than $-40$ dB over half the bandwidth of the read preamplifiers.

The write driver must be able to generate strong currents with well defined wave shapes at high frequencies. In most cases, an input signal indicates when current switching should occur, while other parameters such as amplitude and overshoot are programmable. A rise time close to one nanosecond should be attainable using a recording head with low impedance ($L_h \approx 60$ nH and $R_h \approx 10\ \Omega$). Higher head inductance values would result in degradation of the rise time, due to larger impedance and lower resonance frequency. The limited

**Table 4.2:** *Indicative performances suitable for the R/W module in very high speed tape recording testers. (Evaluation conditions: $I_w = 30$ mA, $L_h = 60$ nH, $R_h = 10\ \Omega$, $I_{mr} = 5$ mA, $R_{mr} = 50\ \Omega$)*

| **Parameter** | **Inductive** (read/write) | **MR** (read) |
|---|---|---|
| Write Current Range (mA) | 2 to 80 | n/a |
| Write Current Rise Time (ns) | 1 | n/a |
| Write Voltage Swing ($V_{pp}$) | 15 | n/a |
| Diff. Output Capacitance (pF) | 4 | n/a |
| Read Passband (MHz) at −3 dB | 0.5 to 150 | 0.5 to 300 |
| −1 dB | 1 to 120 | 1 to 250 |
| Adjustable Read Gain (V/V) | 300 to 1500 | 100 to 500 |
| MR Bias Current Range (mA) | n/a | −15 to 15 |
| Input Noise Voltage ($nV_{rms}/\sqrt{Hz}$) | 0.5 | 0.5 |
| Input Noise Current ($pA_{rms}/\sqrt{Hz}$) | 4 | 5 |
| Diff. Input Capacitance (pF) | 5 | 5 |
| Diff. Input Resistance ($\Omega$) | 1000 | selectable |
| Input Voltage Swing ($mV_{pp}$) | 3 | 10 |

output voltage of the write driver could not therefore ensure fast and ample current changes. Parasitic inductances are also generated by factors such as interconnects and signal paths on the printed circuit board (PCB). They add to the impedance of the head and increase the total inductance of the assembly loading the write driver. Moreover, the head is shunted by a number of capacitances coming from its own windings, output ports of the driver, electrical connections, etc. They may account for a total parasitic capacitance roughly around 10 pF. It is suitable to minimize the parasitic impedances as they limit the operational write bandwidth. Together with the head they form an LC circuit whose resonance frequency decreases inverse proportionally to the square root of the equivalent parallel inductance and capacitance. LC circuits become unstable when operated near their resonance frequency and need to be damped. The equivalent output resistance of the write driver should be sufficiently low for damping, while keeping good load current capabilities as well as linear frequency response. Optimization of the differential output impedance is not straightforward in magnetic tape recording as head inductance values spread within a large range. They turn around hundreds nH in current sys-

tems and can reach 30 nH in modern head designs [14]. The output impedance also has to be matched to the characteristic impedance of the interconnect line to ensure fast current reversal times. Overall, values between 100 Ω and 200 Ω should be considered for a very high speed tester as described in this section. Overdriving the write current at switching was introduced in hard disk recording in order to achieve faster operation. Reversing the current with controlled overshoot helps to reach faster electronic rise times and speed up the magnetic switching of the head yoke [144]. The technique is gaining increased interest in magnetic tape recording, as data rates are pushed further. The write driver should therefore support overshoot with programable amplitude (e.g. 0 to 60%) and duration (e.g. 0.5 to 5 ns).
If only parametric measurements are intended, the data channel would not be necessary. An arbitrary waveform generator (AWG), offering high speed and convenient signal manipulation capabilities, may then be used to generate the write waveform. The generator would support programming of parameters such as signal amplitude and frequency, rise time, overshoot, etc. In that case, the write driver could simply consist of a high throughput transconductance amplifier.

As inductive read heads are still being used in helical-tape systems, an accurate signal preamplifier is considered. This could share the same head interconnect as the write driver. The option to switch between the write driver and the read preamplifier must be implemented without degradation of their specific performances (especially for the writer). A miniature electromechanical relay with outstanding performances in the gigahertz regime could be employed. Its insertion loss at 500 MHz should be better than 0.3 dB and the parasitic capacitance lower than 0.5 pF. The ability to pass in read mode may also serve to adjust the head-to-tape contact of the write heads, independently of the read device. The bandwidth of the preamplifier is lower than that of the write driver as inductive read heads are unlikely to operate at frequencies higher than 150 MHz. Matching the input impedance to that of the head interconnect is not really necessary due to the moderate bandwidth. In fact, it is preferred to have a relatively high input resistance in order to reduce the signal drop. Priority for impedance matching should be given to the write driver. Other preamplifier's features include very low noise and input capacitance, large voltage gain, etc. However, one may find not necessary to use inductive head reading and decide to not implement the preamplifier. The R/W module would become then similar to those employed in hard disks, but with lower bandwidth.

Anisotropic magnetoresistive (AMR) and giant magnetoresistive (GMR) read heads are believed to enable very high densities and data rates in future tape storage systems [13, 14]. Even tunneling magnetoresistive (TMR) devices have been investigated for magnetic tape recording [44]. The preamplifier for MR heads comprises a high bandwidth, accurate amplifier combined with a very low noise biasing source. The MR device is biased by applying either a

constant current through it or a constant voltage across it. The flux changes produced by the magnetic medium cause fast variations of the sensor's resistance, which are sensed by the preamplifier as AC voltages or currents. The amplifier input is therefore AC coupled with the biasing source and the head, resulting in a high pass filter. The time constant of the biasing source is well below that of the read signal.

Voltage sense preamplifiers are most commonly employed in magnetic recording. Current or voltage biasing modes are usually selectable, leading to sensitivity to the absolute resistance variation $\Delta R_{mr}$ or to the relative change $\Delta R_{mr}/R_{mr}$, respectively. The bias source should be programmable and bidirectional. Other suitable features include very low noise, adjustable gain and passband, and selectable differential input resistance. Again, optimum transmission bandwidth is achieved by matching the input resistance of the preamplifier, $R_{in}^{diff}$, to the characteristic impedance of the interconnect, $Z_0^r$. The read line impedance can be optimized for different purposes like achieving maximum signal-to-noise ratio (SNR), frequency independent SNR, or best signal flatness [144, 145]. Line termination and highest SNR is obtained if

$$R_{in}^{diff} = Z_0^r = \sqrt{R_{mr}\frac{v_{an}}{i_{an}}} \ , \tag{4.5}$$

where $v_{an}$ and $i_{an}$ are the input referred amplifier voltage noise and current noise respectively. For a sensor resistance of 50 Ω and an amplifier noise figure as given in Table 4.2, an optimum impedance value of 225 Ω is found. Balanced pairs with such characteristic impedance are possible. Assuming a total parasitic capacitance $C_p = 8$ pF leads to a cutoff frequency of 485 MHz at the preamplifier input, given by $f_{in} = (R_{mr} + R_{in})/(2\pi C_p R_{mr} R_{in})$. For this specific case, $f_{in}$ does not limit the preamplifier passband proposed in Table 4.2. Suitable bandwidth and optimum SNR are therefore achieved for MR sensors with the resistance close to 50 Ω, if $R_{in}^{diff} = Z_0^r = 225$ Ω.

However, other input/line impedance values may be preferred, resulting from different considerations. A differential input resistance $R_{in}^{diff} = 100$ Ω could also present interests, like the wide availability of interconnects with similar characteristic impedances. Moreover, it would ensure a sufficiently wide bandwidth for sensors with high resistance up to 200 Ω, enabling the use of TMR read heads. The relative large track widths employed in tape recording do not constrain the sensor area making possible to achieve magnetic tunnel junctions (MTJ) with low resistance [14]. A comfortable resistance-area product of 50 $\Omega \cdot \mu m^2$ would enable a TMR sensor resistance of 200 Ω at a track width and element height equal to 0.5 $\mu$m. This represents about a tenfold increase compared to the highest track densities achieved nowadays in commercial tape systems. A MR head preamplifier with programmable differential input resistance is desirable for best flexibility. This would employ a feedback loop to vary the input impedance without introducing any thermal (Johnson) noise.

In the tape recording tester, the connections from the R/W module to the measurement and analysis equipment can be relatively long, up to one meter. The lines should be terminated at both sides and shielded in order to ensure very wide bandwidth and low electromagnetic radiation. The sensitive read preamplifiers are generally not suited for driving such lines and using a signal boosting stage is recommended. The final stage should have high output capabilities and may be equipped with an additional gain control facility. This could serve for fine calibration of the amplifier.

## 4.3 Redesign and Optimization of an Existing Tester

The possibility to produce a new tester with ultimate performances as described previously in Section 4.2 was investigated. It was intended to develop the control software plus the read/write instrumentation and to acquire a custom-made electromechanical assembly. The latter includes the drum, the air-spindle, the head positioning mechanisms, and the associated controllers. Specialist manufacturers of tape-drum testers were considered to contract the electromechanical assembly. The author was actively involved in defining its technical specifications as well as suggesting solutions to issues as discussed in Section 4.2. Despite a certain flexibility regarding the technical requirements, it was concluded that a suitable apparatus could not have been guaranteed. It appears that specialist manufacturers are limiting their investments for the development of advanced tape-drum testers.
Building in-house the complete new tester was judged technically feasible but would have required extended development time. The final solution was to redesign and modify an existing tape-drum setup that was already available in the laboratory. Its performances were considerably improved by developing new R/W modules and a very stable head positioning mechanism. The drums were reworked and the control software was rewritten for optimum precision, stability, flexibility, as well as support for new types of measurements.

The upgraded tape-drum tester used for the recording measurements in this thesis is shown in Fig. 4.6. The rotating drum and the new head positioning mechanism are visible. One can see that the air is supplied to the tape drum via an external shaft on top of the drum. Modern approaches would rather be to feed the air via the own shaft of the spindle. Nevertheless, a very stable air bearing with high load capability is employed. The bearing combines a spherical and a flat air surface with the diameter of 100 mm and 120 mm respectively. Its performances were certified recently at a specialized laboratory, finding total error motions (synchronous plus asynchronous) lower than 20 nm and a radial stiffness of 50 N/$\mu$m. These specifications are in line with the requirements for a very high precision tester as formulated in Section 4.2.2. The rotation speed of the spindle is limited to an equivalent relative linear velocity

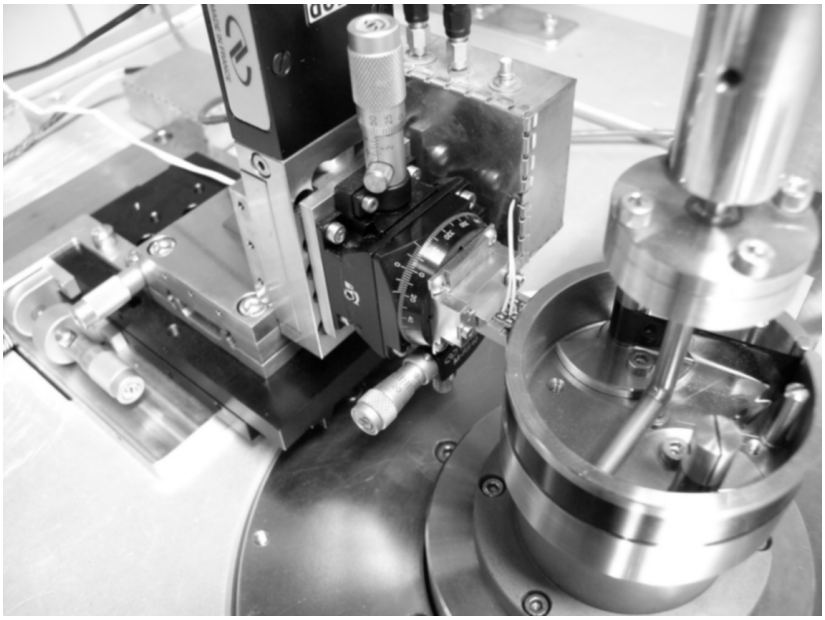

**Figure 4.6:** *View of the upgraded tape-drum tester (drum and head positioning mechanism).*

in a range between 1 and 10 m/s. The spindle controller was tuned to minimize the speed jitter measured from recording Wow-Flutter measurements. An optimum synchronous speed jitter of 0.03 % was obtained. We note that this measurement reflects the variations of the head-to-tape relative velocity and accounts for more factors than just the spindle alone.
The design of the drums is however less advanced and resembles to that in Fig. 4.2 (a). Two drums for 8 mm and 12.7 mm (half-inch) tapes are being used. They have a diameter of 76 mm, allowing to mount short tape samples down to 40 cm. A radial deviation of the tape reference surface around 8 $\mu$m was measured in both cases. This value was found after rectification works on the drums. The air supply channel and the hole pattern hardly ensure an uniform pressure underneath the tape, further affecting the concentricity of its path. If careful adjustments of the tape tension and of the air pressure are performed, the radial deviation of the tape path is found around 12 $\mu$m (zero-to-peak).

**Table 4.3:** *Specifications of the motion components integrated into the head positioning mechanism.*

| Head Motion | Description | Actuator | Stage Main Specifications |
|---|---|---|---|
| Insertion | Translation *y*-axis | Manual | Range: 13 mm<br>Graduations: 5 μm<br>Sensitivity: 0.5 μm<br>Tilt Error: 150 μrad |
| Balance | Translation *x*-axis | Manual | Range: 25 mm<br>Graduations: 20 μm<br>Sensitivity: 1 μm<br>Tilt Error: 200 μrad |
| Tracking | Translation *z*-axis | DC Motor | Range: 8 mm<br>Resolution: 0.055 μm<br>Uni-dir. Repeatability: 1 μm<br>Reversal Value: 3 μm<br>Full-range Accuracy: 10 μm<br>Maximum Speed: 0.3 mm/s<br>Tilt Error: 100 μrad |
| Azimuth | Rotation $\theta_y$ | Manual | Coarse Range: 360°<br>Vernier Graduations: 0.2°<br>Fine Adjustment Range: 10°<br>Actuator Graduations: 1.5 mrad<br>Sensitivity: 75 μrad<br>Eccentricity: 20 μm |
| Roll | Rotation $\theta_x$ (Goniometer) | Manual | Range: ±5°<br>Actuator Graduations: 150 μrad<br>Sensitivity: 15 μrad<br>Goniometric Error: 100 μm |

### 4.3.1 Construction of the Head Positioning Mechanism

The original head positioning mechanisms of the tester were featuring limited stability and precision, unsuitable for recording track widths below 5 $\mu$m. A new platform was designed by the author, aiming at performances approaching those described in Section 4.2.3. The construction was, however, simplified to a certain degree by excluding the piezoelectric stage and the pitch adjustment. The immediate scope of the positioning mechanism was to accurately support track widths close to 1 $\mu$m. The resultant assembly is visible in Fig. 4.6. Its motion components are listed in Table 4.3 together with most significant specifications, as given by the manufacturer. For the head coordinate system

it should be referred to Fig. 4.4.

The tracking motion is ensured by a motorized stage with a rotary encoder whose resolution corresponds to 55 nm. Its control algorithms were optimized to ensure a minimum incremental motion equal to the resolution of the encoder. However, it turned out that the practical motion resolution of the stage was almost double that of the encoder. This was suggested by the staircase appearance of the track profiles measured at an incremental motion equal to the encoder resolution, as presented in Fig. 5.3 (Section 5.2.2). The discrepancy between the actual motion and the encoder output was probably caused by limitations of the gear mechanism. For precise movements, the stage was set to approach the desired position always from the same direction in order to avoid reversal errors. These could be caused by hysteresis (elastic deformations) of the drive mechanism, which is a backlash-compensated lead screw. It was observed experimentally that the positioning accuracy of the stage may vary along its travel range. Care was taken to operate it in a region where performances are optimum, in order to ensure precise tracking. With all precautions, an accuracy better than 100 nm is achieved for short-range motions within 10 $\mu$m. More advanced electromechanical stages with ball screw or direct drive mechanisms would ensure superior performances (resolution, repeatability, accuracy, speed, etc.). However, the precision of the head positioning relative to the tape can further be affected by the stability of the head-to-tape contact. Using a piezoelectric stage to improve tracking would also require more advanced tape-drums in order to ensure consistent performances. If necessary, the design of the present head platform would allow to replace the azimuth rotation stage with a piezoelectric element.

All other adjustments of the head position are manual, with fine sensitivity. Most stages feature stable construction in stainless steel and crossed-roller bearings were chosen where possible. Special attention was given to the conception of the head mounting system, which was optimized for high precision assembling and convenient manipulation. A detailed picture is shown in Fig. 4.7. The head is mounted on a jig which is then mounted in a restraint fixed to the positioning mechanism. This configuration allows to use different jigs designed for specific types of heads. The head in Fig. 4.7 is an Helical Scan Silicon (HSS) chip fixed on a DDS standard brass plate. Other types of plates are often used. The jigs are easily interchangeable and fit to the restraint with cumulative tolerances better than 20 $\mu$m. Two tiny wings are attached by screws to the restraint and allow to easily tighten the jig in firm position. Very good assembling repeatability is achieved. The electrical contacts to the head are done by soldering ensuring robustness and low resistance. The preamplifier is placed very close to the head resulting in a short interconnect around 4 cm.
The separated jig is shown in Fig. 4.8, with the same head mounted on it. The top part of the screw has a conical shape to push the head against the three reference planes machined with tight tolerances. This results in a mounting

precision below 20 $\mu$m for the head types employed. The block shape of the jig is convenient for head manipulations like checking its status under an optical microscope. The total mass of the jig-restraint assembly is just around 40 g, even though they are fabricated in stainless steel. This would enable them to be used with piezoelectric positioners without affecting the response times, which are highly sensitive to load.

In practice, the present head positioning mechanism proved to deliver outstanding performances and operation convenience for narrow track recording. The targeted track width of one micrometer was reached as demonstrated by the track profiles measured in Section 5.2.2. The staircase profiles in Fig. 5.3 suggest that the resolution of the motorized stage was the main factor limiting the precision of the measurement. This is a notable fact as it suggests that improving the design of the positioning mechanism and of the tape-drum would allow to considerable enhance the tracking accuracy. The development of a tape-drum tester supporting track widths down to 200 nm, as described in Section 4.2, seems now feasible.

### 4.3.2 Development of the Read/Write Module

The tape-drum tester is equipped with measurement instruments comprising an arbitrary waveform generator, a spectrum analyzer and an oscilloscope. A wide range of parametric measurements in the frequency domain had been implemented. They are based on writing a square wave and reading the amplitude of the fundamental and sometimes of the harmonics. The read spectrum of square wave recording is basically explained in Section 2.4.2. Frequency and current dependencies of the signal output and overwrite ratio were included, as well as a wide range of measurements dedicated to study track edge effects or nonlinearities of the write process.

A new R/W module was developed for use with inductive heads, which were mainly available during this project. A differential, well balanced architecture was employed for optimum performance and stability. Due to the maximum relative velocity of 10 m/s achieved by the tester, a read bandwidth of 100 MHz was judged sufficient. The read circuit contains a very low noise differential preamplifier coupled with a variable gain amplifier to boost and transmit the signal. The write driver is a fast transconductance differential amplifier with a rise time around 2 ns when loaded with a purely resistive charge. Other features of the read and write amplifiers are given in Table 4.4. The head can be switched between the write and the read circuits using an electromechanical relay for high frequency applications, visible in Fig. 4.9. Its insertion loss at 100 MHz is specified at less than 0.1 dB, while the parasitic capacitance between contacts is 0.4 pF. Close to the relay are the contact pins for the head interconnect. A current probe (transformer) is permanently placed on one of the pins, serving for calibration of the read/write module. It also allows to check

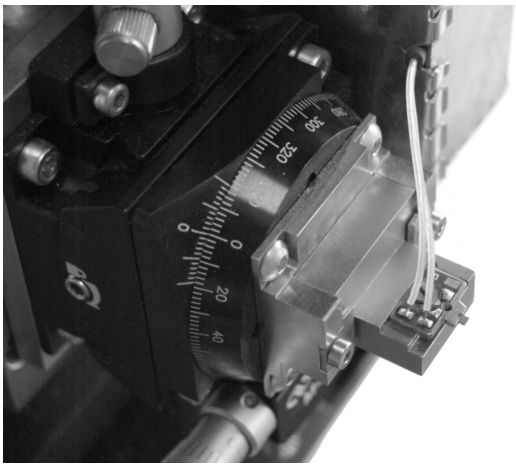


**Figure 4.7:** *Detailed view of the head mounting system.*

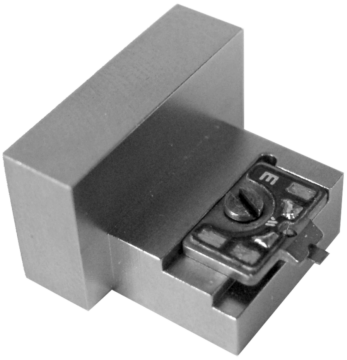

**Figure 4.8:** *Block shaped jig allows precise mounting and easy manipulation (e.g. head replacement and inspection at microscope).*

**Table 4.4:** *Performances of the read and write amplifiers developed. (Evaluation conditions: $I_w = 20$ mA, $L_h = 200$ nH, $R_h = 5\ \Omega$)*

| **Parameter** | **Typical Value** |
|---|---|
| Write Current Range (mA) | 0 to 75 |
| Write Current Rise Time (ns) | 2.5 |
| Write Voltage Swing ($V_{pp}$) | 8 |
| Diff. Output Resistance ($\Omega$) | 350 |
| Diff. Output Capacitance (pF) | 6.5 |
| Read Passband (MHz) at $-3$ dB | 0.05 to 100 |
| $-1$ dB | 0.1 to 60 |
| Adjustable Read Gain (V/V) | 300 to 1500 |
| Input Noise Voltage at 10 MHz ($nV_{rms}/\sqrt{Hz}$) | 0.54 |
| Input Noise Current at 10 MHz ($pA_{rms}/\sqrt{Hz}$) | 3.7 |
| Diff. Input Capacitance (pF) | 4.6 |
| Diff. Input Resistance ($\Omega$) | 2250 |
| Input Voltage Swing ($mV_{pp}$) | 3 |

the response of the amplifiers for specific heads. In write mode, it can be used to monitor the driver's current having a conversion factor of 0.5 mV/mA (into a 50 $\Omega$ load). The probe can also be operated in reverse mode by applying a voltage to its output to induce a signal in the read circuit, simulating that from the replay head. It is a very convenient method to measure the response of the read preamplifier. The probe was built around a ferrite ring core ($\phi = 4$ mm) with low initial relative permeability $\mu_{ri} = 80$ and inductance factor $A_L = 13$ nH. A flat passband within $-1$ dB from 0.8 to 120 MHz was achieved. The probe impedance is negligible compared to that of the preamplifier input and of the inductive heads employed here. The balance of the differential line is therefore not affected. However, for higher bandwidth amplifiers, one may choose to further reduce the probe inductance and place a dummy one on the mate pin. Even better results would be obtained if operational probes are placed on both pins and connected differentially. One may also choose not to implement such current transformer into the read/write module and use a removable probe when necessary.

The high read amplification gain around 1000 V/V may create instabilities at high frequencies if parasitic couplings between output and input are not avoided. Careful consideration was therefore given to factors such as electro-

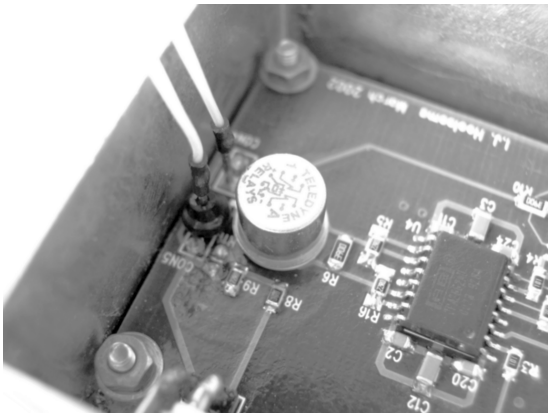

**Figure 4.9:** *Partial view of the R/W module showing the write amplifier, the relay, and the current probe placed on the head port. The read preamplifier is placed very close to the relay on the other face of the PCB.*

magnetic interference and return currents. The R/W module is enclosed in a screening case whose relatively low dimensions (80 mm × 55 mm × 27 mm) allow to be placed very close to the recording head. Double shielded coaxial cables are used to route the signals between the R/W module and the measurement equipment.

### 4.3.3 General Measurement Conditions

The recording experiments presented in this thesis were carried out on the upgraded tape-drum tester described previously. The write signal was generated using a LeCroy LW410A arbitrary waveform generator, featuring a maximum sample rate of 400 MS/s and a rise time of 5 ns. A HP3589A spectrum/network analyzer with a gated sweep option was employed to acquire the preamplified read signal, having a frequency range from 10 Hz to 150 MHz. A resolution bandwidth of 17 kHz was typically employed for the recording measurements. They were performed in the frequency domain, by writing a square wave signal and reading the fundamental. The relative head-to-tape velocity was equal to 3 m/s, ensuring linear frequency operation of the heads investigated. The experiments were generally prepared such that optimum stability and tracking accuracy is achieved.

## 4.4 Conclusion

Performing recording experiments at very high recording density and low track width requires appropriate test equipment. Smooth and accurate head-to-tape contact, high system stability, and precise tracking are essential. Still, recording tape testers suitable for submicron track widths are not readily available. In this work, an existing set-up was modified and partly redesigned in order to deliver suitable performances and operation convenience for recording narrow tracks close to one micrometer. The speed stability, the head-to-tape contact, the cross-track positioning, and the signal conditioning were primarily upgraded. This was achieved by reworking some components such as the tape-drums, and by developing new designs for other modules including the head positioning platform and the read/write circuitry. The head positioning mechanism was conceived to offer operation convenience with a wide range of adjustments and a practical head mounting system. The control software was rewritten to enhance its flexibility and to optimize the performances of the tester. Careful preparation of the recording experiments led to non-repeatable tracking errors below 100 nm, for short-range motions within 10 $\mu$m.

It is expected that considerable better performances are achievable by constructing a whole new tester with optimized design. Such issues were analyzed aiming to develop an ultimate tape-drum tester suitable for track widths down to 200 nm. Extensive design criteria and suggestions were elaborated, covering the main mechanical and electronic components of the setup. A judicious construction is required for the tape-drum while a very precise air spindle should be employed. The resolution of the head positioning mechanism can be enhanced to the nanometer level by integrating a piezoelectric stage. Non-repeatable tracking errors below 35 nm (at $3\sigma$) were judged feasible, and track widths slightly less than 1 $\mu$m could be operated without servo tracking. Recording at track widths close to 200 nm is expected to be possible using servo tracking.

Chapter 5

# Measurements and Interpretation of Track Profiles

Narrow track magnetic recording is affected by edge effects, as introduced in Section 2.5. Side writing and erasing cause the edges of the tracks to be less efficiently recorded than the center. This results in an effective track width inferior to the track pitch. The effects depend on the capability of the recording head to generate a write field well confined in transverse direction, with sharp edges. Similarly, side reading is related to the cross-track resolution of the read head sensitivity function that does not drop abruptly enough at the flanks. It may engender intertrack interference by reading information from adjacent tracks. *Track profiling* techniques have been commonly applied in hard disk recording for studying the edge effects [63, 64, 75, 115, 116, 146, 147]. They involve scanning the read head across a written track or a pattern of multiple tracks to measure the output signal versus transverse location. Very good control of the cross-track position is required. The tracking precision and stability achieved in most tape recording systems is generally not sufficient for accurately performing such experiments. Magnetic imaging techniques such as magnetic force microscopy (MFM) are therefore often preferred. A brief review of magnetic imaging and profiling techniques is presented in this chapter. It is also shown that track profiles can be adequately measured in tape recording using an optimized tape-drum tester which was described in Section 4.3. Helical Scan Silicon (HSS) heads with narrow pole widths down to 1.3 $\mu$m were used to test its capabilities.

The side write asymmetry of a 3.3 $\mu$m wide HSS head is analyzed in the last part of the chapter using an overwrite configuration that enhances the edge effects. The *imbalanced overwrite* method allows for a qualitative study of side

writing and erasing, and it requires moderate tracking precision. The overwrite patterns were studied from track profiles and MFM images processed by fast Fourier transforms (FFT). Weak edge effects were observed at good pole alignment. The experiments were performed with metal evaporated (ME) and metal particulate (MP) tapes having magnetic layers between 50 and 300 nm. More detailed investigations of side write and erase effects are presented in Chapters 6 and 7, using techniques that demand enhanced cross-track positioning accuracy.

## 5.1 Track Profiles versus Magnetic Imaging

Edge effects have been typically investigated using track profiles or magnetic imaging techniques of the recorded patterns. Initial imaging techniques used Bitter colloid decorations observed by optical microscopy [64, 118] or even by scanning electron microscopy (SEM) [148]. The advent of magnetic force microscopy (MFM) [149] made readily available a valuable imaging technique with resolution better than 50 nm and relatively easy sample preparation. MFM became shortly a standard tool for observing recorded tracks and analyzing the nature of side writing and erasing [99, 104, 106, 108, 109, 110]. However, MFM does not sense the magnetization in the sample but the gradient of the force exerted on the scanning tip due to the stray field. The MFM signal is therefore related to the magnetization changes rather than to the magnetization itself, and it is not related in a simple way to the magnetization direction. Moreover, complex interactions between the MFM tip and the magnetization patterns may occur. MFM is an indirect method to observe the magnetization and the interpretation of images is not always straightforward. Lorentz transmission electron microscopy (LTEM) is more closely related to the magnetization in the sample. LTEM was also applied to investigate recorded track edges [65, 150, 151], however, the method requires very complicated sample preparation which restrains its use. Its resolution depends on the magnetization and thickness of the sample and it is worst than 150 nm for media with low $M_r\delta$ around 5 mA (0.5 memu/cm$^2$) [151].

MFM and LTEM imaging techniques can typically not separate between longitudinal and transverse magnetization in the medium. At the track edges, transverse magnetization may be present, the amount of which depends on the orientation ratio of the medium. The read head is rather insensitive to the transverse magnetization, which appears to it as erased [65]. The erase bands sensed by the read head may therefore differ from those observed using other imaging techniques. The problem is even more complex in azimuth tape recording where bits are written under an angle to the medium's easy axis, which can be as high as 30° in recent helical drives (25° for the azimuth angle plus approximately 5° for the track angle). Note that modern tape media

feature relatively high orientation ratios, typically comprised between 2 and 5 (see Table 3.3). The magnetization distribution at the track edges in azimuth recording is therefore not straightforward.

The erase bands as sensed by the read head can be evaluated from track profile measurements. Useful information about the recording and replay process along the cross-track direction is obtainable using such methods. The experiments are fully performed on the recording setup, without involving the use of additional instruments to observe the magnetization patterns. The data is averaged down-track over a considerable distance of several centimeters, reflecting the standard behavior of the recording system. Magnetic imaging techniques cover localized areas with dimensions in the order of micrometers or tens of micrometers. However, spatial resolution better than 50 nm is easily achieved by MFM, making it possible to study fine magnetization structures inside the erase bands. Appropriate measurements of track profiles require precise tracking and good stability of the recording setup, being mainly employed in hard disks. The effective write and read track widths can then be estimated from simple full-track scans (see Section 5.2) [152]. Furthermore, the cross-track sensitivity function of the read head is accessible from microtrack scans. Diverse methods have been developed to evaluate the erase bands, by recording diverse track patterns with partial overlap (edge overwrite).

The effective write width was measured in [63] from *erase profiles* obtained by gradually erasing a written track and reading the remainder. Three distinct write, read, and erase heads were used for the experiment. Erase profile measurements were later adapted to evaluate the erase width, using a single read/write head [115]. A track was written and then progressively erased from both sides by displacing the same recording head. Profiling the output from the narrowed track versus the erase distance allow to calculate the erase width. The method was still being employed until recently [75, 116, 153]. Narrowing the track by erasing it just at one side allows measuring the erase bands at each edge of the head. This technique was initially applied in [146] to analyze the asymmetry of the erase bands due to skew angles in hard disk recording. It is reliable and relatively easy to implement, being reused in other works [114, 154, 155].

*Triple-track profiles* were introduced in [64] to investigate the write, read, and erase widths in hard disks, becoming a popular method for measuring erase bands [100, 111]. It consists in recording a central track in between two side tracks with partial overlap such that it overwrites their edges, producing two erase bands. The complete pattern is scanned then by the read head to acquire a triple-track profile as that shown in Fig. 6.1. An original method to extract the erase bands and relative side read widths is presented in Chapter 6 and applied to analyze edge effects in magnetic tapes.

As previously stated, the application of track profiling techniques in magnetic tape recording is limited by the tracking accuracy of the systems. Anal-

ysis of side writing and erasing by MFM has therefore been often preferred [19, 20, 119, 156, 157]. Measurement of erase bands from track profiles with an accuracy down to around 1 $\mu$m were performed in [158], on a linear tape recording setup. Cross-track profiles were measured with better accuracy in [159] using an original *azimuth displacement* technique to minimize errors caused by tape tracking. The method is applicable to merged thin-fim/MR heads, where the separation between the read and write elements is much larger than the track width (e.g. 50 to 200 times). The scan is achieved by incremental rotation of the head with very small angles, instead of the typical cross-track translation. Read, write, and erase effective widths were measured based on this technique with precision better than 0.5 $\mu$m, as reported in [160, 161].
Tracking control is typically more accurate in tape-drum testers than in linear scan ones (Section 4.1). A tape-drum setup was employed in [74] to analyze the erase bands dependence on the pole geometry of ferrite video heads. A track profiling technique involving three recording heads was employed to measure erase bands to less than 0.5 $\mu$m. A similar tester was also used more recently to investigate the cross-track response of AMR read heads developed for helical scan tape systems [162]. Full-track and microtrack profiles were measured there with a resolution around 0.25 $\mu$m. A tape-drum tester with tracking accuracy better than 0.1 $\mu$m (zero-to-peak) was employed in the work presented here to study the edge effects in magnetic tape recording. Several profiling methods to investigate side writing/erasing and reading were applied.

## 5.2 Full-Track and Microtrack Profiles

### 5.2.1 Profiling Bases

A *full-track profile* is measured by recording a test track and scanning the read head across it to capture the output signal versus position, as schematically shown in Fig. 5.1 (a). A square wave pattern is most often used to write the test track on a previously erased background. The output can be either the down track averaged amplitude (TAA) or the fundamental of the read signal. The experiments reported in this work are performed by reading the fundamental using a spectrum analyzer. It is therefore possible to resolve the individual output from tracks written adjacently at different frequencies.
If square functions are assumed both for the cross-track response of the replay head as well as for the distribution of the written magnetization, a trapezoid track profile is predictable [152]. From the scheme in Fig. 5.1 (a), the trapezoid's segments AD and BC can be related to the effective write width $w_w$ and read width $w_r$:

$$\mathrm{AD} = w_w + w_r \qquad \& \qquad \mathrm{BC} = |w_w - w_r| \; . \tag{5.1}$$

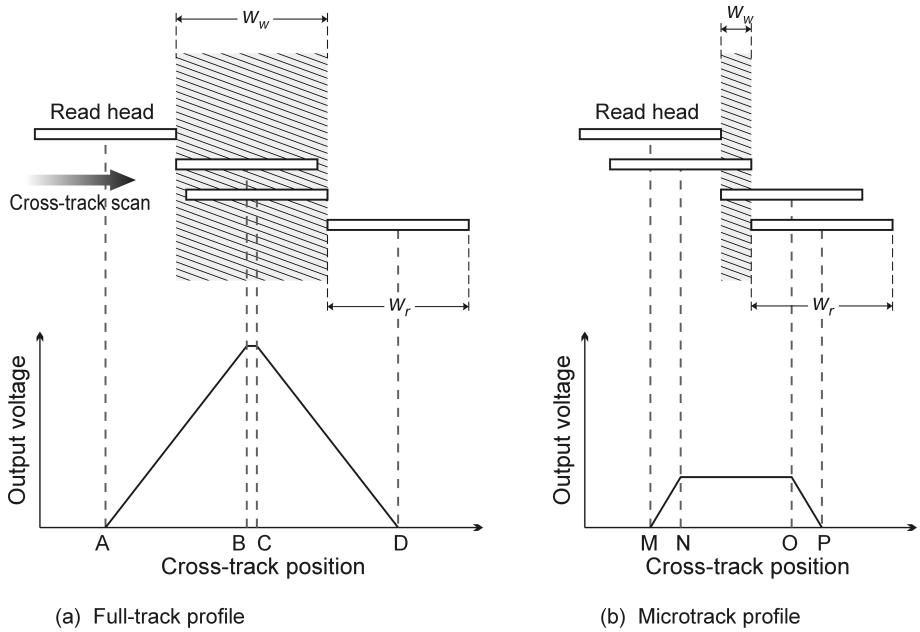


**Figure 5.1:** *Reading of full-track (a) and microtrack (b) profiles.*

Calculating $w_w$ and $w_r$ from Eq. (5.1) is straightforward if the equality relation between them is known, leading to

$$w_w = (\mathrm{AD} - \mathrm{BC})/2 \quad \& \quad w_r = (\mathrm{AD} + \mathrm{BC})/2 \qquad \text{for} \quad w_w < w_r \ , \tag{5.2}$$

$$w_w = (\mathrm{AD} + \mathrm{BC})/2 \quad \& \quad w_r = (\mathrm{AD} - \mathrm{BC})/2 \qquad \text{for} \quad w_w > w_r \ . \tag{5.3}$$

A triangular profile is obtained if the write and read widths are equal ($w_w = w_r = \mathrm{AD}/2$ and $\mathrm{BC} = 0$).

In practice, the edges of the recorded track may be less well defined than the center resulting in a cross track magnetization that does not really correspond to a square function. The effective write width corresponds therefore to the width of an ideal track, defined by a square function, that would create the most similar output. Distortions due to side writing, having a nonlinear contribution to the read signal, are therefore perceived as a decrease of the effective write width. They consequently cause the effective erase bands to increase. Such interpretations make sense from a practical point of view as long as deviations from the assumed square functions are not excessive. Similar considerations apply for the effective read width.

A *microtrack* is obtained by writing a test track and erasing it from the side(s) such that a much narrower track is left. The profile obtained by scanning the read head across is called a *microtrack profile*, which is drawn in Fig. 5.1 (b). The microtrack written width is considerably smaller than the read width ($w_w < w_r$) and they are given by

$$w_w = (\mathrm{MP} - \mathrm{NO})/2 \qquad \& \qquad w_r = (\mathrm{MP} + \mathrm{NO})/2\ . \tag{5.4}$$

If $w_w \ll w_r$, the microtrack profile reproduces closely the sensitivity function of the read head across the track. They are therefore extremely useful to characterize the cross-track response of read heads with a fine level of detail [5, 147, 162, 163]. The width of the microtrack has to be very small for achieving good resolution, however, it must ensure sufficient signal-to-noise ratio (SNR). Moreover, the magnetization within the microtrack has to be well defined, without distortions that may influence the replay process. In fact, preparation of microtracks is not always straightforward. The microtrack's features may depend on the particular method used to create it. The resulting magnetization pattern is most susceptible to its position relative to the full-track width and to the erase technique employed. Microtracks can be produced in the middle of a full-track by erasing at both sides or at the edge by erasing at only one side. They are called here *center-microtracks* and *edge-microtracks* respectively. Edge-microtracks usually suffer more severely from side writing effects [102]. Profiles of a full-track, center-microtrack, and edge-microtracks are shown in Fig. 5.4. The erase method applied to narrow the full-track may also influence the quality of the obtained microtrack. The erasure has to be complete and to leave the edge of the microtrack abrupt and free of distortions. Most consistent results were obtained by using two-sided dc erasure, where two currents of opposite sense are applied consecutively through the recording head. An extensive study of microtrack profiles reported in [147] led to a similar conclusion. Microtracks were also produced in the past by patterning of hard disk media using sputter etching to achieve better resolution than by erasing [164, 165].

### 5.2.2 Track Profiles of HSS Heads

Helical Scan Silicon (HSS) heads were introduced in Section 3.1.1. They feature narrow pole widths and are suitable for high track density recording. Track profiles measured with the three HSS heads from Table 3.1 and ME-2 tape (Table 3.3) are presented in this section. The HSS samples have small pole widths of 1.3 $\mu$m (HSS3-1), 3.5 $\mu$m (HSS1-1), and 6.2 $\mu$m (HSS2-1). The ME-2 tape feature thin magnetic layer $\delta = 50$ nm, and its coercivity is $H_c = 164$ kA/m. A square wave signal was written at $\lambda = 0.5$ $\mu$m and the fundamental was read as a function of the cross-track position. The experiments were performed at the optimum recording current of the heads, equal to 10 mA.

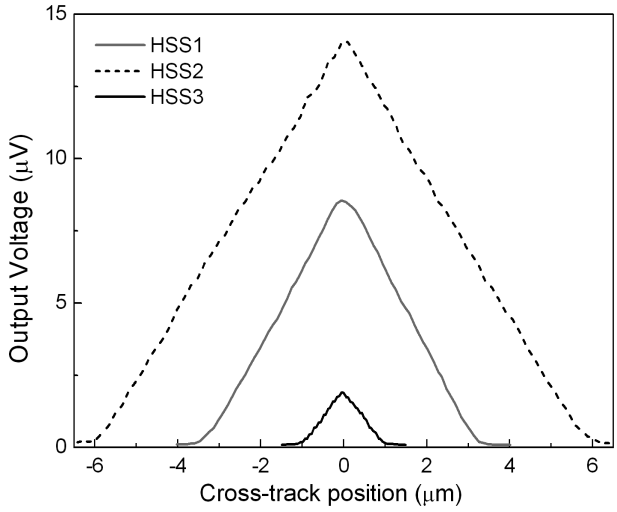


**Figure 5.2:** *Full-track profiles measured with the HSS heads and the ME-2 tape sample ($\delta = 50$ nm and $H_c = 164$ kA/m), for $\lambda = 0.5$ $\mu$m.*

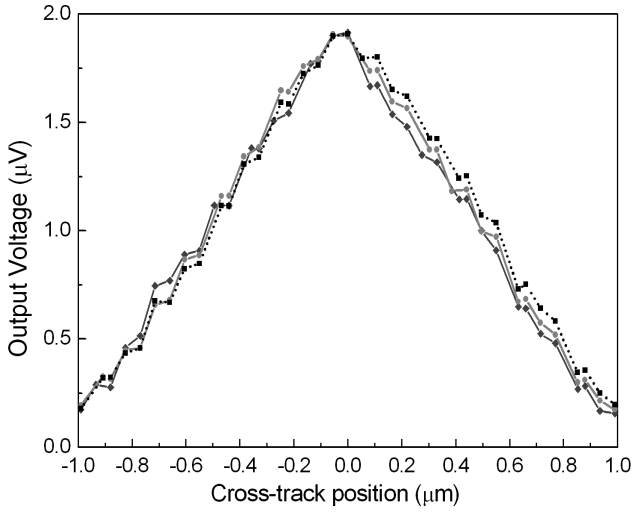


**Figure 5.3:** *Repeatability of cross-track read scans measured with the HSS3-1 head and ME-2 tape. The scan step was 55 nm, equal to the resolution of the position encoder. The staircase profiles suggest that the motion resolution was inferior, between 55 nm and 110 nm.*

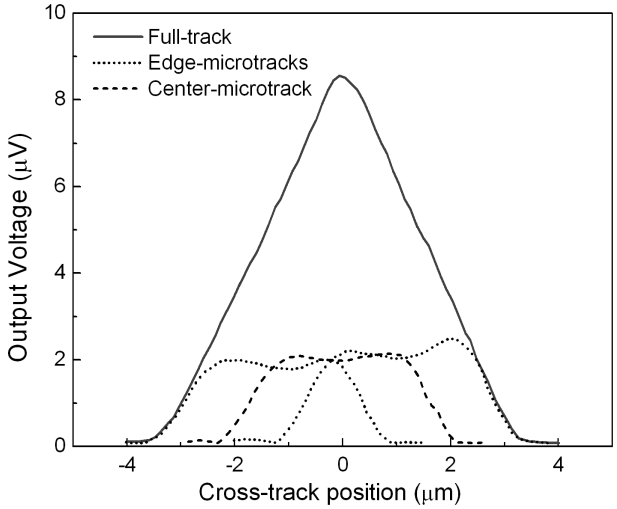


**Figure 5.4:** *Full-track and microtracks profiles measured with the HSS1-1 head and ME-2 tape ($\lambda = 0.5$ $\mu$m).*

Full-track profiles measured with each of the HSS samples are plotted in Fig. 5.2. The shape of the experimental track profiles is almost triangular, suggesting that the effective write and read widths have very close values. The interpretation of track profiles as described in the previous section is most probably satisfactory for these cases. Even the profile of the HSS3-1 head is well defined by a trapezoid/triangle, despite its narrow track width (1.3 $\mu$m) and large azimuth angle (35°). A closer look at multiple profiles measured with this head is revealing for the positioning accuracy of the tester. Three consecutive read scans of the same written track are shown in Fig. 5.3. The cross-track translation of the read head was performed with an incremental motion equal to the encoder resolution of the motorized stage, i.e. 55 nm. However, the stage could not deliver the same resolution, resulting in a staircase profile. Its practical resolution is estimated to be somewhere between 55 and 110 nm (i.e. between one and two encoder pulses). Without considering the errors due to the limited resolution, the positioning repeatability is evaluated around 50 nm. The positioning repeatability is influenced by head-to-tape instabilities and actuator errors, e.g. caused by elastic deformations in the drive mechanism.

Track and microtrack profiles measured with the HSS1-1 head and ME-2 tape are presented in Fig. 5.4. Edge- and center-microtracks were created as described in Section 5.2.1, their width being around 0.8 $\mu$m. Note that there are not significant differences between the microtrack profiles, meaning that side writing effects are not yet obvious at this particular wavelength ($\lambda = 0.5$ $\mu$m).

However, their plateau is not completely flat as one would expect. A kind of side reading interactions with phase deviations due to the azimuth angle of the head is suspected. The read scans were performed with a step of 110 nm, corresponding to two pulses of the position encoder. No staircase effect is noticeable in the output profiles as it was the case for the head HSS3-3 in Fig. 5.3. It is deduced that the cross-track positioning stage is able to consistently perform incremental motions of 110 nm.

## 5.3 Imbalanced Overwrite Method

Magnetic recording heads may present asymmetric write characteristics across the track width, depending on their construction and system operation. As pointed out in [146, 154, 155], side writing becomes asymmetric and erase bands worsen in hard disk drives when bits are written with a skew angle. In guardband-less helical scan tape systems, recording is performed with an azimuth angle that can be as large as 25° [20]. In such cases, the magnetic poles of the magnetic head are not symmetrical with respect to the tape running direction, presenting asymmetric field gradients at the gap edges. Asymmetric side writing may also be caused by uneven alignment of the poles.

An overwrite technique that can be applied to qualitatively analyze side writing and erasing of recording heads was developed. Overwrite is a complex process, where the residual signal is mainly determined by incomplete erasure due to insufficient write field, and overwrite modulation due to transition shifts [127, 166]. Both influences are usually more pronounced at the track edges than on-track, caused by the degradation of the write field [127, 167]. Edge effects can be enhanced by recording the original track at higher current than the overwriting data. They become clearly visible in the cross-track profiles of the overwrite pattern, allowing the study of side writing and erasing. This *imbalanced overwrite* method is particularly suitable to observe the side write asymmetry of recording heads. It is easy to implement and it is not demanding in terms of tracking accuracy. Imbalanced overwrite is an indirect observation method, however, it provides good qualitative insight into side write and erase effects.

### 5.3.1 Overwrite Procedure

The method involves writing a track deeply embedded into the recording medium by using high current and long wavelength. The width of the resulting track is large as this configuration is favorable to excessive side writing. The cross-track distribution of the magnetization is schematically shown for a relatively thick medium in Fig. 5.5 (a). The embedded track is then overwritten at shorter recording wavelength and lower current. The overwriting signal erases

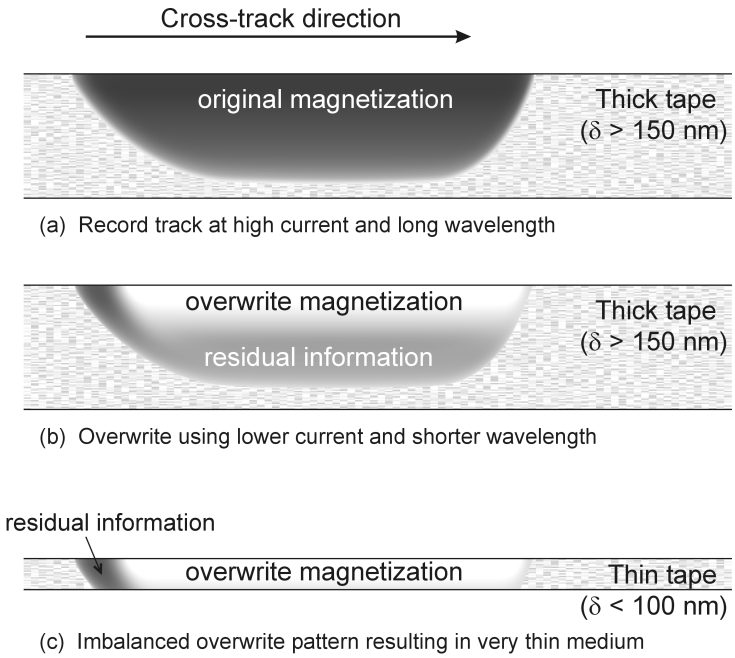


**Figure 5.5:** *Schematic representation of the imbalanced overwrite procedure and cross-track distribution of the magnetization pattern. An asymmetric write head was assumed.*

partially the embedded track, while it writes new information. Because the width of the embedded track is very large, its edges are hard to erase by the overwriting signal at moderate currents. This results in enhanced edge effects that significantly affect the residual information. Substantial residual data is therefore left at the edges and in the deep sublayers of the medium, as drawn in Fig. 5.5 (b). The edge effects are mainly strong if the pole alignment of the write head is poor. In Fig. 5.5, it was assumed that the recording head is well aligned at the right-hand side and misaligned at the left-hand side. The residual information is therefore asymmetrically distributed at the track edges. In the case of a very thin medium there is almost no residual left on-track as indicated in Fig. 5.5 (c). The residual information is concentrated then in the edges of the track.

The cross-track distribution of the residual and overwriting data can be traced by track profiles, allowing to monitor the extents to which old information is erased and new information is written. If the recording parameters for the embedded track are not varied, its residual is determined just by the overwriting

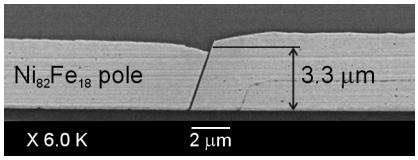


**Figure 5.6:** *SEM image of the magnetic poles of the HSS1-2 head sample.*

field. The evolution of the write and erase processes can therefore be studied as a function of the overwrite current and/or wavelength. The overwrite patterns (residual and overwriting tracks) can also be analyzed from MFM images.

### 5.3.2 Analysis of Side Write Asymmetry

The imbalanced overwrite method is applied to investigate the side write asymmetry of a narrow HSS head, labeled HSS1-2. It is an early stage prototype whose magnetic poles were particulary misaligned at one side, as visible in Fig. 5.6. A misalignment equal to 0.55 $\mu$m was measured from a SEM image with higher amplification. However, the alignment is very good at the opposite gap corner. The HSS1-2 head has a mean pole width of 3.3 $\mu$m, gap length of 0.11 $\mu$m, and azimuth angle equal to 20°. Three tape samples were selected for this study, with the thickness of the magnetic layers between 50 and 300 nm. Two samples are metal particulate, MP-1 and MP-2, the latter featuring higher coercivity and slightly lower magnetic layer thickness $\delta$. The third sample, ME-2, is metal evaporated having intermediate coercivity $H_c = 164$ kA/m and very low $\delta$ of 50 nm. Their main properties are resumed in Table 3.3.

In all experiments, the embedded track was written at 2.73 $\mu$m wavelength and 40 mA current. This is about two times higher the optimum recording current of the HSS1-2 sample ($I_w = 18$ mA). The wavelength of the overwriting track was fixed at 0.5 $\mu$m, while the current was varied from 5 to 40 mA. The profiles of the residual and of the overwriting track were read back in a single scan to avoid introducing offsets by two consecutive passes. The measurements presented here were performed with the tapes running in the same direction, with the narrower pole of the HSS1-2 head being the trailing pole.

#### Track Profiles of Overwrite Patterns for ME and MP media

Typical imbalanced overwrite profiles measured with the ME-2 sample are shown in Fig. 5.7. At $I_{owr} = 7.5$ mA, the profile of the residual signal is slightly distorted and seems to be shifted from the overwriting track. The shift comes from the fact that side writing is not symmetric in the embedded track,

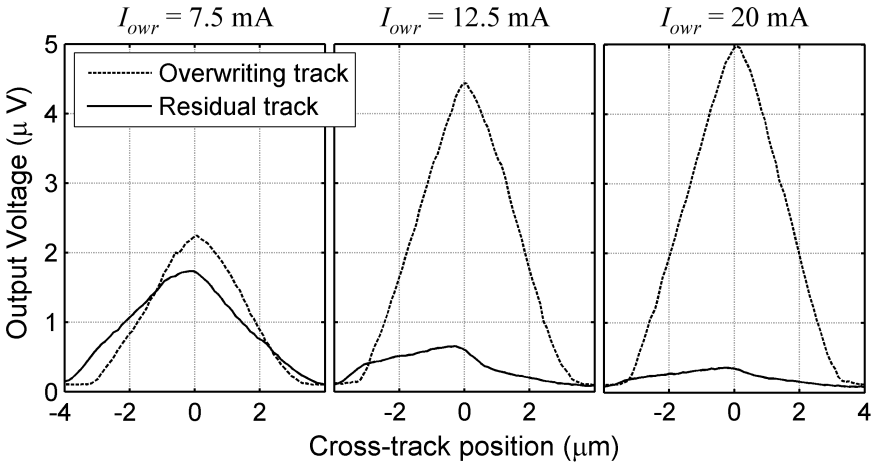


**Figure 5.7:** *Imbalanced overwrite profiles showing side write asymmetry, measured with the ME-2 tape.*

and it extends further at one edge than at the other. If the overwrite current is increased to $I_{owr} = 12.5$ mA, the embedded track is efficiently erased except at one edge. The residual signal is mainly concentrated in the edge where side writing was strong in the embedded track, corresponding to the side of the head with poor pole alignment. This edge is hard to erase at moderate overwrite currents, probably because the overwrite field is too weak at that flank of the embedded track. Nevertheless, the opposite edge seems to be erased as efficiently as the track center. The information in the hard-to-erase edge is better removed at higher current, $I_{owr} = 20$ mA. At the opposite side, no edge effects are visible at either current.
The width of the overwriting track is almost invariant with the recording current above $I_{owr} \approx 10$ mA. Still, a gradual spread of the erasure is observed at the misaligned edge as indicated by the embedded residual information. This means that the side erase width was gradually progressing but not the side write width, which would cause an increase of the erase band. At high current, the (over)write field expands further at the misaligned edge than at the well aligned one. However, the (over)write bubble is distorted at the misaligned edge and cannot effectively record information at short wavelength. The transition length is larger than the bit size due to the poor side field gradient and erasure mainly occurs. Therefore, increasing the current mainly produces a spread of the erase band at the misaligned edge. At the well aligned edge, both side write and erase effects are well confined.

Similar overwrite experiments were also performed using the MP-1 and

MP-2 samples. The profiles of the overwriting tracks do not differ significantly from those measured with ME-2. It was observed also for the MP tapes that the overwrite track width is roughly constant at moderate and high currents $I_{owr}$. The profiles of the residual data measured in all the samples at low overwrite currents, $I_{owr} = 5$ mA and $I_{owr} = 10$ mA, are shown in Fig. 5.8. Lower amplitude corresponds to higher overwrite current. At $I_{owr} = 5$ mA, the embedded track is slightly erased and no asymmetry in the profile of the residual signal is yet visible. The output is higher in the MP samples due to the strong residual signal in the bottom layers of the media. The width of the embedded track is almost the same in the samples MP-1 and ME-2, but is narrower in MP-2 probably because of its higher coercivity. If the overwrite current is increased to $I_{owr} = 10$ mA, the profiles become asymmetric. The effect is most pronounced in the sample ME-2 and least visible in the sample MP-2. The reduced sensitivity of the MP samples is attributed to the on-track residual signal coming from the bottom layers, which is high compared to the unerased signal at the edge. Edge effects are less strong in the sample MP-2 due to its larger coercivity, yet it has thinner magnetic layer than MP-1. In fact, the maximum recording depth of the HSS1-2 head with the MP-2 tape is estimated around 100 nm using Eq. (2.16). It is limited by the high tape coercivity, small gap length of the head, and the moderate saturation magnetic flux density $B_s$ of its permalloy poles. The recording depth is about half the thickness of the recording layer ($\delta = 200$ nm) and significant on-track residual information is expectable.

The appearance of the residual signal at increased overwrite currents is shown in Fig. 5.9 for $I_{owr} = 15$ mA and $I_{owr} = 30$ mA. At $I_{owr} = 15$ mA, most residual information in the thin ME-2 tape is concentrated in the hard-to-erase edge. The rest of the track seems to be uniformly erased. That is, at the edge with good pole alignment, the erasure is as efficient as in the track center. In the MP-1 sample, the amount of distortion is somewhat higher than at $I_{owr} = 10$ mA, probably because on-track erasure is stronger while a significant amount of information is still present in the hard-to-erase edge. In the MP-2 sample, edge effects and on-track amplitude seem to have been proportionally reduced. The cross-track profiles of the residual information become almost symmetric at $I_{owr} = 30$ mA. The current is high enough for spreading a strong field across the complete embedded track, able of erasing it uniformly. It is interesting to note that doubling the overwrite current from 15 to 30 mA strongly affects the erasure of the hard-to-erase edge, while the residue at the other edge and on-track remains nearly the same. In the ME-2 sample, the on-track residue looks unchanged. The on-track overwrite process is probably dominated by modulation in this sample, which is typical for thin recording layers [168]. The embedded track is more difficult to erase in the MP samples, due to the thick magnetic layers. The combination of incomplete erasure and modulation should underlie the overwrite process in these thick samples.

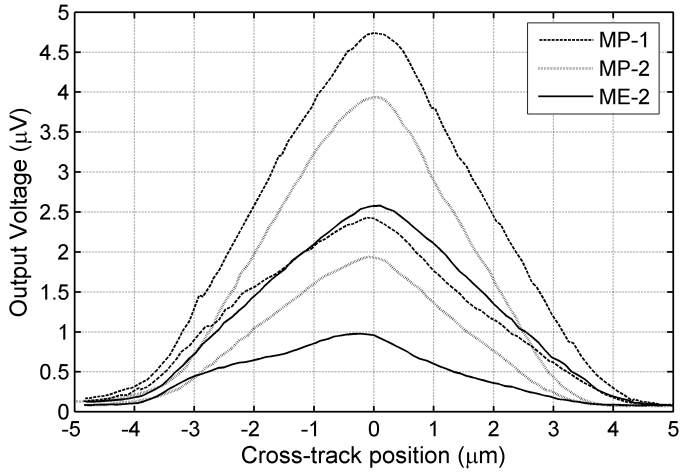


**Figure 5.8:** *Profiles of the embedded track residue measured with each tape sample for two low overwrite currents: $I_{owr} = 5$ mA and $I_{owr} = 10$ mA. Smaller amplitude corresponds to higher overwrite current.*

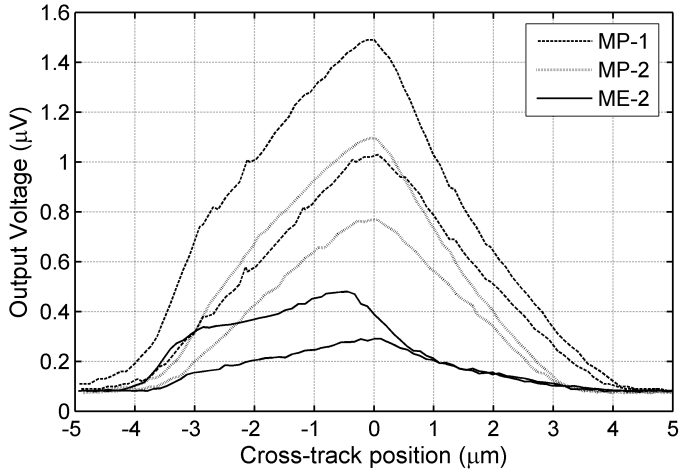


**Figure 5.9:** *Profiles of the embedded track residue measured with each tape sample for moderate and high overwrite currents: $I_{owr} = 15$ mA and $I_{owr} = 30$ mA.*

### MFM Study of Overwrite Patterns

The imbalanced overwrite patterns recorded in the ME-2 sample were also imaged by MFM. Multiple images corresponding to overwrite currents ranging between 5 and 20 mA are presented in Fig. 5.10. At small overwrite currents below 10 mA, the residue of the embedded track is considerably wider than the overwriting track. It is noticed that very strong phase shifts of the transitions are visible at its edges, due to the excessive side writing. After overwriting at larger currents (e.g. $I_{owr} = 12.5$ mA), residual information is only visible at one edge of the track. This edge is gradually better erased by increasing the overwrite current. At $I_{owr} = 20$ mA, just little residual information is noticeable in the hard-to-erase edge. These observations are in good agreement with the corresponding cross-track profile in Fig. 5.9.

The distributions of the residual and overwrite information across the track was extracted from MFM images via one dimensional FFT processing. They reflect the configuration of the magnetization pattern. The MFM-FFT scans confirmed that the width of the overwrite track is marginally affected at currents higher than $I_{owr} \approx 10$ mA. It is mainly the side erasure at the misaligned edge which spreads gradually. Typical scan results are plotted in Fig. 5.11. The overwrite currents are the same as in Fig. 5.7 to allow direct comparison between track profiling and MFM-FFT techniques. The same effects are visible in the MFM scans but with much better resolution. It is observed here again that at low current, $I_{owr} = 7.5$ mA, the overwrite process is dominated by incomplete erasure, which is more pronounced at the edges than on-track. Residual data is most substantial in the hard-to-erase edge, being very asymmetrically distributed across the track width. At the edge with good pole alignment, the residue is just slightly stronger than on-track. At $I_{owr} = 12.5$ mA, on-track erasure becomes more efficient and residual signal is mainly present in the hard-to-erase edge. Increasing the current to 20 mA does not affect much the on-track residual, but improves the erasure in the hard-to-erase edge. On-track overwrite is dominated by modulation at currents higher than 12.5 mA, while edge effects caused by incomplete erasure are present only in the hard-to-erase edge.

### Discussion of the Results

The cross-track profiles of the overwrite patterns and the MFM images show strong side write asymmetry of the investigated prototype head. At the edge with poor pole alignment, the write field is not well confined to the gap region and side writing is strong at long wavelength. However, at short wavelength erasure mainly occurs due to the poor side field gradient. The side written information in the embedded track is incompletely erased by the overwriting track at the misaligned edge. A gradual spread of the side erasure was observed by increasing the overwrite current, whereas the effective side written

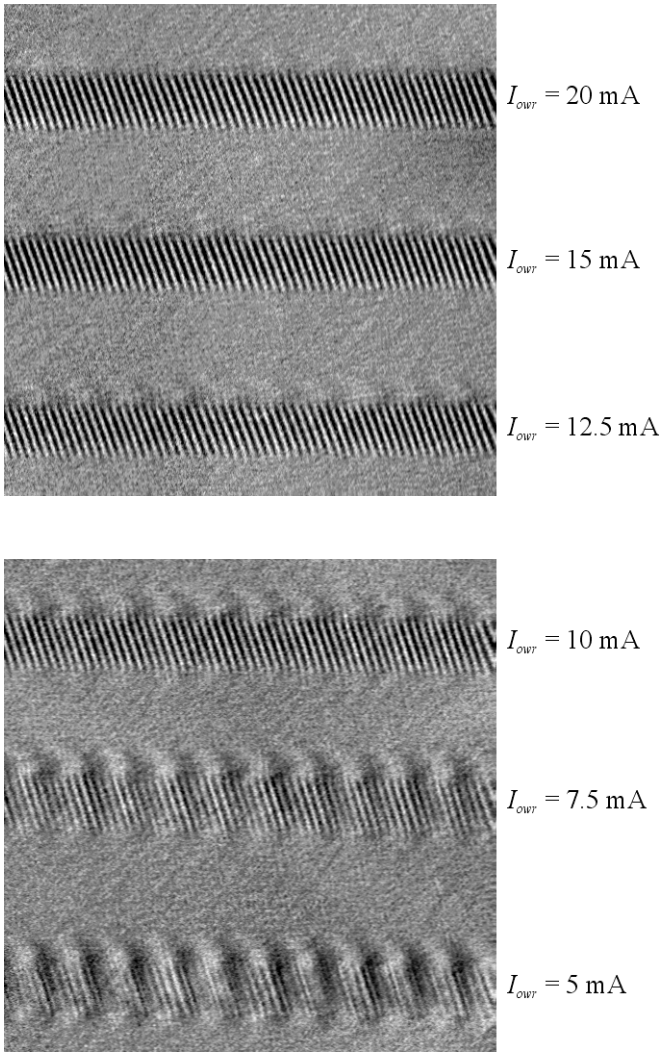


**Figure 5.10:** *MFM images (30 $\mu$m $\times$ 30 $\mu$m) representing six overwrite patterns written in the ME-2 sample at different currents $I_{owr}$.*

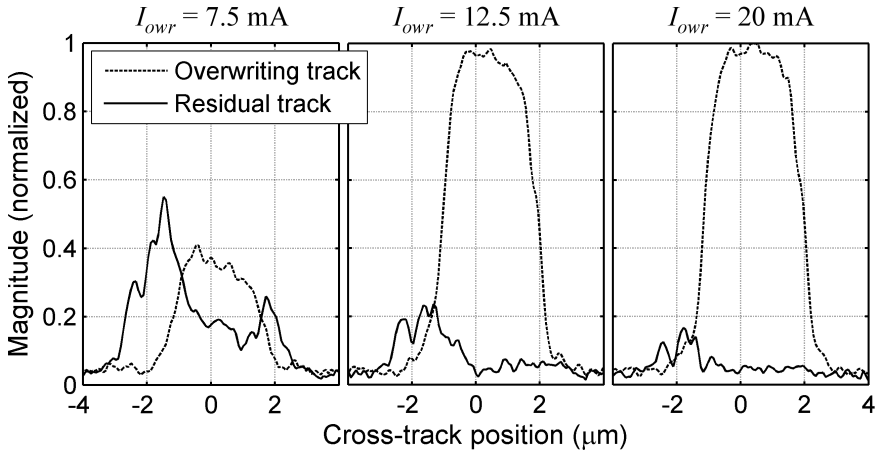


**Figure 5.11:** *Magnitude of the residual and overwriting signal across the track obtained from MFM images by FFT processing (ME-2 tape).*

width did not vary considerably. This can be related to a steady increase of the erase band with the recording current. At the well aligned edge, the erasure of the embedded track is almost as efficient as in the track center. This suggests that side writing is weak at that edge, due to finely confined side fringing field. Sharp side fields are suited to minimize edge effects such as erase bands. The azimuth angle may also cause side write asymmetry in the case of symmetrically aligned poles.

Imbalanced overwrite experiments were also performed with the MP tapes running in opposite direction. Strong side writing was still observed at the misaligned edge while it was well contained at the other edge. The profiles of the embedded residual information were very similar to those presented here. However, at the misaligned edge, the width of the overwrite track showed some increase with the overwrite current. This is explained by the fact that the side field gradient and geometry achieved at the larger trailing pole is more favorable to write short transitions. The side fields of misaligned heads were modeled in several works [5, 112, 113]. At the misaligned edge, better erase bands are therefore obtained for the tape moving direction resulting in a wider trailing pole. Still, they are larger than the erase bands achieved at good pole alignment.

The asymmetry observed by this method is not directly associated with the asymmetry of the write bubble at the overwrite current/frequency. It is also related to the asymmetry of the embedded pattern. Most probably, the high current used to write the embedded track causes saturation of the recording poles of the head. Serious distortion of the write bubble is likely to occur and

consequently of the recorded pattern. This is clearly visible at the edges, where strong transition phase shifts are observed in the MFM images (Fig. 5.10). On-track aberrations are also expected such as strong phase shifts within the depth of the medium or surface erasure. However, such distortions are not believed to significantly affect the principle of the investigation method. In fact, the residual information in the hard-to-erase edge was used as a reference to monitor the evolution of the write bubble at the overwrite current. The dependence of the write bubble on the overwrite current was obvious around the optimum recording current (e.g. from 12.5 mA to 25 mA), at the misaligned edge. Such dependence was not visible for the well aligned edge, even in reversed recording direction. Therefore, an asymmetry of the (over)write bubble due to the misaligned poles can be deduced. There was a gradual spread of the side erasure at the hard-to-erase edge, related to stronger side write. This is not a direct observation method, however, it gives a good picture of side write and erase effects. The analysis can be simply conducted from track profiles and does not require high scan accuracy.

#### Additional Comments on the Method

The imbalanced overwrite method can also be used to evidence the effects of the head azimuth angle or of the trailing pole on side write performances. Recording heads such as HSS samples (Fig. 3.2) and MIG-1 (Fig. 3.3) were investigated. The experiments were mainly performed with ME-2 tape and the method was slightly modified to achieve better sensitivity. After obtaining an overwrite pattern like in Fig. 5.5 (c), the head is displaced to erase half side of the track. Removing the magnetization at one edge allows to emphasize side writing and erasing effects at the other edge. Each edge can therefore be analyzed individually and with better detail. Moreover, the embedded track can be recorded at currents closer to the optimum write current, reducing the distortions of the pattern. Measurements were performed for both moving directions of the tape to examine the effect of the trailing pole. It was found that the alignment of the head poles is the most influencing factor for side writing/erasing and, to a less extent, the gap length. The side write performance also depends on the specific trailing pole, as it is the rear of the write bubble which determines the transition length and shift. The influence of the trailing pole was visible for heads with misaligned gap corners, such as MIG-1 or HSS1-2. At the same edge, side writing was better for the tape moving direction leading to a wider trailing pole. The results are in agreement with the asymmetric erase bands observed in helical scan recording systems [19]. Uneven side writing was hardly noticeable for HSS heads with very good alignment, even though the azimuth angle leads to asymmetric trailing poles. Such issues are investigated in more detail in Chapter 7, using an original technique based on the investigation of microtracks.

## 5.4 Conclusion

Side writing and erasing are generally evaluated using recording measurements such as track profiles or magnetic imaging techniques like MFM. While it achieves better resolution, MFM is an indirect and localized observation technique of the magnetization in the medium. It is a useful tool to examine track edge distortions such as phase shifts of the transitions, however, the erase bands may be reproduced differently by MFM than they are sensed by the read head. The influence of the track edges on the output of the read head is approachable by track profile measurements and the erase bands can be evaluated using appropriate techniques. Their implementation typically demands precise cross-track positioning of the head.

An imbalanced overwrite method suitable for qualitative studies of side writing was developed, requiring moderate track profiling capabilities. Edge effects become excessive if the original track is recorded at long wavelength and high current, so that its width is very large. Its edges are therefore hard to erase by the overwriting signal at practical currents and serve as references to monitor the side writing and erasing of the latter. The method is very sensitive to side write asymmetry and was applied to study a 3.3 $\mu$m wide HSS head, with the gap length of 0.11 $\mu$m. It was an early stage prototype with very good pole alignment at one edge and a misalignment of 0.55 $\mu$m at the other edge. The overwrite patterns were investigated from cross-track profiles with three types of ME and MP media, showing significant side write asymmetry. At the gap corner with poor pole alignment, write fields were not well confined in the gap region resulting in strong side writing. At the well aligned edge, side write effects were hardly noticeable. The experiments suggest that good alignment of the magnetic poles is crucial for reducing side writing.
The method proved to be very sensitive with the thin ME media ($\delta = 50$ nm), where the on-track residue was low and edge effects were dominant. Edge effects were still visible in thicker MP media ($\delta = 200$ nm and $\delta = 300$ nm) and appeared to attenuate at high coercivity ($H_c = 195$ kA/m). The overwrite patterns written in the ME tape were also imaged by MFM and analyzed by FFT processing. Good agreement was found between the track profiles and the MFM images, the latter providing increased level of detail.

Chapter 6

# Novel Interpretation Model of Triple-Track Profiles

The triple-track profiling technique was introduced to study track edge effects in hard disk recording [64]. A triple-track pattern is created by first recording in a first step two side tracks at equal frequency and separated by a distance shorter than the write width. A central track is afterward recorded in between by partially overlapping and overwriting their edges, such that two erase bands are produced. The triple-track profile is acquired by scanning the read head across the pattern and capturing the output signal. The central track and the side tracks must have different frequencies such that their respective outputs can be effectively separated by filtering. If a spectrum analyzer is used, the signal fundamentals can be precisely addressed with narrow resolution bandwidth. The erase bands can be extracted from triple-track profiles as originally described in [64]. They were evaluated assuming constant read width of the replay head across the whole pattern. The practice is therefore appropriate only if the central and side tracks have very close frequencies, resulting in approximately equal read widths. A new interpretation technique able to deal with much different frequencies is presented here. It allows measuring the erase bands as well as the relative side read widths. The method is shown to be appropriate for investigating edge effects in high density tape recording. It was applied to study Helical Scan Silicon (HSS) heads and metal-in-gap (MIG) heads with narrow track widths between 3.5 $\mu$m and 6.2 $\mu$m. Different metal evaporated (ME) and metal particulate (MP) tapes were employed. Finally, erase bands obtained by triple-track profiling are compared with results from erase profiles and magnetic force microscope (MFM) imaging.

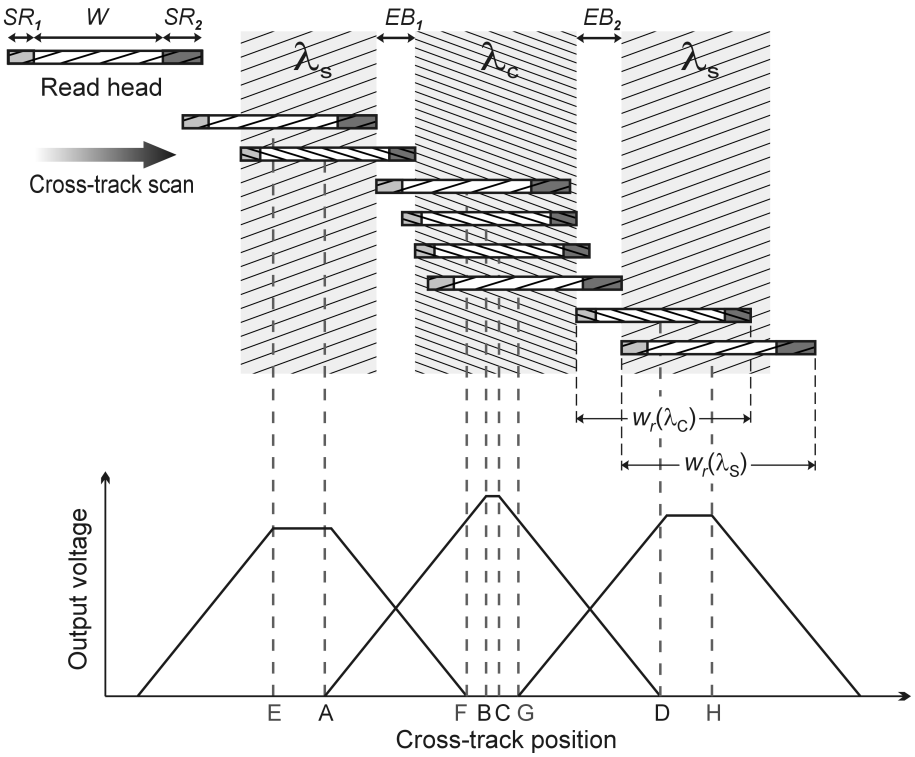


**Figure 6.1:** *Schematic diagram of a triple-track pattern and predicted replay profiles. Wavelength dependence of side reading is considered. The read width was assumed to be larger than the write width.*

## 6.1 Model Description

The effective read width of a replay head increases with the recording wavelength due to side reading [62, 98]. This aspect is treated in more detail in Section 2.5.2. Moreover, side read as well as side write could manifest differently at each edge of the head depending on its symmetry. From these considerations, a more consistent model for the effective read width is proposed, described by

$$w_r = W + SR_1(\lambda) + SR_2(\lambda) \ , \tag{6.1}$$

where $W$ is a reference width, wavelength independent, and $SR_1(\lambda)$ and $SR_2(\lambda)$ account for side reading at each flank of the head. Their values depend on the wavelength. The response of the read element across the track is assumed to be a square function, as previously discussed in Section 5.2.1.

By applying the read head model from Eq. (6.1) to a triple-track pattern, one can predict the output profiles drawn in Fig. 6.1. This scheme and the resulting calculations assume a read width larger than the write width for the central track, i.e. $w_w(\lambda_c) \leq w_r(\lambda_c)$. The model is latter extended to the case when $w_w(\lambda_c) > w_r(\lambda_c)$. The side tracks have equal wavelength, $\lambda_s$, and their edges are overwritten by a central track at wavelength $\lambda_c$. When the acquisition is switched from $\lambda_s$ to $\lambda_c$, there is a relative change in the effective side read width given by

$$\Delta SR_i(\lambda_c, \lambda_s) = SR_i(\lambda_c) - SR_i(\lambda_s) \qquad \text{for} \quad i = 1,\, 2\ . \tag{6.2}$$

We note that $\Delta SR_i$ is null if the wavelengths of the central and side tracks are equal ($\lambda_c = \lambda_s$).
In terms of side erase bands and relative side read widths, we find from the diagram in Fig. 6.1 the following relations:

$$\begin{aligned} \mathrm{EA} &= EB_1 - \Delta SR_2 \qquad \& \qquad \mathrm{FC} = EB_1 + \Delta SR_1\ , \\ \mathrm{BG} &= EB_2 + \Delta SR_2 \qquad \& \qquad \mathrm{DH} = EB_2 - \Delta SR_1\ , \end{aligned} \tag{6.3}$$

where the erase bands, $EB_1$ and $EB_2$, can be asymmetrical. Erase bands and side read widths specific to each edge cannot be extracted from Eq. (6.3). Hence, we consider their mean values:

$$EB = (EB_1 + EB_2)/2\ , \tag{6.4}$$

$$\Delta SR = (\Delta SR_1 + \Delta SR_2)/2\ . \tag{6.5}$$

From Eqs. (6.3) and (6.4) we find two distinct equations giving the mean erase band independently:

$$EB' = (\mathrm{BG} + \mathrm{EA})/2 \qquad \& \qquad EB'' = (\mathrm{FC} + \mathrm{DH})/2\ , \tag{6.6}$$

where, in the ideal case, $EB = EB' = EB''$. The same can be applied to Eqs. (6.3) and (6.5) to get

$$\Delta SR' = (\mathrm{FC} - \mathrm{EA})/2 \qquad \& \qquad \Delta SR'' = (\mathrm{BG} - \mathrm{DH})/2\ . \tag{6.7}$$

It is noted that no information from the right side track is needed to determine $\Delta SR'$, and no information from the left side track is needed to calculate $\Delta SR''$. In a real case, we may find two different values for the same quantity due to measurements errors and/or model approximations (e.g. square functions for the read head response and magnetization across the track). The difference between the values of $\Delta SR'$ and $\Delta SR''$ (or $EB'$ and $EB''$) can be interpreted as an indication for the precision of the measurement, and it is useful to average them for getting finer results:

$$\Delta SR = (\Delta SR' + \Delta SR'')/2 \qquad \& \qquad EB = (EB' + EB'')/2\ . \tag{6.8}$$

One can remark from Eqs. (6.6) and (6.7) that $\Delta SR' - \Delta SR'' = -(EB' - EB'')$.

It should be reminded that Eqs. (6.3), (6.6), and (6.7) apply for the case when $w_w(\lambda_c) \leq w_r(\lambda_c)$. In the contrary situation, when $w_w(\lambda_c) > w_r(\lambda_c)$, the erase bands and the relative side read widths are readily found to be expressed as

$$\begin{aligned} EB' &= (\mathrm{CG} + \mathrm{EA})/2 \quad \& \quad EB'' = (\mathrm{FB} + \mathrm{DH})/2 \ , \\ \Delta SR' &= (\mathrm{FB} - \mathrm{EA})/2 \quad \& \quad \Delta SR'' = (\mathrm{CG} - \mathrm{DH})/2 \ , \end{aligned} \tag{6.9}$$

using the same notations for the profiles as in Fig. 6.1. The write width of the side tracks is considered to be always smaller than their corresponding read width. This is normally the case as the side tracks are partially erased by the central track.

## 6.2 Experimental Procedure

An algorithm to interpret experimental triple-track profiles according to the model introduced in the previous section was developed. The program fits each individual track scan into a trapezoid and then calculates the erase bands and relative side read widths. The fitting method may influence the robustness and the accuracy of the estimations. Special attention was therefore given to optimize it and extensive tests were performed for validation. A linear fit based on least squares minimization was implemented for the side ramps of the profile, which is a straightforward procedure. The fitting was usually performed from 10% to 90% of the maximum amplitude (or 20% to 80% for heads with strong edge effects). Fitting the top plateau of the profile is less evident as distortions are often present in this region, as visible in Fig. 5.4 and Fig. 6.4. The principle of the method retained was to intermediately place the plateau at the maximum amplitude of the profile and then trying to lower it by fitting the points contained within its central region. The size of the central region was taken as 50% of the plateau length.

The triple-track profile measurements were performed in the frequency domain using a spectrum analyzer for signal capture. After recording the triple-track pattern, the output was read back in a single scan by switching between the acquisition frequencies at each head position. The step of the scan was generally 110 nm for heads with the pole width below 4 $\mu$m, and 165 nm for the larger ones. The tape-to-head velocity was relatively low at 3 m/s, in order to ensure very smooth contact and linear frequency response for all the heads investigated. The triple-track patterns were read back using the same inductive head as for writing. All tracks were recorded under the same azimuth angle as a single head was used for each measurement. Alternating positive and negative azimuth angles, as in real drives, is believed to have little or no influence on

the erase bands. It is rather the corresponding trailing pole of the write head which influences the side writing behavior.

## 6.3 Analysis of Triple-Track Profile Measurements

Experimental data reflecting the capabilities of the triple-track profiling model to analyze edge effects in magnetic tape recording is presented in this section. Measurements performed with two inductive heads are analyzed, featuring similar track widths and gap lengths but very different construction. One is the HSS2-1 sample introduced in Section 3.1.1. It is fabricated using advanced thin-film technology and its magnetic poles are very well aligned, as visible in Fig. 3.2 (b). The second device is a metal-in-gap (MIG) ferrite head, labeled MIG-1, described in Section 3.1.2. An image of its magnetic poles is shown in Fig. 3.3. The MIG-1 and HSS2-1 heads have close pole widths of 5.5 $\mu$m and 6.2 $\mu$m respectively. They also feature equal gap lengths of 0.2 $\mu$m, while their first gap nulls were found at wavelengths around 0.23 $\mu$m. The azimuth angle is 10° for MIG-1 and 15° for HSS2-1. However, the alignment of their magnetic poles is substantially different, being worst for the MIG-1 head. This is typical for ferrite heads as they are fabricated using micromachining processes with limited miniaturization capabilities.
The measurements were performed using the ME-2 tape sample, having a thin magnetic layer $\delta = 50$ nm (see Table 3.3). The wavelengths of the central and side tracks were $\lambda_c = 0.6$ $\mu$m and $\lambda_s = 0.5$ $\mu$m respectively. The heads were operated at their optimum recording current, of 10 mA for HSS2-1 and 20 mA for MIG-1.

### 6.3.1 Well Aligned HSS Head

Typical triple-track profiles measured with the head HSS2-1 are given in Fig. 6.2 and Fig. 6.3. Such plots are generated by the program employed to interpret the experimental data. The effective read width of the HSS2-1 was found to be slightly larger than the write width ($w_r > w_w$), such that Eqs. (6.6) and (6.7) were used in the program. The two triple-track scan measurements in Fig. 6.2 present sharp profiles which are accurately fitted by trapezoids. Deviations of the experimental data that could be related to edge effects are not noticeable. Low values were calculated indeed for the effective erase band $EB$, equal to 0.26 $\mu$m and 0.21 $\mu$m for each respective measurement. There is a difference of 0.05 $\mu$m between the two estimations, which is acceptable for the recording tester and model employed. Note that the two profiles correspond to distinctly recorded triple-track patterns, not just different read scans. The relative side read width should approach zero as the central and side tracks have close wavelengths. The $\Delta SR$ values extracted from the two patterns were 0.04 $\mu$m and

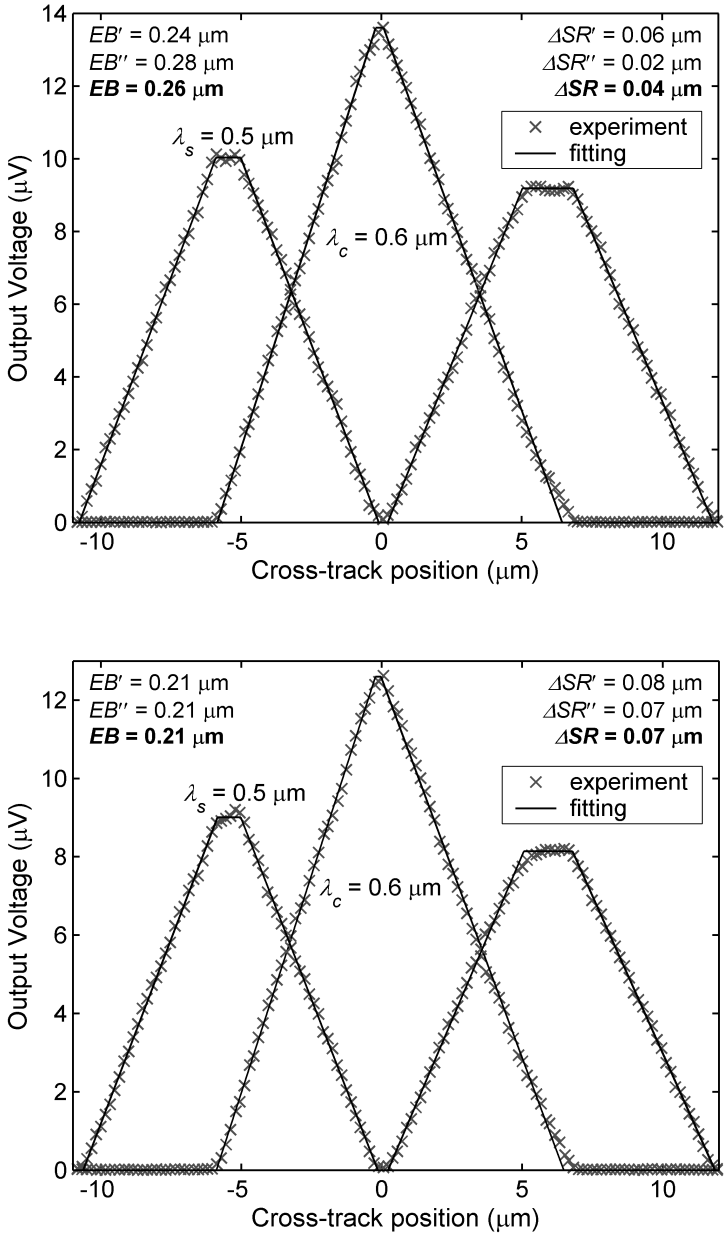


**Figure 6.2:** *Two triple-track profiles measured with the HSS2-1 head and ME-2 tape. The erase band's estimations differ with 0.05 μm.*

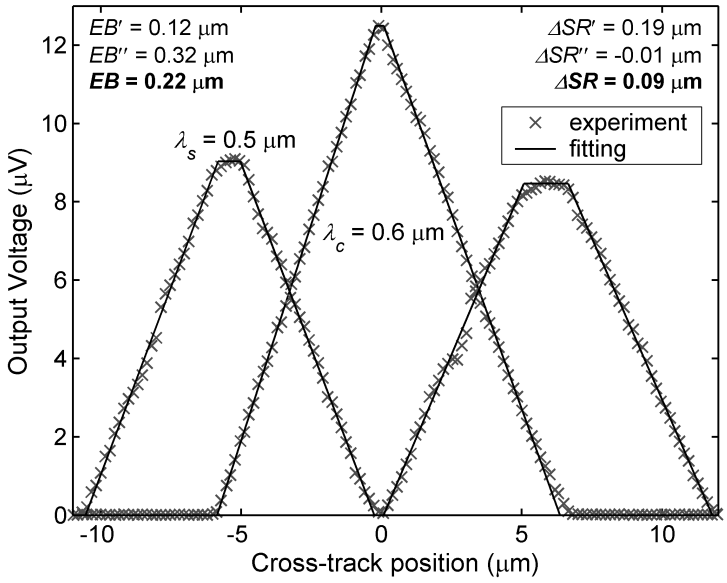


**Figure 6.3:** *Triple-track profile measured with the HSS2-1 head and ME-2 tape, featuring some instabilities.*

0.07 $\mu$m respectively, but slightly smaller amounts were expected (e.g. between 0.01 $\mu$m and 0.03 $\mu$m). However, the difference is not significant and could be due to measurement errors and/or model approximations.

Each triple-track profile in Fig. 6.2 led to close values for $EB'$ and $EB''$ (or $\Delta SR'$ and $\Delta SR''$). According to our model, this would suggest that the read scans were performed rather accurately. The triple-track profile from Fig. 6.3 presents some instabilities, despite being measured in exactly the same conditions. The output fluctuations seem to be more pronounced for the side tracks than for the central one, even though they were read together in the same scan. Therefore, they may also be caused by other sources than just positioning inaccuracies. Such instabilities may sometimes appear in the measurements, their origin being not fully understood. A significant gap of 0.2 $\mu$m between the values of $EB'$ and $EB''$ is noticed. The spread indicates that the precision of the estimations is limited and can be probably related to the fluctuations observed in the profile. However, the final value of the erase band $EB$, calculated by averaging $EB'$ and $EB''$ as in Eq. (6.8), is in the same range as those found from the more accurate profiles in Fig. 6.2. The same apply for the relative side read width $\Delta SR$. That is, the measurement is still usable despite the instabilities observed. Taking the average value of $EB'$ and $EB''$, as well as of

$\Delta SR'$ and $\Delta SR''$, is indeed effective for getting finer results.

### 6.3.2 Ferrite MIG Head

Two triple-track profile experiments performed with the MIG-1 head are shown in Fig. 6.4. Its effective write width is judged to be somewhat larger than the read width, implying the use of Eq. (6.9) in the evaluation model. They are approximately equal at $\lambda = 0.6$ $\mu$m, as the fit to the central track is almost triangular. The triple-track scans measured with the MIG-1 head are less sharp as those obtained with the HSS3-1 head. The corners of the profiles are not well defined and alterations from the trapezoid format are visible, being probably due to relatively strong edge effects. The top of the side tracks' profiles is not flat as expected, the deviations being antisymmetric wit respect to the central track. Both side writing and reading are suspected to cause distortions. In such cases, the lateral fitting of the profiles has to be applied to the region where the output varies rather linearly. For the profiles measured with the MIG-1 head, the fitting was performed from 20% to 80% of the maximum amplitude. Relatively wide erase bands were calculated for the MIG-1 head from the triple-track experiments in Fig. 6.4. The erase bands $EB$ obtained from the two patterns are coherent, equal to 0.84 $\mu$m and 0.89 $\mu$m respectively. The relative side read width $\Delta SR$ is higher than expected in both cases, being 0.14 $\mu$m and 0.16 $\mu$m. Some difference between $EB'$ and $EB''$ is noticeable in each case, without being excessive. Although the measurements shown good repeatability, some issues were left to be considered. They include the rather high $\Delta SR$ and the deviations observed in the profiles, their origin as well as the influence on the parameters calculated.

In a triple-track pattern, one edge of each side track is overwritten (erased) by the central track. It is expected that the overwritten edge is exempted of severe magnetization distortions caused by side writing, such as important phase shifts. However, such distortions may be present in the other edge of the side track. This affected edge can be simply cleaned by dc erasure. Triple-track patterns were therefore prepared with the MIG-1 head, which was also employed to dc erase the outer edge of the side tracks. Two experimental profiles are shown in Fig. 6.5, obtained by dc erasing the side tracks at slightly different positions. The improved shape of the side tracks profiles is immediately visible. Their fitting is more accurate and the plateaux are flat. The profiles are still rounded at the corners due to side reading, however, deviations caused by side writing were mainly eliminated. The triple-track profiles comply more accurately with the model, and are processed with increased precision. The differences between $EB'$ and $EB''$ are very small for both measurements. The relative side read width $\Delta SR$ is around 0.06 $\mu$m, which is less than half the values obtained previously without using erasure. The smaller $\Delta SR$ is certainly more accurate. The values calculated for the erase bands are in line with those

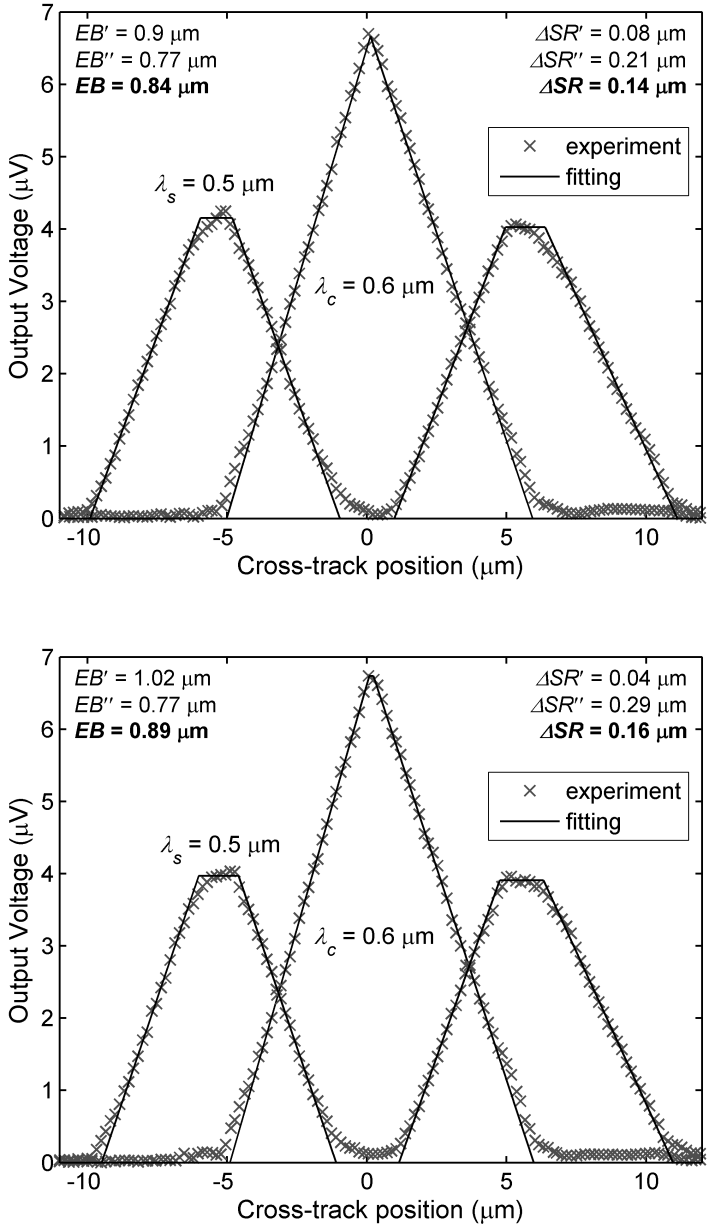


**Figure 6.4:** *Two triple-track profiles measured with the MIG-1 head and ME-2 tape. Good repeatability, however, edge effects are visible in the track scans which are not accurately fitted by trapezoids.*

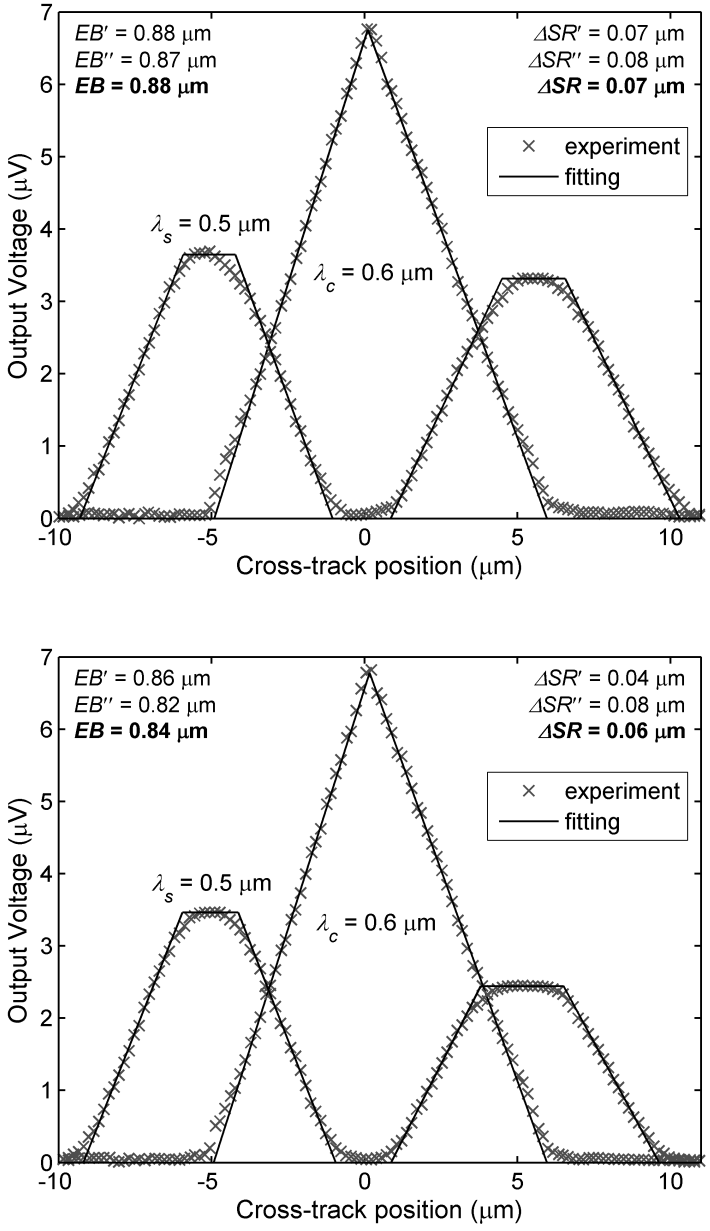


**Figure 6.5:** *Triple-track profiles measured with the MIG-1 head and ME-2 tape, with the outer edge of the side tracks being dc erased. Fitting of the side tracks is improved by erasing the edges.*

extracted from the earlier measurements.
It seems that the profiles' alterations in the non-erased case affected the evaluation precision of $\Delta SR$ but not of $EB$. These inaccuracies were found to be caused to a large extent by side writing at the outer edge of the side tracks. The edge written magnetization suffer from distortions such as transition broadening and phase shifts [99, 104, 105, 107]. Its contribution to the read signal beside the on-track data is therefore nonlinear. This would alter the shape of the track profiles, especially if side writing is strong as for the MIG-1 head. The triple-track profiles in Fig. 6.4 were clearly affected. The effect was most visible for the side tracks from the asymmetry of their top plateaux. The asymmetry came from the fact that side written magnetization was only present in one edge, the other being overwritten by the central track. The edges of the central track were probably also affected by side writing. The effects were less visible due to the triangular shape of the profile and the more symmetric configuration. However, side writing is far from being balanced for this head as its trailing poles have asymmetric edges (Fig. 3.3). This was also found experimentally from *imbalanced overwrite* and *microtracks* (Section 7.3) measurements.

### 6.3.3 Discussion on Measured Erase Bands

The edge effects of the MIG-1 head are considerably stronger than for the HSS2-1 head. The erase bands measured from triple-track profiles were around 0.86 $\mu$m and 0.23 $\mu$m respectively, for a write wavelength equal to 0.6 $\mu$m. The large erase band of the MIG-1 head is due to the poor alignment of its magnetic poles. Similarly high values for ferrite recording heads were found in other works as well [19, 74]. Using mechanical trimming to align the poles of MIG heads was reported to result in considerably narrower erase bands [19, 20]. They were around 0.4 $\mu$m, measured from magnetic force microscope (MFM) images of overlapping tracks written at wavelengths of 0.5 $\mu$m and 0.7 $\mu$m. The head azimuth angle was 25° and the poles were trimmed parallel to the head-to-tape motion direction. The alignment along this direction was shown by micromagnetic modeling to be very efficient in confining the side writing [169]. The erase bands reported for the trimmed MIG heads are however higher than those measured in this work with the HSS2-1 head. Possible reasons could be better pole alignment of the HSS2-1 head, smaller azimuth angle, and higher tape coercivity. ME tapes with similarly low $M_r\delta$ were used in both cases, the coercivity of the ME-2 sample being slightly superior to that mentioned in [20].

### 6.3.4 Accuracy of the Triple-Track Model

The triple-track profiling model introduced here proved in multiple experiments to be suitable for investigating side writing and reading in narrow track tape recording. The tracking precision and stability of the recording setup is however

important for getting fine results and may be limiting factors. Even slight temperature variations during the read scan may influence the accuracy of the data. The measurements were therefore cautiously prepared and the evaluation errors of $EB$ and $\Delta SR$ are estimated at

$$\begin{aligned} \varepsilon(EB) &< \pm(0.1 \cdot EB + 0.1\ \mu m)\ , \\ \varepsilon(\Delta SR) &< \pm 0.15\ \mu m\ . \end{aligned} \tag{6.10}$$

In many cases, the precision was better than given in Eq. (6.10). It is reminded that the measurements were performed on a recording tester with tracking accuracy finer than $\pm 0.1$ $\mu$m, for short-range travels within 10 $\mu$m. Superior results should be achievable using a more advanced tester with low pressure, stable head-to-tape contact and precise actuation, as described in Section 4.2. The precision seemed generally to be slightly worse for $\Delta SR$ than for $EB$. It was observed from the triple-track profile measurements of the MIG-1 head that $\Delta SR$ is more likely to be influenced by side writing distortions. Inductive replay heads typically present constant read sensitivity across the track. Their response is therefore rather well approximated by a square function, if edge effects are moderate. It is especially at very long wavelengths (e.g. exceeding 2 $\mu$m) that side reading becomes excessive and the approximation does not hold any longer. However, such low densities are not of practical interest.

Anisotropic magnetoresistive (AMR) heads often present asymmetric read response [5, 120, 162], mainly depending on the biasing schemes employed. Giant magnetoresistive (GMR) heads feature symmetric sensitivity, however, their response may be influenced by side reading at very narrow track widths and considerable magnetic spacing. If the cross-track read response is far from being a square function, the triple-track interpretation method presented here is not applicable. More complex techniques should then be employed. It is possible, for instance, to model the output track profiles using a head sensitivity function other than square (e.g. with Gaussian edges). The distribution function of the magnetization may also be reconsidered. However, this would involve a series of new assumptions whose general applicability would still be limited. A better suited technique is believed to consist in measuring the sensitivity function of the read head from the output profile of a microtrack (Section 5.2.1). The triple-track profile is then processed by deconvolving the read response leading to the effective cross-track distribution of the magnetization. Estimation of the erase bands is then possible, for each edge of the write head. The main interest of the method comes from minimizing the number of a priori assumptions. However, the profiling measurements should be performed with very high mechanical accuracy and small scan steps, in order to optimally perform the deconvolution. The width of the microtrack has to be much below that of the read head in order to correctly reproduce the sensitivity function. The method is therefore limited by the erase resolution to create narrow microtracks and the read signal amplitude to measure their profiles.

## 6.4 Edge Effects of a 3.5 $\mu$m HSS Head

Triple-track profiles were applied to study the edge effects of the HSS1-1 head sample, presented in Section 3.1.1. It has a narrow pole width of 3.5 $\mu$m and its gap length is 0.11 $\mu$m. The gap null could not be precisely evaluated from the recording spectrum because of the poor SNR at very short wavelengths, below 0.16 $\mu$m. The alignment of its magnetic poles is perfect at one edge while it is somewhat worse at the other, as visible in Fig. 3.2 (a). The triple-track experiments were performed using ME and MP tapes, namely the ME-1 and MP-2 samples introduced in Table 3.3. The erase bands and the side read widths were evaluated at different recording densities and currents. If not otherwise stated, the optimum recording current equal to 10 mA was employed. The tape moving direction was the same for all measurements, with the narrower pole at the trailing side.

The erase bands are expected to depend on the wavelength of the central track rather than that of the side tracks. The erase width of the central track is given by the write bubble of the recording head (Section 2.5.1) and, in principle, it should not be affected by the pattern in the side tracks. Only if the demagnetizing field is comparable to the medium's switching field, one may imagine the erase width being dependent on the wavelength of the side tracks. This is typically not the case, as nowadays magnetic tapes are far from being employed close to their self-demagnetization limit. The effective write width of the central track is determined by side writing characteristics at its own recording frequency. Nevertheless, side writing may be influenced to a certain extent by magnetic interactions with the adjacent track, resulting in effects such as transition phase shifts [67, 108] and erase band modulation [109, 110].

A set of triple-track profile experiments was performed with the MP-2 tape to check the effect of the side tracks' wavelength on the erase bands. The central track was employed at fixed frequency to overwrite the side tracks recorded either at long or short wavelengths. An example is presented here, where the central track was recorded at $\lambda_c = 0.41$ $\mu$m. The wavelength of the side tracks was $\lambda_s = 1.5$ $\mu$m and $\lambda_s = 0.4$ $\mu$m for the triple-track profiles shown in Fig. 6.6 and Fig. 6.7 respectively. The erase bands calculated in each case are very close, the small difference of 0.02 $\mu$m being well below the accuracy limit of the measurement. Similar results were obtained using slightly larger central track wavelengths ($\lambda_c = 0.51$ $\mu$m and $\lambda_c = 0.62$ $\mu$m). In these measurements there is not a clear influence of the side track wavelength on the erase band widths. They are mostly affected by the recording density of the central track.

The edge effects of the HSS1-1 head were studied in more detail versus the frequency of the central track. Its wavelength was varied between 0.3 $\mu$m and 1.5 $\mu$m, while that of the side tracks was fixed at 0.5 $\mu$m. A triple-track profile measured at $\lambda_c = 0.35$ $\mu$m with the ME-1 tape sample is given in Fig. 6.8.

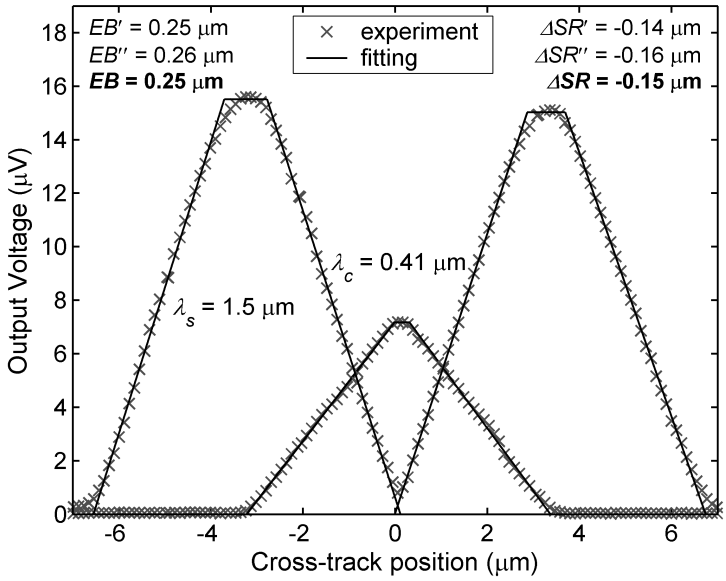


**Figure 6.6:** *Triple-track profile measured with the HSS1-1 head and MP-2 tape, at long wavelength of the side tracks ($\lambda_s = 1.5$ $\mu$m).*

It is observed that the profiles are well fitted by trapezoids and edge effects seem to be contained. The same is valid for the triple-track experiments from Fig. 6.6 and Fig. 6.7, performed with the MP-2 tape. It is also interesting to compare the profiles from Fig. 6.7 and Fig. 6.8 achieved at similar recording wavelengths but with different tapes. The top plateau of the central track scan is visibly larger with the MP-2 tape than with ME-1. This is explained by the narrower write width obtained with the MP-2 tape which has higher coercivity. The erase width is also narrower as indicated by the clearance between the side track scans (given by "FG" in Fig. 6.1). Note that the effective read width of the HSS1-1 head is larger than the write width in both cases.

The erase bands are plotted versus the recording density of the central track in Fig. 6.9. The measurements were performed at the optimum recording current ($I_w = 10$ mA) with the ME-1 and MP-2 tapes, but also at higher current $I_w = 20$ mA with the ME-1 sample. The erase bands measured at $I_w = 10$ mA with the two tapes differ just slightly, seeming to be a little narrower for MP-2. It is probably due to its higher coercivity, although the recording processes in the two types of media are not directly comparable because of different easy axis and microstructure. The erase bands are well confined in both cases without exceeding 0.35 $\mu$m even at short wavelengths around 0.31

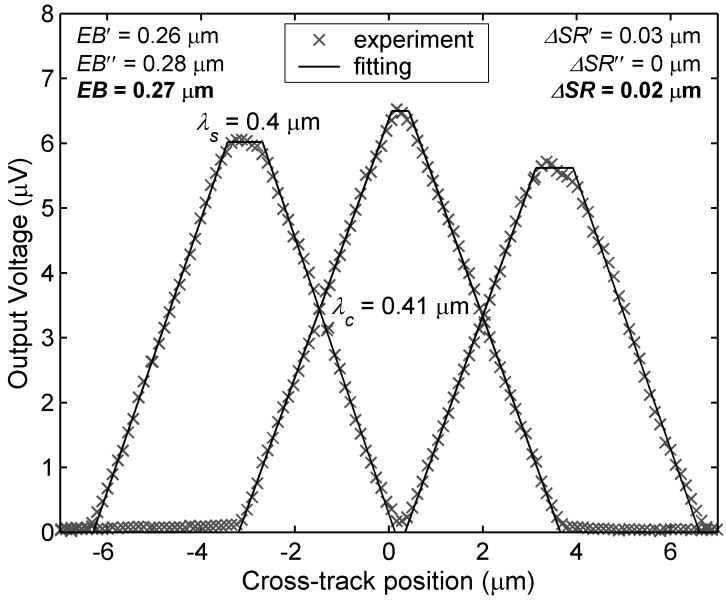


**Figure 6.7:** *Triple-track profile measured with the HSS1-1 head and MP-2 tape, at short wavelength of the side tracks ($\lambda_s = 0.4$ $\mu m$).*

$\mu$m. They are below 0.2 $\mu$m at long recording wavelengths. The erase bands are increased with about one third by doubling the recording current in the ME-1 tape. It is expected that their deterioration is worse at the edge of the head where the alignment of the magnetic poles is not optimum. Saturation of the poles' tips may occur at such high current resulting in the degradation of side writing performances, as suggested by micromagnetic modeling [107, 170]. Pole saturation arising from the gap corners was also observed experimentally by mapping the high frequency field of a recording head using a modified MFM [171]. It is interesting to note that all the curves in Fig. 6.9 have almost identical slopes, despite the different tapes and write currents employed. The slope may therefore depend on head properties that are not strongly affected by the write current. Moreover, at optimum current, the erase bands are marginally influenced by the recording media, whereas they are strongly dependent on the write head. This was clearly seen in Section 6.3 when comparing the erase bands of the HSS2-1 and MIG-1 heads. In fact, the erase bands of the HSS2-1 and HSS1-1 samples are relatively close. The HSS2-1 head has very well aligned poles and a gap length of 0.20 $\mu$m, while HSS1-1 has shorter gap length of 0.11 $\mu$m but the alignment is perfect only at one edge. It is reminded that the erase band evaluated by the triple-track model introduced here represents the

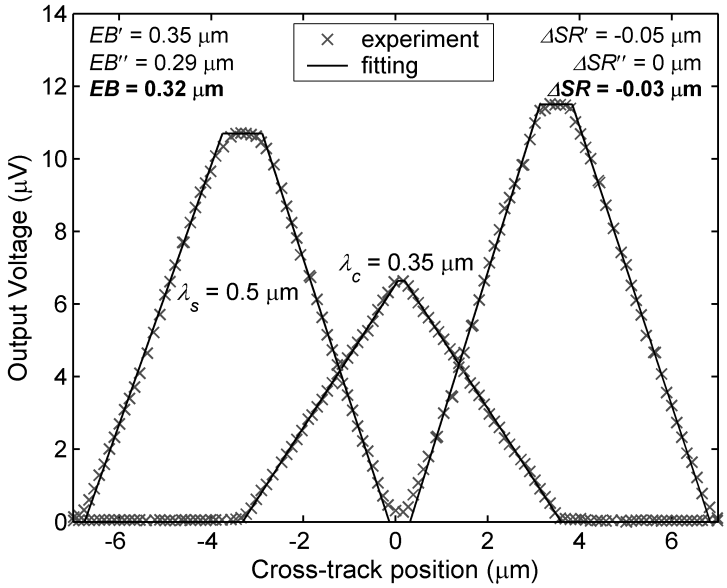


**Figure 6.8:** *Triple-track profile measured with the HSS1-1 head and ME-1 tape.*

average of the bands measured at each edge of the head (Section 6.1). The erase bands at the well aligned edge of the HSS1-1 are therefore expected to be even narrower than the values determined from the triple-track profiles. A similar head is studied in Section 6.5 and it is shown that the erase bands at the aligned edge are considerable smaller than at the misaligned edge.

The relative side read widths measured from the same triple-track profiles as above are plotted versus the wavelength $\lambda_c$ in Fig. 6.10. The curves are more noisy than for the erase bands, the evaluation of $\Delta SR$ featuring in general worst repeatability as already stated before. However, their dependence on the wavelength is roughly the same for the two tapes and write currents employed. This was expectable as side reading is mostly determined by the replay head assuming a well defined magnetization pattern. It was shown in Section 6.3.2 that the values calculated by our model for $\Delta SR$ may be influenced by strong magnetization distortions due to side writing. The similar $\Delta SR$ curves in Fig. 6.10 indicates that such distortions are not considerable with the HSS1-1 head, even at high write current. This is consistent with the narrow erase bands found.
A simplistic theoretical estimation of $\Delta SR$ is possible from Eq. (2.31), which

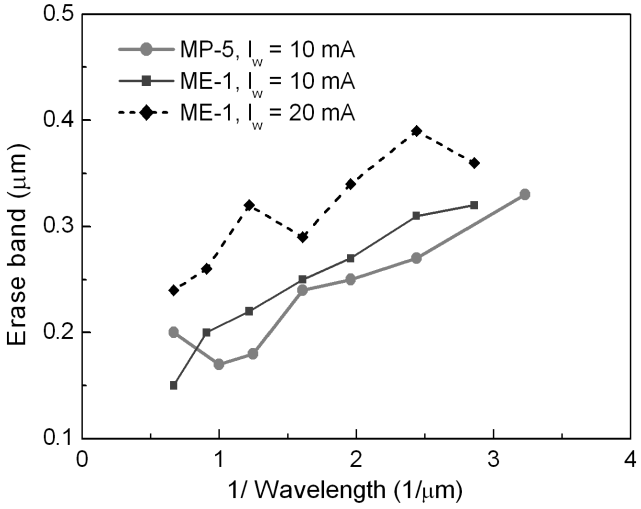


**Figure 6.9:** *Wavelength dependence of the erase bands measured for the HSS1-1 head with ME-1 and MP-2 tapes. Two recording currents were employed with the ME-1 tape.*

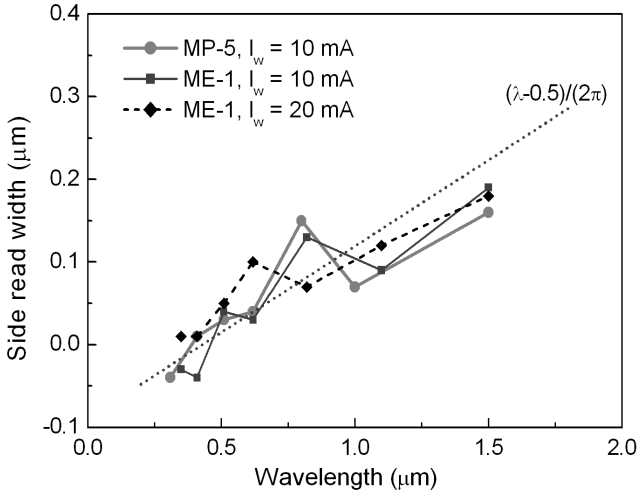


**Figure 6.10:** *Wavelength dependence of the side read width relative to $\lambda_s = 0.5$. The simplistic theoretical prediction from Eq. (6.11) is plotted in dotted line.*

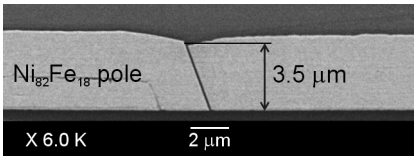


**Figure 6.11:** *SEM image of the recording poles of the HSS1-3 head.*

can be derived using Eqs. (6.1) and (6.2) to give

$$\Delta SR(\lambda_c) = \frac{\lambda_c - \lambda_s}{2\pi} \ , \tag{6.11}$$

where $\lambda_s$ is constant and equal to 0.5 $\mu$m in the present case. The line given by Eq. (6.11) is also plotted in Fig. 6.10. This theoretical estimation is based on a number of constraining assumptions such as $\lambda \gg \pi g_r$ and no azimuth angle. In azimuth recording, side reading over a wide write track is more complex. The side read voltage has variable phase, diverging from the on-track signal, resulting probably in reduced side read widths. This may explain the slower increase of the measured $\Delta SR$ with the wavelength than that given by Eq. (6.11). However, one should consider that Eq. (6.11) is a rather rough approximation in this case and the precision of the measurements is also limited. Side reading can be reduced by decreasing the gap length of the read heads, which is also required for improved sensitivity at short wavelengths. Moreover, shielded MR heads will be mainly employed and they offer better immunity to side reading at long wavelengths than inductive devices.

## 6.5 Track Profiles and MFM Imaging

The erase bands of a HSS1 type head similar to that investigated in Section 6.4 were analyzed using track profiling techniques and MFM imaging. The construction and the dimensions of the recording poles of the HSS1-3 sample are identical to those of the HSS1-1. That is, they have a pole width of 3.5 $\mu$m, a gap length of 0.11 $\mu$m, and an azimuth angle of $-20°$. The alignment of their poles is also very similar, both featuring a misalignment of 0.25 $\mu$m at one edge. However, they present slight differences in the structure of the magnetic circuit. An image of the recording poles of the HSS1-3 head is shown in Fig. 6.11.
The recording experiments were performed with the ME-2 tape, moving in the same direction as for the measurements presented in Section 6.4. The magnetization transitions were therefore written at the narrower pole of the HSS1-3 head. The optimum recording current of 10 mA was used. The ME-2 tape features a thin magnetic layer of 50 nm with coercivity of 164 kA/m (see Table 3.3). Triple-track profiles and *erase profiles* (described below) were applied

to analyze the erase bands of the HSS1-3 head. The triple-track patterns were recorded at fixed wavelength of the side tracks, $\lambda_s = 0.52$ $\mu$m, while that of the central track was varied between 0.27 $\mu$m and 2.14 $\mu$m. The erase bands were evaluated from the read profiles employing the model extensively discussed in this chapter. Triple-track patterns were also prepared for analysis by MFM imaging. The MFM tip employed has a resolution rated around 30 nm. The images were processed by one-dimensional fast Fourier transforms (FFT), applied line by line along the track direction. Care was taken to minimize the angular deviation from the track direction, which was less than 0.1°. The length of the scan lines was 20 $\mu$m for the images processed by FFT, implying a maximum transverse deviation below 30 nm. Its effect on the MFM signal profiles should not be significant.

### 6.5.1 Triple-Track and Erase Profiles

The erase bands of the HSS1-3 head were also measured from erase profiles, using a technique similar to that described in [146]. The method is based on progressively dc erasing one edge of a track and finding the width of the narrowed track where the read signal vanishes. This width approximates well the erase band at that edge. The dc erasure has to be performed at the same current as used to record the track. The track may be rewritten prior to each edge erase action. In fact, this would ensure a more robust measurement because positioning errors are not cumulated during multiple motions of the head. It also averts the effects of temperature variations and allows for averaging over several measurement cycles for the same erase offset ($EO$). This is very useful in tape recording, where the positioning accuracy is limited. The method employed here can be described by the following algorithm, $z$ being the cross-track position:

1. ac erase region locally
2. write test track ($z = 0$)
3. position the head at $z = EO$
4. dc erase the edge of the test track (same current as for writing)
5. position the head at $z = RO$
6. read signal
7. position the head at $z = 0$

A read offset ($RO$) was used in order to center the head with the narrowed track and avoid effects such as side reading or slight positioning errors. We note that $RO$ must have opposite sign than that of $EO$ (i.e. $RO$ is negative if $EO$ is positive). The erase offset is typically varied from some negative value close to the track width to a positive value (or vice versa). The measurement cycle can be repeated several times for each $EO$ value in order to average the data and get finer results.

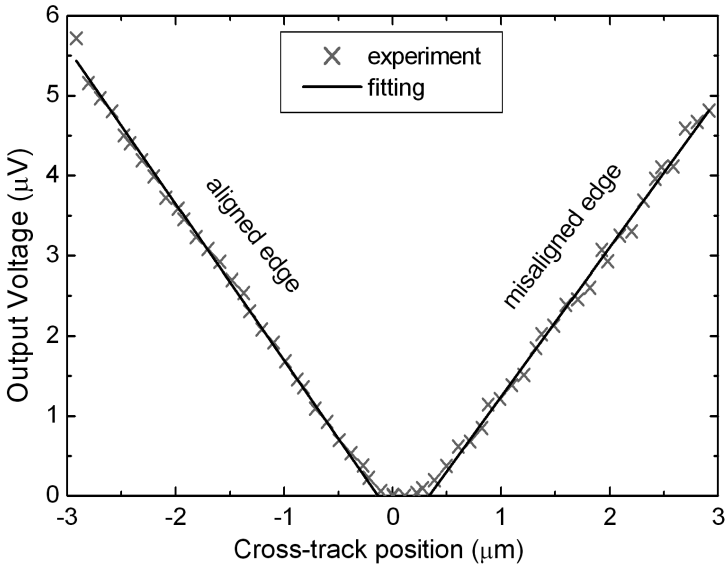


**Figure 6.12:** *Erase profile measured with the HSS1-3 head and ME-2 tape ($\lambda_c = 0.37$ $\mu$m). The asymmetry of the profile is caused by the larger erase band at the misaligned edge of the head.*

Erase profiles were applied to study the erase bands of diverse heads (e.g. MIG-2T and HSS2-1) and proved to give consistent results (not included in this thesis). The method is less sensitive to the experimental conditions than triple-track profiling and allows to study each edge of the head. However, it is not a direct measurement method as it employs erasure of the track edge rather than overwriting. Erase profiles were employed here to study the dependence of the erase bands on the edge of the HSS1-3 head. A typical measurement is shown in Fig. 6.12 for a recording wavelength of the test track equal to 0.37 $\mu$m. Three measurement cycles were performed and averaged for each data point and *RO* was plus or minus 0.5 $\mu$m. The two ramps of the experimental data are fitted linearly between 10% and 90%. The intercepts of the fitting lines with the horizontal axis approximate the erase bands at each edge of the head. It is easily noticed that the erase profile is asymmetric. This is due to the larger erase band caused at the misaligned edge of the HSS1-3 head. We deduced erase bands of 0.13 $\mu$m and 0.32 $\mu$m for the well aligned edge and the misaligned edge respectively. The absolute slopes of the two ramps are almost identical with less than 5% difference, indicating that the asymmetry is not related to inaccuracies of the cross-track positioning.

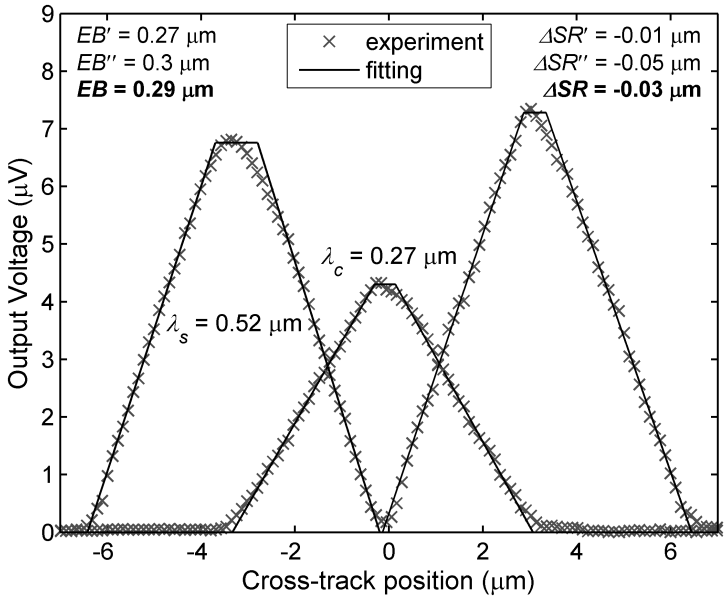


**Figure 6.13:** *Triple-track profile measured with the HSS1-3 head and ME-2 tape, at short wavelength* $\lambda_c = 0.27$ *μm.*

A typical triple-track profile measured with the HSS1-3 head is shown in Fig. 6.13, for $\lambda_c = 0.27$ $\mu$m. The profiles are adequately fitted by trapezoids, meaning that the method is applicable even at very short wavelengths and the tracks are not distorted. The erase bands seem to be well confined and a value around 0.29 $\mu$m was deduced. The erase bands measured from triple-track profiles and erase profiles are plotted versus the inverse of the wavelength in Fig. 6.14. The values extracted from triple-track profiles represent the average of the two erase bands created at each edge of the head. They were estimated for each specific edge using erase profiles. The erase band measured by triple-track profiling at a given wavelength is therefore expected to be about the average of those deduced from erase profiles. This is the case in Fig. 6.14 at medium and short wavelengths. At long wavelengths, the erase bands determined from triple-tracks are somewhat smaller than obtained by the other technique. This is believed to be caused by the modulation of the erase band when the partially overlapping tracks are written at large wavelengths. The erase band is quasi-null when the transitions in the adjacent tracks are in-phase, whereas there is a clear erased region in the out-of-phase case. This effect is clearly visible in the MFM image from Fig. 6.15 and was already reported before [108, 109, 110]. Modulation of the erase bands does not occur when the edge of the track is

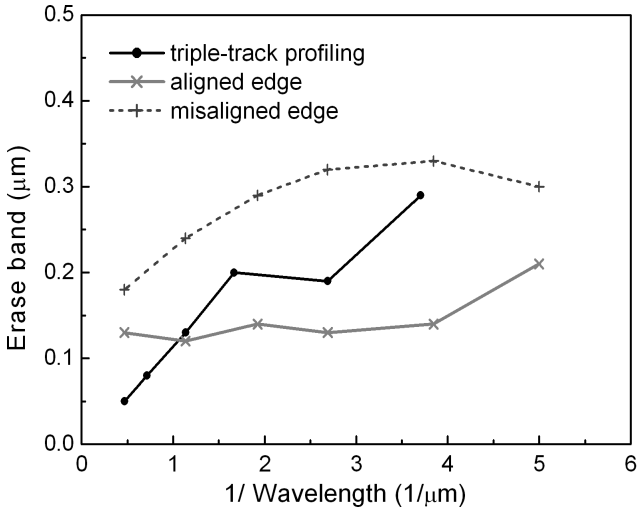


**Figure 6.14:** *Erase bands measured from triple-track profiles and erase profiles. The erase bands were addressed at each edge of the head using erase profiles.*

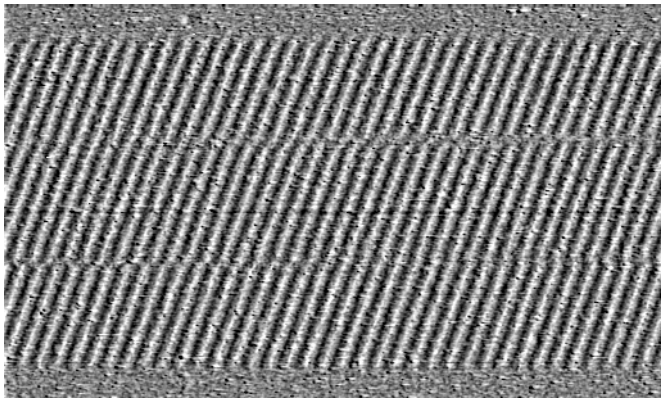

**Figure 6.15:** *MFM image (20 $\mu m$ × 12 $\mu m$) showing modulation of the erase bands. The wavelengths of the tracks are $\lambda_c = 0.51$ $\mu m$ and $\lambda_s = 0.52$. The larger erase band toward the top of the image was generated by the misaligned edge of the HSS1-3 head.*

dc erased. The values measured from erase profiles are therefore larger than deduced from triple-track profiles.
However, the modulation observed could also be caused to some extent by magnetic interactions between the MFM tip and the recorded patterns. When the transitions in the adjacent tracks are in-phase, the forces acting on the tip at the track edge are constructive. The same forces are destructive when the transitions are out-of-phase. Examination of Fig. 6.15 reveals that, in the out-of-phase case, the erase band is notably higher at the misaligned edge than at the well aligned one. The modulation of the erase band is therefore caused to a large extent by side writing effects. The aligned edge produces a sharp side field resulting in reduced modulation. Considerably narrower erase bands at that edge were also found from erase profile measurements as plotted in Fig. 6.14. They are around 0.2 $\mu$m even at the very short recording wavelength of 0.2 $\mu$m (254 kfc/in). These are believed to be the smallest erase bands reported to date in magnetic tape recording.

The erase bands measured from triple-track profiles with the HSS1-3 head and the ME-2 tape were smaller that those found for the HSS1-1 head and the ME-1 and MP-2 media (Section 6.4). The recording poles of the HSS1-3 and HSS1-1 heads are very similar, however, it is not known if they influenced the different results. The thin recording layer of the ME-2 tape and its higher coercivity compared to the ME-1 sample certainly contributed to reduce the erase bands. The side read widths deduced for the HSS1-3 head were very close to those measured with the HSS1-1 head and therefore are not presented here.

### 6.5.2 MFM Study of Erase Bands

Triple-track patterns were prepared for MFM imaging in the same conditions as those studied by track profiling. Typical images are shown in Fig. 6.16 and Fig. 6.17 for different values of the central track wavelength. The color scale is linear. At short wavelength, $\lambda_c = 0.26$ $\mu$m, the erase band at the misaligned edge is clearly distinguished while that at the well aligned edge is less evident. At long recording wavelength, in Fig. 6.17, some dependence of the track edges on the phase difference of the transitions in adjacent tracks is observed. This is noticeable especially at the side where the poles of the HSS1-3 head are misaligned. The effect was previously discussed concerning the pattern in Fig. 6.15, where it was better visible.

The magnitude (and phase) of the MFM signal along the track direction can be calculated by applying one dimensional FFT. It allows to extract the profile of the MFM signal across the imaged track patterns, giving a basic picture of the magnetization distribution. Results obtained using this technique are shown in Fig. 6.18, corresponding to the recorded patterns imaged in Fig. 6.16 and Fig. 6.17. The MFM-FFT profiles from the upper plot in Fig. 6.18 (with $\lambda_c = 0.26$ $\mu$m) exhibit higher noise. Both MFM images processed by FFT had

a scan line of 20 $\mu$m and were acquired in the same conditions except for the scan rate. The scan rate was 1.5 Hz for the upper plot and 1.0 Hz for the lower plot. A small enough rate is therefore recommended for reducing the noise. Note that a root mean square substraction of the noise floor was applied to the data from Fig. 6.18. This caused some increase of the noise amplitude at small signal. The data was normalized to the mean magnitude of the on-track signal at each wavelength.
The MFM-FFT profiles obtained for the pattern prepared at short wavelength of the central track ($\lambda_c = 0.26$ $\mu$m) clearly show asymmetric erase bands. They were determined from the half amplitude of the scans to be 0.27 $\mu$m for the misaligned edge and 0.1 $\mu$m for the well aligned edge. These values are just slightly smaller than those determined from erase profiles, by approximately 50 nm. This deviation could be well accounted for by the tip resolution and some slight misalignment error between the FFT lines and the track direction. Both measurement techniques show almost equivalent relative asymmetry of the erase bands, confirming that this effect is indeed present. However, the asymmetry is less evident at long wavelength of the central track, $\lambda_c = 0.88$ $\mu$m. The erase bands measured at half amplitude are about null. Finite erase bands superior to 0.1 $\mu$m were determined at the same wavelength from erase profiles as well as triple-track profiles (Fig. 6.14). The estimations from the half amplitude of the MFM-FFT profiles are therefore not accurate for this pattern. The slope of the MFM-FFT signal at the misaligned edge is somewhat worse than at the aligned edge, probably due to increased side write interaction. This is consistent with the stronger modulation of the erase bands observed at the misaligned edge in the images from Fig. 6.15 and Fig. 6.17. Phase shifts of the transitions depending on the magnetization patterns in the overlapping tracks were also noticed. The phase shifted regions of the transitions have a non-linear contribution to the read signal being sensed less effectively. They contribute more efficiently to the magnitude of the MFM-FFT signal but should influence its phase.

It was deduced also from other recorded patterns that better agreement between MFM-FFT and track profiling techniques is found at short recording wavelengths. The long range magnetic interactions between the MFM tip and the magnetization patterns could be somewhat increased at large wavelengths. Also, the estimation of the erase bands from the half amplitude of the FFT scan may not be the most appropriate method. In some works, the erase bands were evaluated from the power profiles of the MFM-FFT signal [109]. However, using that method here proved to considerably overestimate the erase bands both at short and long recording wavelengths. A similar conclusion was also drawn in [110], where a method based on the phase of the MFM-FFT signal is proposed. The erase band was defined as the region between the overlapping tracks (written at the same wavelength) where the phase coherency is significantly lost. We applied the method to study the erase bands of a thin-film write

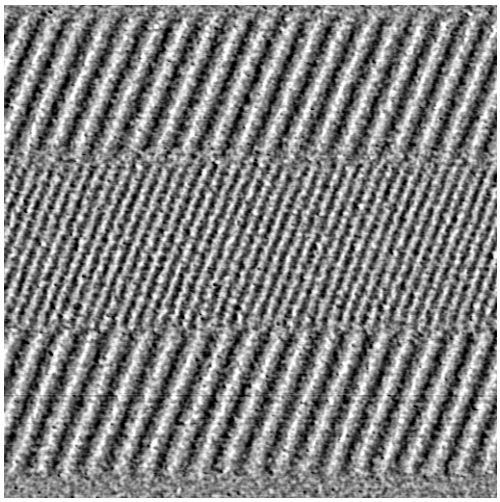

**Figure 6.16:** *MFM image (10 $\mu$m $\times$ 10 $\mu$m) of a triple-track pattern written at $\lambda_c = 0.26$ $\mu$m and $\lambda_s = 0.52$. The larger erase band toward the top of the image was generated by the misaligned edge.*

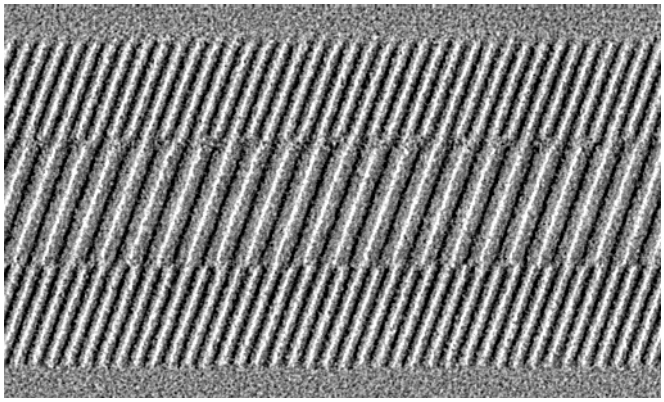

**Figure 6.17:** *MFM image (20 $\mu$m $\times$ 12 $\mu$m) of a triple-track pattern written at $\lambda_c = 0.88$ $\mu$m and $\lambda_s = 0.52$.*

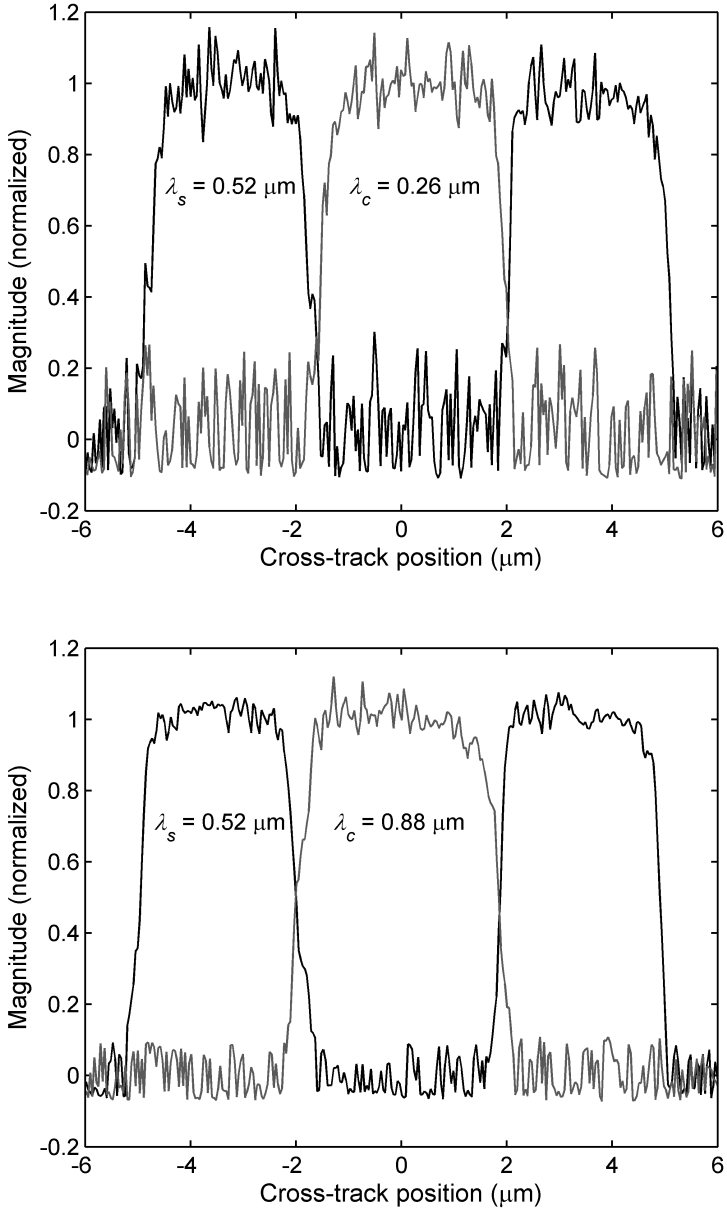


**Figure 6.18:** *MFM signal profiles of two triple triple-track patterns obtained by one-dimensional FFT. They correspond to the patterns from Fig. 6.16 and Fig. 6.17 respectively.*

head, not presented in this thesis, and MP tape. At short wavelengths, it was found that the erase bands measured by phase coherency were close to those determined from the magnitude. At long wavelengths, the erase bands were overestimated by phase coherency, whereas they were underestimated by the magnitude method. A method considering both the magnitude and the phase information could eventually lead to more precise determinations. This would make sense as both parameters influence the response of the read head. More advanced interpretation techniques of the MFM images should be investigated, especially as the erase bands are getting narrower.

## 6.6 Conclusion

A novel model to interpret triple-track profiles was introduced, allowing to extract the erase bands and side read widths. The model is based on representing the read head as the sum of a reference width, wavelength independent, and two side read effective widths that are wavelength dependent. The technique proved to be suitable to investigate edge effects in narrow track tape recording. It was employed to determine the erase bands and side read widths of HSS and MIG heads with pole widths down to 3.5 $\mu$m. The accuracy of the estimations was typically better than 0.1 $\mu$m. The method could be applied to analyze even narrower heads, especially if a recording tester with better tracking capabilities is employed.

The erase bands of a HSS head were found to be few times smaller than for a MIG head with equal gap length of 0.2 $\mu$m. The good pole alignment of the HSS heads is effective to confine side writing and erasing. Two similar HSS1-type heads were extensively studied, featuring very good pole alignment at one side and a misalignment of 0.25 $\mu$m at the other side. Their gap length was 0.11 $\mu$m, and the triple-track profiles were measured using three ME and MP tapes. The smallest erase bands were found with the ME-2 sample, probably due to its thin recording layer and good coercivity ($\delta = 50$ nm and $H_c = 164$ kA/m). They were below 0.3 $\mu$m at recording wavelengths close to 0.25 $\mu$m. It was proved from erase profiles and MFM images processed by FFT that the erase bands are unevenly distributed between the head edges. They were considerable narrower at the well aligned edge, being around 0.2 $\mu$m even at a very short wavelength of 0.2 $\mu$m (254 kfc/in). These are the lowest erase bands reported to date in magnetic tape recording. This is a notable result as it demonstrates that much improved control of side writing is achieved using well aligned heads with short gap length and thin tapes with large coercivity. Recording heads with higher saturation flux density ($B_s > 1.6$ T) and thin tapes with increased coercivity ($H_c > 200$ kA/m) would further reduce the erase bands.

Chapter 7

# Side Write Effects on Microtracks

The recording process at track widths much narrower than the poles of write heads can be studied from measurements of microtracks. They are generally obtained by erasing the side(s) of a wider track, as described in Section 5.2.1. In this chapter, microtracks are studied in order to better understand the requirements for achieving submicrometer tracks in tape recording, especially from a side write point of view. A technique to study the side write phenomenon from the frequency and current response of microtracks is introduced. The method is based on investigating the recording characteristics of microtracks created in the center and at the edges of the track. The edge-microtracks are affected by side writing while the center-microtracks are not, or just weakly by the erase process. A relative study can therefore be performed to evidence the side write effects on microtracks. The deterioration of the transitions at each edge of the write head can be analyzed as a function of the frequency and/or of the recording current. The method is very sensitive to side write asymmetry.

## 7.1 Experimental Considerations

The recording characteristics of microtracks were studied for HSS and MIG ferrite heads, with great emphasis on their edge effects. Results obtained with the HSS2-1 (Fig. 3.2) and the MIG-1 (Fig. 3.3) samples are presented as they are representative for two different technologies. They have close pole widths of 6.2 $\mu$m and 5.5 $\mu$m respectively, as well as equal gap lengths of 0.2 $\mu$m. A second ferrite head MIG-2T, from the same batch as MIG-1, was also analyzed. It has opposite azimuth angle and slightly larger gap length around 0.22 $\mu$m. However, very good alignment of its recording poles was achieved by trimming the edges using Focused Ion Beam (FIB). An image of the trimmed sample is

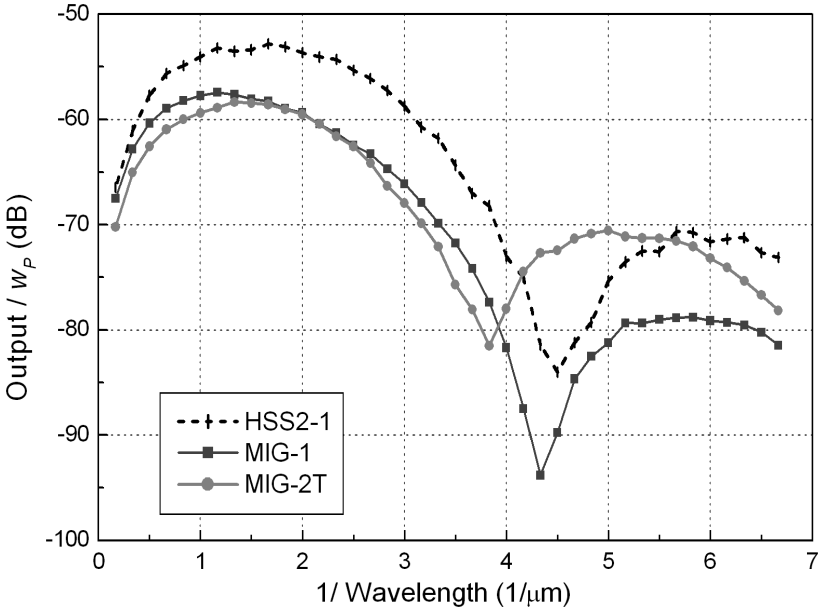


**Figure 7.1:** *Recording spectra of the HSS2-1, MIG-1, and MIG-2T samples measured with ME-2 tape, normalized to 1 μm pole width.*

shown in Fig. 3.4. All heads are presented in more detail in Section 3.1.

The recording experiments were carried out at a relative velocity of 3 m/s, using the ME-2 and MP-3 tape samples, introduced in Table 3.3. The optimum recording current was 10 mA for the HSS2-1 head and 20 mA for the MIG samples. The HSS2-1 head needs low write current due to its solenoid thin-film coil with high number of turns and good efficiency. All logarithmic scales employed in this section are referenced to an absolute voltage of 1 $\mathrm{mV_{rms}}$, meaning that −60 dB corresponds to 1 $\mu\mathrm{V_{rms}}$. The recording spectra of the HSS2-1 and MIG heads are given in Fig. 7.1, the output being normalized to 1 $\mu$m pole width. That is, the output signal of each head is divided to its pole width $w_p$ measured in micrometers. The HSS2-1 head feature the highest signal, probably due to better sensitivity. At low recording density, the MIG-1 sample presents slightly higher output than MIG-2T. The efficiency of their magnetic structures should be very close as they feature similar construction, but the effective track width of MIG-1 is increased at short wavelengths due to important side writing. However, at short wavelengths side writing acts to reduce the effective track width and the MIG-1 head presents the worst frequency degradation. Its strong edge effects are caused by the poor alignment of the magnetic poles. To the contrary, the output of the MIG-2T head is very

little degraded at high density due to marginal side writing and small magnetic spacing. Trimming was efficient to align the poles and their surface was not damaged by the FIB etching.

The side write phenomenon is explored in this chapter by studying the frequency and current response of microtracks created at the edges and in the center of the track. The center-microtracks were prepared by erasing at both sides of a recorded track; the edge-microtracks were prepared by erasing at one side only. As explained in Section 5.2.1, it is important to employ an erase method that leaves sharp edges when narrowing the full-track. Different erase techniques were studied in order to minimize related artifacts. They were tested by comparing the microtracks prepared using one erase cycle and ten erase cycles. Minimal differences should result with a good erase method. We preferred two-sided dc erasure, consisting in a cycle of erasing twice with dc currents of opposite sense. The frequency responses of center-microtracks prepared using one and ten erase cycles are shown in Fig. 7.2, for the HSS2-1 and MIG-1 heads. In the case of the HSS2-1 head, there is hardly any difference between one and ten erase cycles. This is probably due to a very well confined write field, related to the good pole alignment. The situation is different with the MIG-1 head, where the signal from the microtrack created with ten erase cycles is evidently lower. However, the reduction does not seem to depend much on frequency.

## 7.2 Effect of Poles Alignment on Recording Spectra

Recording spectra of microtracks were measured with the HSS2-1, MIG-1, and MIG-2T heads in combination with ME-2 tape to analyze the side writing influence on submicron tracks. The frequency response of edge-microtracks obtained with the HSS2-1 head is plotted in Fig. 7.3. After writing a full track, the head was offset with plus or minus 0.8 $\mu$m to erase most part of the track. The erase offset, $EO$, is given in the figure for each curve. The read offset, $RO$, was null when the head was replaced at the original write position for playback. Reading was also performed with the head centered on the microtrack, in which case $RO$ was $+2$ $\mu$m or $-2$ $\mu$m. The recording spectra of two center-microtracks are also included in the same figure for reference. Their erase offsets were $EO = -/+3.45$ $\mu$m and $EO = -/+3.70$ $\mu$m respectively. The edge-microtracks measured with the HSS2-1 head exhibit very similar frequency behavior, for both edges and read positions. Their frequency decay is higher than of the center-microtracks, due to the degradation of the transitions at the track edges at short wavelengths. This can be interpreted as an effective track width reduction. The spectra of the edge-microtracks are contained in between the spectra of the two center-microtracks, for the frequency range investigated. At very long wavelength, the edge-microtracks have an effective

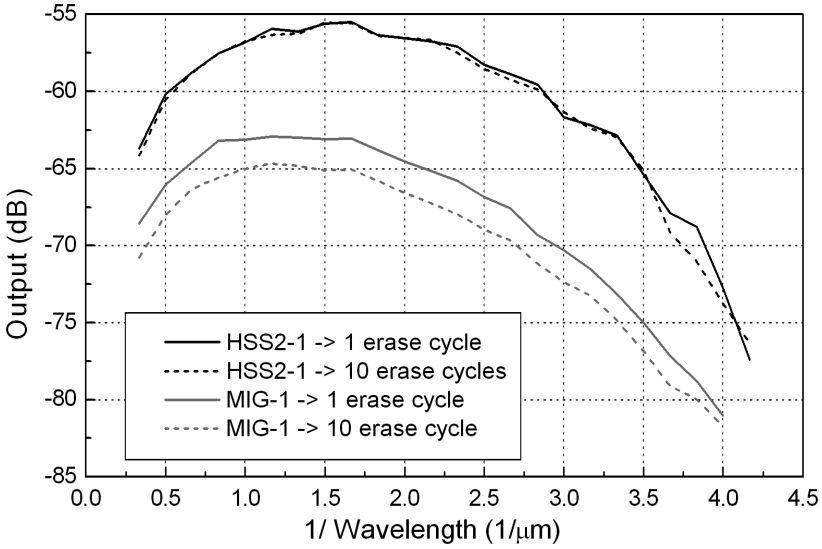


**Figure 7.2:** *Influence of the number of erase cycles on the recording spectrum of center-microtracks, for the HSS2-1 and MIG-1 heads.*

width close to that of the center-microtrack obtained with $EO = -/+3.70$ $\mu$m. At the short wavelength limit, their effective width is approaching that of the thinner center-microtrack, defined with $EO = -/+3.45$. The effective track width reduction of the edge-microtracks is therefore slightly smaller than the difference between the widths of the two center-microtracks. Accordingly, it is less than 0.5 $\mu$m up to very short wavelengths around $\lambda = 0.2$ $\mu$m. The effective track width reduction at $\lambda = 0.4$ $\mu$m was found close to 0.3 $\mu$m (from a center microtrack with $EO = -/+3.55$ $\mu$m, not shown in the figure).

Measurements of edge and center-microtracks performed with the MIG-1 head are plotted in Fig. 7.4. The edge microtracks present excessive deterioration of the signal with increasing recording density. Their erase offsets had to be increased considerably when compared with the HSS2-1 head (1.6 $\mu$m instead of 0.8 $\mu$m), due to much stronger side erasing. At both edges, the output is significantly higher when the head is centered on the edge-microtrack for reading. This means that the MIG-1 head is able to write information more faraway from its gap edge than it can read. In other words, side writing is stronger than side reading. The edge-microtracks are very different for each side of the MIG-1 head. The signal is decaying much faster at one edge causing an effective track width reduction around 1.5 $\mu$m at the wavelength $\lambda = 0.3$ $\mu$m (estimated using the center-microtracks as references). Note that the signal cannot drop below the noise floor which is around $-84$ dB. The effective

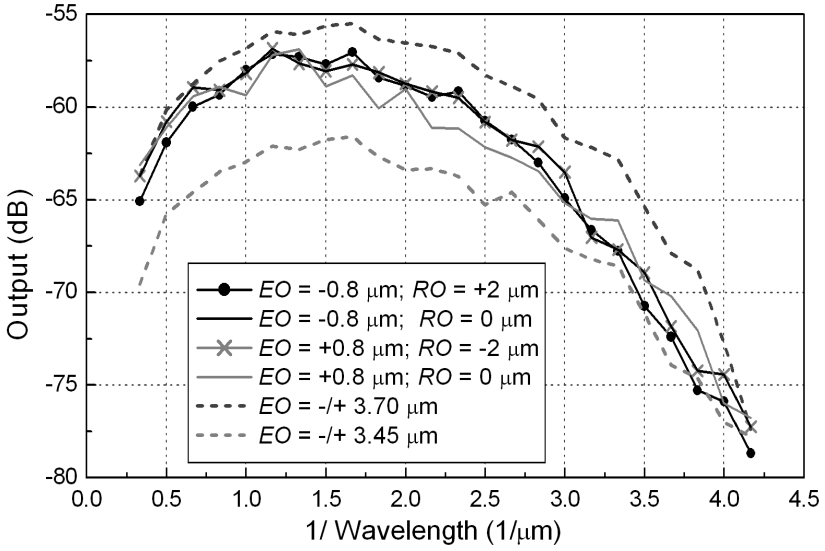


**Figure 7.3:** *Recording spectra of microtracks measured with the HSS2-1 head and ME-2 tape.*

track width reduction is considerably less at the other edge, close to 0.5 $\mu$m (at $\lambda = 0.3$ $\mu$m). It was found that the situation becomes the other way around when changing the tape moving direction, which is detailed in Section 7.3. The track width reduction averaged for the two edges at $\lambda = 0.3$ $\mu$m is around 1.0 $\mu$m. The misalignment of the recording poles of the MIG-1 head is responsible for strong side writing and consequent degradation of the track edges at high recording density.

The MIG-2T head with trimmed magnetic poles is expected to present better side write performances than MIG-1. Recording spectra of edge and center microtracks measured with MIG-2T are shown in Fig. 7.5. Measurements of edge microtracks are included just for the case when the head was centered on the microtrack for reading. Very similar data was obtained when no read offset was used ($RO$=0). The erase offsets of the edge microtracks were $EO = +1$ $\mu$m and $EO = -1$ $\mu$m, and their spectra are almost identical. They are contained within the frequency curves of two center-microtracks, created at $EO = -/+ 2.2$ $\mu$m and $EO = -/+ 2.4$ $\mu$m. The effective track width reduction at each edge, caused by side writing, is therefore estimated around 0.4 $\mu$m at $\lambda = 0.3$ $\mu$m. These results are comparable with those for the HSS2-1 head. The improvements obtained with the ferrite MIG-2T head by trimming of its magnetic poles are evident. However, such performances are intrinsic to HSS heads, manufactured using advanced thin-film technology.

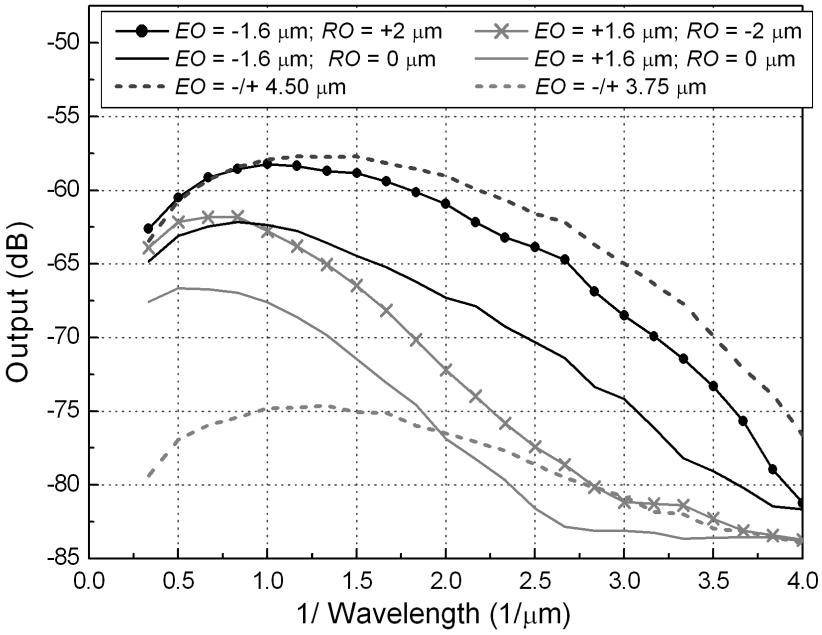


**Figure 7.4:** *Microtracks' spectra measured with the MIG-1 head. Edge microtracks are asymmetric and present strong degradation with increasing density.*

Side write effects can be consistently traced from recording spectra measurements of edge and center-microtracks. The edge-microtracks are strongly influenced by side writing, which results in a reduction of the effective track width. The degradation of the edge-microtracks is enhanced at high recording density and depends strongly on the pole alignment of the write head. The track width reduction for the poorly aligned MIG-1 head is almost three times higher than for HSS2-1 and MIG-2T. The results are in good agreement with the erase bands measured for the MIG-1 and HSS2-1 samples from triple-track profiles (Section 6.3). In fact, the track width reduction deduced from microtrack's spectra corresponds closely to the erase bands of the heads. This is explainable by the fact that at very long wavelengths the erase bands are close to null, as side writing is not yet limited by the poor field gradient. The erase bands increase with the recording density due to the effective track width reduction caused at the edges.

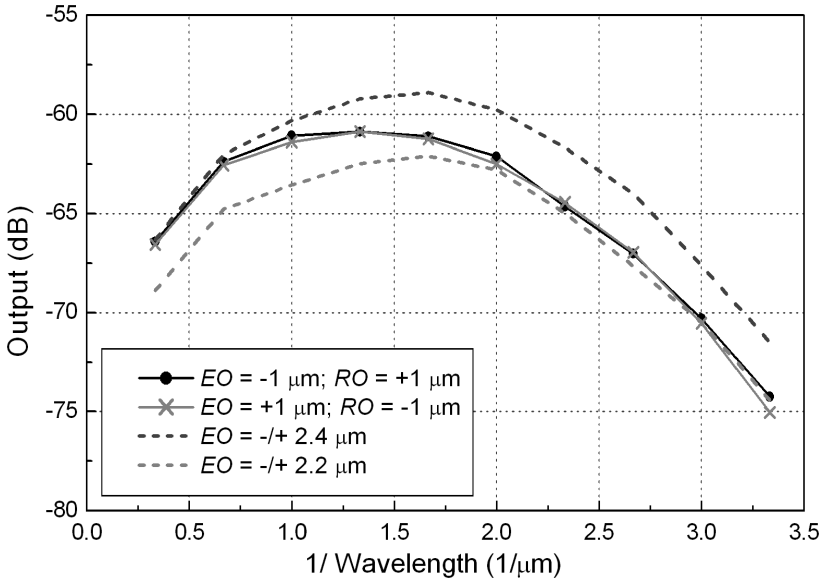


**Figure 7.5:** *Microtracks' spectra measured with the MIG-2T head, revealing limited deterioration of edge microtracks.*

## 7.3 Side Write Dependence on the Trailing Pole

In the previous section it was observed that side writing of the MIG-1 head was strongly asymmetric. The source of asymmetry was studied in more detail from microtracks measurements performed with the MP-3 tape (Table 3.3). The MP-3 tape allows to experiment in both recording directions without having to replace a new sample on the drum tester. It is therefore sufficient to rotate the drum in clockwise (CW) or counterclockwise (CCW) direction. Moreover, the thin magnetic layer of the MP-3 tape ($\delta = 70$ nm) is suitable to evidence edge effects by avoiding depth nonlinearities related to the recording process. The measurements presented in the previous section were performed in CCW direction.

Frequency and current dependence curves of microtracks were acquired for both tape moving directions. The center-microtracks' measurements were identical in both measurement directions, within the error margin of the experiments. Side erasure does not depend on the recording direction, which was expectable. However, the edge-microtracks feature very different properties depending on the tape moving direction. Their recording spectra are given in Fig. 7.6. Playback was performed with the head centered on the microtracks such that the measurements are not affected by side read. It is observed that

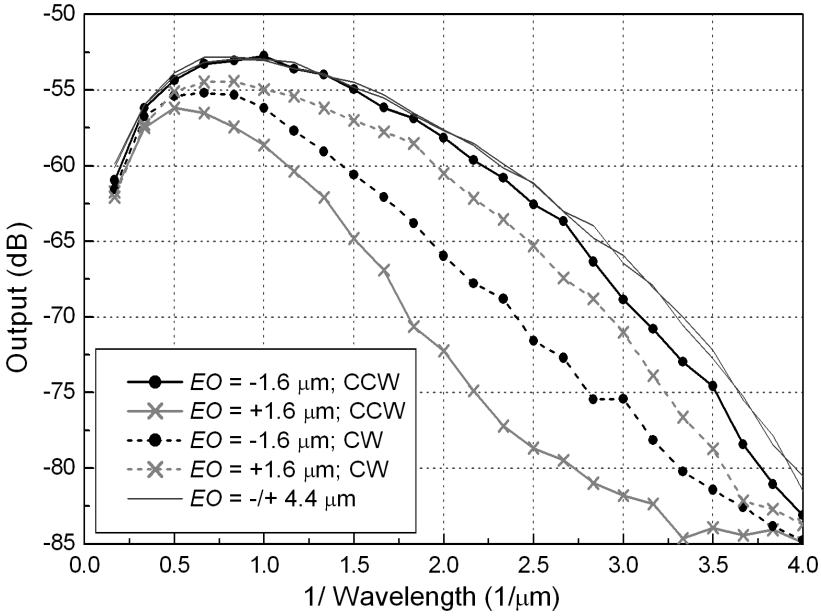


**Figure 7.6:** *Spectra of edge-microtracks measured with the MIG-1 head and MP-3 tape for both recording directions ($I_w = 20$ mA). The center-microtrack is not influenced by the recording direction.*

for a given tape moving direction, the signal degradation with the recording density is worse at a specific edge than at the other. The situation is reversed for the opposite recording direction. The side write asymmetry is much more pronounced in CCW than in CW direction. In fact, side writing depends more strongly on the recording direction than on a specific edge. However, the edge with positive erase offset ($EO = +1.6$ $\mu$m) presents overall worse signal degradation.

In order to understand the side write process of the MIG-1 head, one has to consider the misalignment of its poles at each edge. It is convenient to mark the edges of each pole as in Fig. 7.7. They are here referred to as $PE_1$, $PE_2$, $PE_3$, and $PE_4$. When the edge-microtrack is created with negative erase offset (e.g. $EO = -1.6$ $\mu$m), this is written by the trailing pole-edge $PE_1$ in CCW direction, or $PE_2$ in CW direction. For positive erase offset (e.g. $EO = +1.6$ $\mu$m), the trailing pole-edge is $PE_3$ in CCW direction, or $PE_4$ in CW direction. It can therefore be deduced from Fig. 7.6 that side writing is worst for the trailing pole-edge $PE_3$, the microtrack vanishing completely around $\lambda = 0.3$ $\mu$m. Some improvement is visible for $PE_2$, which causes an effective track width reduction close to 1.1 $\mu$m at $\lambda = 0.3$ $\mu$m (deduced from center microtracks). $PE_1$

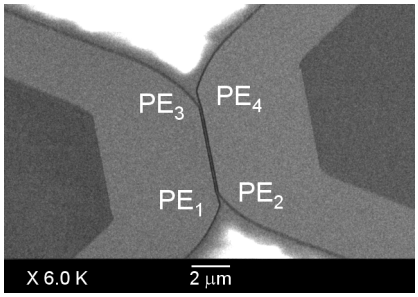


**Figure 7.7:** *SEM image of the MIG-1 head with each edge of the poles numbered for referencing.*

**Table 7.1:** *Approximative track width reduction caused by side writing at each pole-edge, at the recording wavelength* $\lambda = 0.3$ $\mu$*m.*

| | $PE_1$ | $PE_2$ | $PE_3$ | $PE_4$ |
|---|---|---|---|---|
| Track width reduction ($\mu$m) | 0.5 | 1.1 | 1.6 | 0.8 |

presents the best side write performances, which are slightly poorer at $PE_4$. They engender track width reductions around 0.5 $\mu$m and 0.8 $\mu$m respectively, at $\lambda = 0.3$ $\mu$m. These values are summarized in Table 7.1.

The head misalignment at a given edge causes one pole to be wider than the other. The pole-edges $PE_1$ and $PE_4$ are wider than $PE_2$ and $PE_3$. Reported calculations and modeling of write fields for misaligned heads show that the gradient is considerable worse at the narrower pole than at the larger one [5, 112, 113]. Side writing is therefore aggravated at the narrower pole, with pronounced transition broadening and high phase shifts. This results in strong deterioration of the track edges, as seen for $PE_2$ and $PE_3$. The alteration is less severe for the wider pole-edges $PE_1$ and $PE_4$. Moreover, the misalignment of the poles is not identical at both edges, being more important at the side with $PE_3$ and $PE_4$. Side writing is therefore worse at $PE_3$ than at $PE_2$, and at $PE_4$ than at $PE_1$. The degradation of the edge-microtracks' spectra is more acute for $PE_2$ than for $PE_4$, meaning that the effect of the recording direction is stronger than that of the increased misalignment.

The dependence of edge and center-microtracks on the write current was also investigated. The dc erase current for creating the microtracks was not varied, but only the write current. The curves measured at the recording wavelength $\lambda = 0.5$ $\mu$m are shown in Fig. 7.8. It is again observed that side

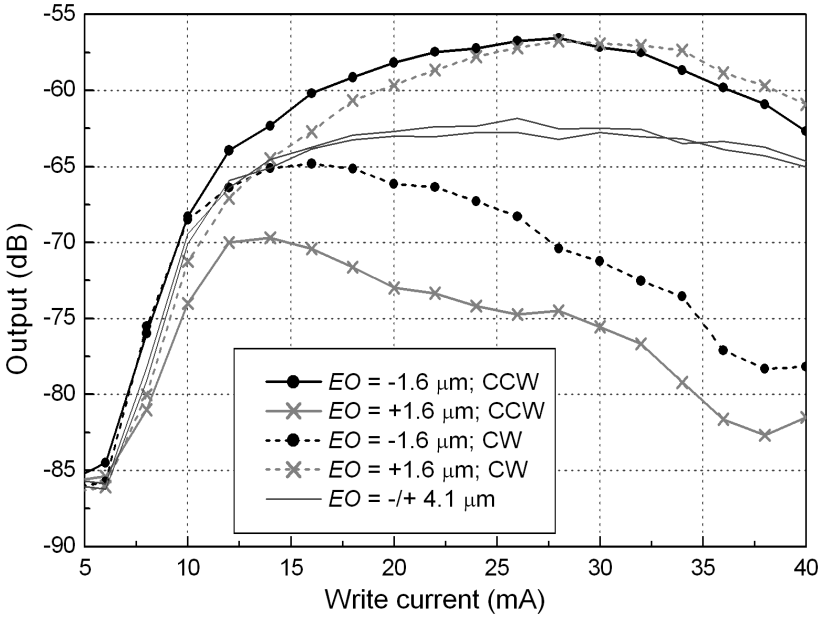


**Figure 7.8:** *Current curves of edge and center-microtracks measured with the MIG-1 head and MP-3 tape for both recording directions, at* $\lambda = 0.5$ *μm. Increasing the current mainly affects the edges.*

writing is anti-symmetric with respect to the tape moving direction. Each edge presents worse degradation in one direction than in the other, due to the asymmetric write fields at the trailing poles of the head. The output of the center-microtracks is increasing until the the recording current reaches approximately 18 mA, after which it is roughly constant. A slight decrease is noticeable at currents above 34 mA. It is deduced that on-track recording does not change much at currents between 18 mA and 34 mA, at that particular wavelength. For the edge-microtracks, the signal is initially increasing and then starts dropping. The drop is very pronounced and starts from 14 mA for the trailing pole-edges $PE_2$ and $PE_3$, where side writing is worst. For $PE_1$ and $PE_4$, the signal is steadily increasing until 28 mA, followed by a moderate decrease.

Increasing the current causes the write bubble to extend in cross-track direction. The amplitude of the side field increases and side writing/erasing spreads further at the track edges. Magnetization transitions are written at the edges only if the gradient is good enough. Moreover, they may present strong distortions such as phase shifts, having nonlinear contribution to the read signal. At the narrow trailing pole-edges, $PE_2$ and $PE_3$, strong degradation of the tran-

sitions starts from very low currents close to 14 mA. Even though the write bubble is expanding, the effective side written information is shrinking. The output vanishes almost entirely at 40 mA, especially for $PE_3$. In the case of the microtracks defined by the pole-edges $PE_1$ and $PE_4$, the replay signal increases until higher current around 28 mA. The gradient of the side field is more appropriate to write transitions at these wider trailing poles and the phase shifts are limited. However, noticeable deterioration of the side writing is visible at write currents above 28 mA.
Dependence of microtracks on the write current was also measured for heads with with very good pole alignment, like HSS2-1 and MIG-2T. The influence of the current on side writing was found to be considerable less. At good pole alignment, the spread of the side field is limited by the saturation of the pole tips. Distortion of the write bubble is likely to occur due to the saturation [170], however, it is much less than that caused at misaligned poles. In the latter case, the side field spreads considerable at high write current and the gradient is much degraded. Strong phase shifts are also involved. Similar interpretations were deduced from the study of the HSS1-2 head presented in Section 5.3.2, based on imbalanced overwrite measurements.

## 7.4 Conclusion

The method to create edge-microtracks is similar to that used to record narrow tracks in many modern tape drives, with the main difference that dc erasure was applied here. In helical-scan systems, the tracks are typically recorded with wider write heads using partial overlap. A similar technique is employed in linear-scan systems, known as *shingling*. The investigation of microtracks is therefore a relevant technique to approach the recording issues related to future high track densities. Edge-microtracks are strongly affected by side writing and their frequency decay is considerably worse than of the center-microtracks. Side write effects can be investigated with a high level of detail from recording spectra and current dependence of microtracks. The method allows studying the alteration of the transitions at each edge of the head.

Side writing causes the transitions to bend and to broaden at the track edge. The bend of the transitions introduces a phase shift between the edge and the track-center, contributing to the deterioration of the output at short wavelengths together with the transition broadening. This results in a reduction of the effective track width corresponding to an increase of the erase bands. The effects are strong at poor pole alignment and depend on the write field gradient at the trailing pole. Asymmetric poles may therefore engender erase bands depending highly on the recording direction, as for the MIG-1 head. However, the 15° azimuth angle of the HSS2-1 head did not induce noticeably asymmetry of the side writing. Even with very well aligned heads as HSS2-1 and MIG-2T,

side writing causes a reduction of the effective track width around 0.5 $\mu$m at high recording density ($\lambda = 0.2$ $\mu$m). This is a serious limitation for reaching submicron track widths in tape recording. Write heads with shorter gap length and higher saturation magnetic flux as well as thin media with higher coercivity are needed to reduce the erase bands.

Chapter 8

# Conclusion

As track widths in magnetic tape recording are approaching the symbolic threshold of one micrometer, increasingly better control of the track edges is required. In this work, the recording process at narrow tracks was investigated with emphasis on edge effects. Side writing and erasing were primarily treated, as they represent critical limitations for increasing the track density. Side reading was also addressed, however, it is not believed to be a severe issue for modern tape storage systems.
The thesis presents an extensive study of edge effects, providing an improved understanding of narrow track tape recording. Diverse investigation methods were applied and explored, some being based on original concepts. The principles for developing a recording tester with ultimate performances aimed at track widths down to 200 nm were also laid down.

## 8.1 Edge Effects

Narrow track recording and edge effects were studied using advanced Helical Scan Silicon (HSS) heads as well as metal-in-gap (MIG) heads. Their pole widths were comprised between 1.3 $\mu$m and 6.2 $\mu$m. Metal particulate (MP) and metal evaporated (ME) tapes were employed, with the thickness of the recording layer down to 50 nm. The erase bands of a HSS head with perfectly aligned poles were found to be few times smaller than for a MIG head with equal gap length of 0.2 $\mu$m. The poorly defined gap corners of the MIG head caused extensive side writing and degradation of the track edges. Considerable better results, comparable to the HSS head, were obtained with a MIG head whose magnetic poles were aligned by Focused Ion Beam (FIB) trimming.
The HSS heads proved good capabilities for writing narrow tracks with well

defined edges due to the good alignment of their poles and short gap lengths. Erase bands within 0.25 $\mu$m were measured at very short recording wavelengths down to 0.2 $\mu$m, at the well aligned edge of a HSS head with 0.11 $\mu$m gap length. They were obtained using a ME tape with thin recording layer of 50 nm and coercivity of 164 kA/m, being the smallest erase bands reported to date in magnetic tape recording. The results demonstrate that much improved control of side writing and erasing is achieved using well aligned heads with short gap length and thin tapes with high coercivity.

In order to write narrow tracks with sharp edges, write heads should feature well defined gap corners with good pole alignment and short gap length. High saturation pole materials and recording tapes with large coercivity are also necessary. Short write gaps require thinner magnetic layers in order to avoid recording nonlinearities within the depth of the media (e.g. $\delta < g/2$). Moreover, thin media with high coercivity are also suitable for achieving short transition lengths and high linear density.

## 8.2 Test and Investigation Methods

The recording experiments were performed on a tape-drum tester adapted for high stability and accuracy. An existing setup was modified and partly redesigned in order to considerably improve the speed stability, head-to-tape contact, cross-track positioning, and signal conditioning. The upgraded tester proved to deliver suitable performances and operation convenience for recording narrow tracks close to one micrometer. The cross-track positioning accuracy was better than 100 nm for short-range travels within 10 $\mu$m.
It is expected that superior features are achievable by constructing a tester with overall optimized design. The related issues were analyzed aiming to develop an advanced tape-drum tester suitable for track widths close to 200 nm. This would require low pressure, stable head-to-tape contact and non-repeatable tracking errors below 20 nm. Extensive design criteria and suggestions were elaborated, covering the main mechanical and electronic components of the setup.

The accuracy of the upgraded tape-drum tester allowed to implement diverse methods to investigate narrow track recording and edge effects. Some techniques were specifically developed in this work while others were adapted from the hard disk research, such as triple-track profiling. However, a novel model was developed for the interpretation of triple-track profiles, allowing to determine both the erase bands and the side read widths. The precision of the estimates was usually better than 0.1 $\mu$m, limited by the tracking accuracy of the tester. Triple-track profiling is a powerful technique for detailed studies of edge effects, requiring accurate control of the cross-track position. The erase bands measured from triple-track profiles, erase profiles, and magnetic force

microscope (MFM) images showed good agreement at short recording wavelengths. The results tended to diverge at long wavelengths, especially for the MFM technique. The increased side write interaction at the overwritten edges and the different sensitivity of the MFM tip to the modulated information were mainly held responsible.
Investigation of microtracks was found to be a relevant technique to approach the recording process at very narrow track width and to address critical issues such as side writing. Edge-microtracks are strongly affected by side writing while center-microtracks reflect the on-track recording performance. It was shown that analyzing the frequency and/or current responses of microtracks is an efficient method to characterize complex side write effects.

## 8.3 Recommendations

According to current tape storage prospects, submicron tracks should be reached in less than ten years. Read heads with track widths down to 0.45 $\mu$m have been already demonstrated, using giant magnetoresistive (GMR) sense elements [13]. Erase bands below 0.2 $\mu$m will be required, implying write heads with short gap lengths around 100 nm or less, well aligned poles, and high saturation flux density (e.g. $B_s > 1.6$ T). Fabricating such devices may be challenging for high angle azimuth recording. The HSS heads present a number of significant innovations such as integrated azimuth angle and very good pole alignment. The tapes should feature thin recording layers eventually below 50 nm, as well as high coercivity in excess of 200 kA/m. Metal sputtered (MS) tapes, with $\delta \approx 30$ nm and $H_c > 250$ kA/m, are believed to be promising candidates for such developments. However, ME and MP media are continuously evolving and are expected to meet the density growth requirements for the next years.

Suitable experimental equipment and investigation methods must be employed for investigating the recording process at submicron tracks. The development of a tape-drum tester with tracking accuracy around 20 nm is judged feasible, and the main design issues were treated in this work. Using such tester, track profiling techniques could be applied to measure erase bands and side read widths with a resolution probably better than 50 nm. This is comparable to that of MFM imaging and has the advantage that the complete characterization is performed at once on the recording setup. Moreover, MFM is an indirect observation technique of the magnetization in the medium and may not reproduce the patterns as they are sensed by the read head. It provides, however, very good detail to examine track edge distortions such as phase shifts of the transitions. It is thus a useful complementary tool which has to be applied circumspectly.
A meaningful method for predicting the performances of future narrow track tape systems is to analyze the recording properties of microtracks. They were

investigated here with a focus on edge effects. However, signal-to-noise ratio (SNR) and error rate measurements could also be applied for addressing overall system issues. Sensitive read heads like GMR devices should be employed for such characterizations.

# Bibliography


[1] F. Yale, "Tape Drive Market Shares: Worldwide, 2003," Gartner Dataquest, Mar. 2004.

[2] R. C. Abraham, "Compact Tape Outlook 2003," Freeman Reports, 12010 MacDonald Drive, Ojai, CA 93023-9714, USA, 2004.

[3] C. Tsang, M.-M. Chen, T. Yogi, and K. Ju, "Gigabit density recording using dual-element MR/inductive heads on thin-film disks," *IEEE Trans. Magn.*, vol. 26, no. 5, pp. 1689–1693, 1990.

[4] T. D. Howell, D. P. McCown, T. A. Diola, Y. Tang, K. R. Hense, and R. L. Gee, "Error rate performance of experimental gigabit per square inch recording components," *IEEE Trans. Magn.*, vol. 26, no. 5, pp. 2298–2302, 1990.

[5] C. Tsang, "Design and performance considerations in high areal density longitudinal recording," *J. Appl. Phys.*, vol. 69, no. 8, pp. 5393–5398, 1991.

[6] M. Futamoto *et al.*, "Investigation of 2 Gb/in$^2$ magnetic recording at a track density of 17 kTPI," *IEEE Trans. Magn.*, vol. 27, no. 6, pp. 5280–5285, 1991.

[7] H. N. Bertram, H. Zhou, and R. Gustafson, "Signal to noise ratio scaling and density limit estimates in longitudinal magnetic recording," *IEEE Trans. Magn.*, vol. 34, no. 4, pp. 1845–1847, 1998.

[8] R. Wood, "Detection and capacity limits in magnetic media noise," *IEEE Trans. Magn.*, vol. 34, no. 4, pp. 1848–1850, 1998.

[9] J. Chen and J. Moon, "Detection signal-to-noise ratio versus bit cell aspect ratio at high areal densities," *IEEE Trans. Magn.*, vol. 37, no. 3, pp. 1157–1167, 2001.

[10] "Magnetic Tape Storage Roadmap," INSIC, 3655 Ruffin Road, Suite 335, San Diego, CA 92123-1833, USA, Feb. 2002.

[11] R. G. Biskeborn and J. H. Eaton, "Flat-profile tape recording head," *IEEE Trans. Magn.*, vol. 38, no. 5, pp. 1919–1921, 2002.

[12] E. R. Childers, W. Imaino, J. H. Eaton, G. A. Jaquette, P. V. Koeppe, and D. J. Hellman, "Six orders of magnitude in linear tape technology: The one-terabyte project," *IBM J. Res. Dev.*, vol. 47, no. 4, pp. 471–482, 2003.

[13] T. Ozue, M. Kondo, Y. Soda, S. Fukuda, S. Onodera, and T. Kawana, "11.5-Gb/in$^2$ recording using spin-valve heads in tape systems," *IEEE Trans. Magn.*, vol. 38, no. 1, pp. 136–140, 2002.

[14] K. Suzuki, T. Shirai, T. Watanabe, Y. Mikami, S. Fukuda, and T. Ozue, "Recording characteristics at a channel rate over 300 Mb/s in a helical-scan tape system," *IEEE Trans. Magn.*, vol. 40, no. 4, pp. 2419–2421, 2004.

[15] G. Cuntze, T. Hughes, S. Magnusson, W. Nichtl-Pecher, D. Norton, and M. Pechtold, "Magnetoresistive read heads for high-density data applications," *IEEE Trans. Magn.*, vol. 37, no. 5, pp. 3839–3843, 2001.

[16] Y. Soda, N. Nagai, K. Kasuga, T. Shirai, M. Kondo, and T. Ozue, "Reliability tests of the MR head in helical-scan tape systems," *IEEE Trans. Magn.*, vol. 37, no. 4, pp. 1716–1718, 2001.

[17] Y. Soda, H. Ono, and T. Ozue, "Effect of surface resistance of metal evaporated tape on discharge current," *IEEE Trans. Magn.*, vol. 39, no. 5, pp. 2347–2349, 2003.

[18] Y. Soda, Y. Ito, I. Kobayashi, H. Takekuma, and Y. Takahashi, "A resistive ferrite substrate for the GMR head in digital tape systems," *IEEE Trans. Magn.*, vol. 40, no. 4, pp. 2218–2220, 2004.

[19] N. Nagai, T. Shirai, S. Fukuda, T. Ozue, and S. Onodera, "A narrower side erase band for use with helical scan systems," *IEEE Trans. Magn.*, vol. 35, no. 5, pp. 2691–2693, 1999.

[20] K. Tsuneki, K. Iesaka, Y. Yanagi, Y. Senshu, and Y. Kotani, "Development of a consumer VCR format and a high-density magnetic recording using an MR head," *IEEE Trans. Consumer Electron.*, vol. 48, no. 3, pp. 783–789, 2002.

[21] K. Ejiri, T. Sugizaki, R. Taguchi, K. Majima, K. Muto, T. Uehara, and H. Okuda, "Investigation of particulate media with an ultra-thin magnetic layer suitable for MR heads on a rotating drum," *IEEE Trans. Magn.*, vol. 37, no. 4, pp. 1605–1608, 2001.

[22] M. McCorkle, "Fujifilm NANO CUBIC coating technology - potential for 1 TB data storage tapes and 3 GB flexible magnetic disk," THIC Meeting, Del Mar CA, Jan. 2002. [Online]. Available: http://www.thic.org/Agenda_0201.html

[23] "Super DLTtape$^{TM}$ II Media," White Paper, Quantum Corporation, Jan. 2004. [Online]. Available: http://www.dlttape.com/DLTtape/Technology/White+Papers.htm

[24] M. P. Sharrock, "Recent advances in metal particulate recording media: Toward the ultimate particle," *IEEE Trans. Magn.*, vol. 36, no. 5, pp. 2420–2425, 2000.

[25] D. J. Sleiter and M. P. Sharrock, "Magnetic time effects in small metallic particles for recording: orientation dependence," *IEEE Trans. Magn.*, vol. 40, no. 4, pp. 2413–2415, 2004.

[26] D. E. Speliotis, "Performance of MP$^{++}$ and BaFe$^{++}$ tapes in high density recording applications," *IEEE Trans. Magn.*, vol. 31, no. 6, pp. 2877–2882, 1995.

[27] T. Suzuki, T. Tanaka, and K. Ikemizu, "High density recording capability for advanced particulate media," *J. Magn. Magn. Mater.*, vol. 235, no. 1-3, pp. 159–164, 2001.

[28] M. P. Sharrock and L. W. Carlson, "The application of barium ferrite particles in advanced recording media," *IEEE Trans. Magn.*, vol. 31, no. 6, pp. 2871–2876, 1995.

[29] Y. Maezawa, H. Yoshida, and K. Shinohara, "Characteristics of ME tape made at 1 $\mu$m/s deposition rate," *IEEE Trans. Magn.*, vol. 35, no. 5, pp. 2688–2690, 1999.

[30] B. Xu, K. Motohashi, S. Onodera, and W. D. Doyle, "Magnetic characteristics and recording properties of thin Co-CoO metal evaporated tapes," *IEEE Trans. Magn.*, vol. 37, no. 4, pp. 1630–1633, 2001.

[31] K. Motohashi and S. Onodera, "Thickness and oxidation dependence of magnetic properties of ultrathin obliquely evaporated Co-CoO media," *IEEE Trans. Magn.*, vol. 39, no. 5, pp. 2350–2352, 2003.

[32] K. Shimizu, J. Tachibana, Y. Arisaka, and K. Sato, "Read-write characteristics and magnetic properties of Co-CoO obliquely evaporated film on a cobalt oxide underlayer," *IEEE Trans. Magn.*, vol. 40, no. 4, pp. 2398–2400, 2004.

[33] B. Bian, J. A. Bain, S.-J. Kwon, and D. E. Laughlin, "High coercivity Co-alloy thin films on polymer substrates," *IEEE Trans. Magn.*, vol. 37, no. 4, pp. 1640–1642, 2001.

[34] H.-S. Lee, J. A. Bain, and D. E. Laughlin, "The application of sputtered thin film in advanced recording tape media," *IEEE Trans. Magn.*, vol. 40, no. 4, pp. 2404–2406, 2004.

[35] L. T. Nguyen, A. Hozoi, and J. C. Lodder, "NiAl seedlayer for obliquely sputtered thin film tape," *IEEE Trans. Magn.*, vol. 40, no. 4, pp. 2401–2403, 2004.

[36] L. T. Nguyen and J. C. Lodder, "Growth of oblique sputtered Co and CoCrPt for high density tape recording," *J. Magn. Magn. Mater.*, 2005, to be published.

[37] J. J. M. Ruigrok, E. A. Draaisma, and H. W. V. Kesteren, "Design of thin-film tape heads," *Philips J. Res.*, vol. 51, pp. 21–57, 1998.

[38] R. G. Biskeborn and J. H. Eaton, "Hard-disk-drive technology flat heads for linear tape recording," *IBM J. Res. Dev.*, vol. 47, no. 4, pp. 385–400, 2003.

[39] R. H. Dee, J. Cates, and J. M. Schmalhorst, "Advanced multi-track tape head for high-performance tape recording application," *IEEE Trans. Magn.*, vol. 35, no. 2, pp. 712–717, 1999.

[40] A. Veloso, R. H. Dee, and P. P. Freitas, "Quasi-static and dynamic analysis of spin valve tape heads with synthetic free and pinned layers versus heads with a conventional free layer and a synthetic pinned layer," *IEEE Trans. Magn.*, vol. 38, no. 5, pp. 1928–1930, 2002.

[41] R. H. Dee, "Comparison of MR and GMR spin-valve heads for magnetic recording on MP tape," *IEEE Trans. Magn.*, vol. 38, no. 5, pp. 1922–1924, 2002.

[42] K. Hallamasek, M. Boots, F. Souchon, R. Hida, M. Panabire, J.-B. Albertini, and B. Viala, "GMR head for helical-scan recording with a 5000-h head life," *IEEE Trans. Magn.*, vol. 39, no. 5, pp. 2387–2389, 2003.

[43] T. Ozue, T. Shirai, K. Kamatani, H. Kano, Y. Ikeda, S. Onodera, and T. Kawana, "Magnetoresistive heads for helical-scan tape systems," *IEEE Trans. Magn.*, vol. 35, no. 2, pp. 729–733, 1999.

[44] E. Nakashio, J. Sugawara, S. Onoe, and S. Kumagai, "Flux guide type tunnel-valve head for tape storage applications," *IEEE Trans. Magn.*, vol. 38, no. 5, pp. 1925–1927, 2002.

[45] B. Bhushan and P. P. Ambekar, "Effect of magnetic tape thickness on friction and wear in a linear tape drive," *Wear*, vol. 255, no. 2, pp. 1323–1333, 2003.

[46] H. Osaki, "Recent research of tape/drive tribology," *Tribol. Int.*, vol. 36, no. 4-6, pp. 349–360, 2003.

[47] H. Tetsukawa, "Spin-valve head with corrosion resistance for tape recording system," *IEEE Trans. Magn.*, vol. 40, no. 6, pp. 3541–3544, 2004.

[48] N. Nagai, S. Kuroda, and T. Ozue, "Observations on the lubricant and the DLC layer of ME tapes and HDD disks with nanometer resolution," *J. Magn. Magn. Mater.*, vol. 241, no. 2-3, pp. 338–340, 2002.

[49] S. T. Patton and B. Bhushan, "Micromechanical and tribological characterization of alternate pole tip materials for magnetic recording heads," *Wear*, vol. 202, no. 1, pp. 99–109, 1996.

[50] Y. Kamatani, N. Nagai, M. Kondo, and T. Ozue, "Wear of the MR head in helical-scanning tape systems," *IEEE Trans. Magn.*, vol. 35, no. 5, pp. 2379–2381, 1999.

[51] J. L. Sullivan, M. A. Wild, and M. S. Hempstock, "The tribology of linear tape/head interfaces and its impact on signal performance," *Tribol. Int.*, vol. 36, no. 4-6, pp. 261–267, 2003.

[52] E. Sourty, J. L. Sullivan, and L. A. M. D. Jong, "Pole tip recession in linear recording heads," *IEEE Trans. Magn.*, vol. 39, no. 3, pp. 1859–1861, 2003.

[53] N. Nagai, Y. Kamatani, M. Kondo, S. Onodera, and T. Ozue, "Clear stains and their behavior in helical scan tape systems," *IEEE Trans. Magn.*, vol. 36, no. 5, pp. 2699–2701, 2000.

[54] C. Nastasa and J. L. Sullivan, "Transfer film formation on helical scan data recording heads," *Tribol. Int.*, vol. 36, no. 4-6, pp. 247–254, 2003.

[55] P. P. Ambekar and B. Bhushan, "Effect of operating environment on headtape interface in a linear tape drive," *J. Magn. Magn. Mater.*, vol. 261, no. 1-2, pp. 277–294, 2003.

[56] M. L. Williams and R. L. Comstock, "An analytical model of the write process in digital magnetic recording," in *A.I.P. Conf. Proc. Magn. Mater.*, vol. 5, 1971, pp. 738–742.

[57] H. N. Bertram and R. Niedermeyer, "The effect of spacing on demagnetization in magnetic recording," *IEEE Trans. Magn.*, vol. 18, no. 6, pp. 1206–1208, 1982.

[58] A. Roesler and J.-G. Zhu, "Novel magnetic characterization of the headmedium interface in metal particle tape systems," *IEEE Trans. Magn.*, vol. 37, no. 5, pp. 3850–3859, 2001.

[59] J. Marion, "One terabyte and beyond - the technology for high capacity serpentine recording," THIC Meeting, Del Mar CA, Jan. 2002. [Online]. Available: http://www.thic.org/Agenda_0201.html

[60] T. Schwarz, "Technology development for a standard cartridge multi-terabyte tape system," THIC Meeting, San Jose CA, Mar. 2004. [Online]. Available: http://www.thic.org/Agenda0403.html

[61] D. A. Lindholm, "Magnetic fields of finite track width heads," *IEEE Trans. Magn.*, vol. 13, no. 5, pp. 1460–1462, 1977.

[62] G. Hughes and D. Bloomberg, "Recording head side read/write effects," *IEEE Trans. Magn.*, vol. 13, no. 5, pp. 1457–1459, 1977.

[63] A. van Herk and H. Bijl, "Measurement of side-write, -erase, and -read behavior of conventional narrow track disk heads," *IEEE Trans. Magn.*, vol. 16, no. 1, pp. 114–119, 1980.

[64] T. Lin, J. A. Christner, T. B. Mitchell, J.-S. Gau, and P. K. George, "Effects of current and frequency on write, read, and erase widths for thin-film inductive and magnetoresistive heads," *IEEE Trans. Magn.*, vol. 25, no. 1, pp. 710–715, 1989.

[65] T. C. Arnoldussen, L. L. Nunnelley, F. J. Martin, and R. P. Ferrier, "Side writing/reading in magnetic recording," *J. Appl. Phys.*, vol. 69, no. 8, pp. 4718–4720, 1991.

[66] J.-G. Zhu, X. G. Ye, and T. C. Arnoldussen, "Effect of in-plane easy axis orientation in narrow track recording," *IEEE Trans. Magn.*, vol. 29, no. 1, pp. 324–329, 1993.

[67] X. G. Ye, J.-G. Zhu, and T. C. Arnoldussen, "Track edge overwrite and easy-axis orientation in narrow track recording," *IEEE Trans. Magn.*, vol. 29, no. 6, pp. 3978–3980, 1993.

[68] E. Yarmchuk, "Spatial structure of media noise in film disks," *IEEE Trans. Magn.*, vol. 22, no. 5, pp. 877–882, 1986.

[69] M. W. Muller, R. S. Indeck, E. S. Murdock, and R. Ornes, "Track edge fluctuations," *J. Appl. Phys.*, vol. 67, no. 9, pp. 4683–4685, 1990.

[70] T. T. Lam and J.-G. Zhu, "Phase dependence of track edge noise in MR head written overlapping tracks," *IEEE Trans. Magn.*, vol. 31, no. 6, pp. 3111–3113, 1995.

[71] T. Korenari, S. Tsuboi, T. Okumura, H. Matsutera, and K. Tagami, "Analysis of track-edge noise in thin-film recording media," *IEEE Trans. Magn.*, vol. 33, no. 4, pp. 2509–2512, 1997.

[72] W. R. Bennett, B. Zhang, and H. J. Richter, "Influence of orientation ratio on reverse erase-edge noise and track-edge dipole distribution," *IEEE Trans. Magn.*, vol. 34, no. 3, pp. 743–749, 1998.

[73] J. K. Lee and P. I. Bonyhard, "A track density model for magnetoresistive heads considering erase bands," *IEEE Trans. Magn.*, vol. 26, no. 5, pp. 2475–2477, 1990.

[74] M. Kawaguchi, K. Tsuneki, and Y. Kubota, "The side-erasing effect in narrow track recording," *IEEE Trans. Magn.*, vol. 27, no. 6, pp. 4900–4902, 1991.

[75] J. L. Su, K. Ju, J. Lo, and G. Countryman, "Side fringing of thin-film heads with pole trimming," *IEEE Trans. Magn.*, vol. 26, no. 5, pp. 2463–2465, 1990.

[76] K. Stoev *et al.*, "Demonstration and characterization of 130 Gb/in$^2$ magnetic recording systems," *J. Appl. Phys.*, vol. 93, no. 10, pp. 6552–6554, 2003.

[77] Y. Maezawa, H. Yoshida, and K. Shinohara, "Tunneling magnetoresistive heads beyond 150 Gb/in$^2$," *IEEE Trans. Magn.*, vol. 40, no. 1, pp. 307–312, 2004.

[78] E. O. Samwel, T. Bolhuis, D. Speliotis, and J. C. Lodder, "Vectorial measurements of the angular coercive field," *J. Magn. Magn. Mater.*, vol. 193, no. 1-3, pp. 337–341, 1999.

[79] O. Karlqvist, "Calculation of the agnetic field in the ferromagnitic layer of a magnetic drum," *Trans. Roy. Inst. Technol. Stockholm*, vol. 86, pp. 3–27, 1954.

[80] B. K. Middleton, "Recording and reproducing processes," in *Magnetic Recording Technology*, 2nd ed., C. D. Mee and E. D. Daniel, Eds. McGraw-Hill, 1996, ch. 2.

[81] H. N. Bertram, *Theory of Magnetic Recording.* Cambridge University Press, 1994.

[82] E. P. Valstyn and C. R. Bond, "Williams-Comstock model with finite-length transition functions," *IEEE Trans. Magn.*, vol. 35, no. 2, pp. 1070–1076, 1999.

[83] H. N. Bertram, A. J. Armstrong, J. K. Wolf, and I. A. Beardsley, "Theory of nonlinearities and pulse asymmetry in high density tape recording," *IEEE Trans. Magn.*, vol. 28, no. 5, pp. 2701–2706, 1992.

[84] B. K. Middleton and P. L. Wisely, "The development and application of a simple model of digital magnetic recording to thick media," *IERE Conf. Proc.*, vol. 35, pp. 33–42, 1976.

[85] B. K. Middleton, A. K. Dinnis, and J. J. Miles, "Digital recording theory for thick media," *IEEE Trans. Magn.*, vol. 29, no. 5, pp. 2286–2288, 1993.

[86] D. Wei, H. N. Bertram, and F. Jeffers, "A simplified model of high density tape recording," *IEEE Trans. Magn.*, vol. 30, no. 5, pp. 2739–2749, 1994.

[87] S. R. Cumpson, B. K. Middleton, and S. E. Stupp, "A thick media recording model for quantitative study of media with arbitrary easy axis orientations," *IEEE Trans. Magn.*, vol. 33, no. 3, pp. 2405–2411, 1997.

[88] H. J. Richter, "A generalized slope model for magnetization transitions," *IEEE Trans. Magn.*, vol. 33, no. 2, pp. 1073–1084, 1997.

[89] L. T. Nguyen, A. Lisfi, and J. C. Lodder, "Obliquely sputtered Co/Cr thin film tape for bidirectional recording," *J. Appl. Phys.*, vol. 93, no. 10, pp. 7786–7788, 2003.

[90] H. N. Bertram and I. A. Beardsley, "The recording process in longitudinal particulate media," *IEEE Trans. Magn.*, vol. 24, no. 6, pp. 3234–3248, 1988.

[91] N. H. Yeh, R. Niedermeyer, and C. R. Olson, "Transition asymmetry in high density digital recording," *IEEE Trans. Magn.*, vol. 26, no. 5, pp. 2175–2177, 1990.

[92] A. J. Armstrong, H. N. Bertram, R. D. Barndt, and J. K. Wolf, "Nonlinear effects in high-density tape recording," *IEEE Trans. Magn.*, vol. 27, no. 5, pp. 4366–4376, 1991.

[93] N. H. Yeh, R. Niedermeyer, and C. R. Olson, "Nonlinear distortion in helical-scan tape recorders," *IEEE Trans. Magn.*, vol. 28, no. 5, pp. 2707–2709, 1992.

[94] H. N. Bertram, "The effect of the angular dependence of the particle nucleation field on the magnetic recording processes," *IEEE Trans. Magn.*, vol. 20, no. 6, pp. 2094–2104, 1984.

[95] B. K. Middleton, "The dependence of recording characteristics of thin metal tapes on their magnetic properties and on the replay head," *IEEE Trans. Magn.*, vol. 2, no. 1, pp. 225–229, 1966.

[96] D. A. Lindholm, "Dependence of reproducing gap null on head geometry," *IEEE Trans. Magn.*, vol. 11, no. 6, pp. 1692–1696, 1975.

[97] H. N. Bertram and D. A. Lindholm, "Dependence of reproducing gap null on medium permeability and spacing," *IEEE Trans. Magn.*, vol. 18, no. 3, pp. 893–897, 1982.

[98] A. van Herk, "Side fringing fields and write and read crosstalk of narrow magnetic recording heads," *IEEE Trans. Magn.*, vol. 13, no. 4, pp. 1021–1028, 1977.

[99] M. R. Madison, T. C. Arnoldussen, T. Y. Chang, R. W. Wood, and F. D. Scott, "Erase band and transition charge-model and MFM," *IEEE Trans. Magn.*, vol. 32, no. 5, pp. 3878–3880, 1996.

[100] L. Mei, M. E. Schabes, and N. H. Yeh, "Coercivity and frequency dependence of track widths and erase bands in thin film media," *IEEE Trans. Magn.*, vol. 34, no. 4, pp. 1546–1548, 1998.

[101] A. Hozoi, J. P. J. Groenland, J.-B. Albertini, and J. C. Lodder, "Novel profiling model and side effects of helical scan silicon heads," *IEEE Trans. Magn.*, vol. 38, no. 5, pp. 1916–1918, 2002.

[102] A. Hozoi and J. C. Lodder, "Recording performances of perfectly aligned HSS heads," *IEEE Trans. Magn.*, vol. 40, no. 4, pp. 2422–2424, 2004.

[103] J.-G. Zhu, X. G. Ye, and T. C. Arnoldussen, "Side writing phenomena in narrow track recording," *IEEE Trans. Magn.*, vol. 28, no. 5, pp. 2716–2718, 1992.

[104] D. J. Seagle, M. C. Barsotti, M. L. Osborn, and V. M. Tobin, "Transition curvature analysis," *IEEE Trans. Magn.*, vol. 35, no. 2, pp. 619–624, 1999.

[105] T. Hamaguchi, T. Ichihara, F. Tomiyama, M. Hara, K. Akagi, and H. Takano, "A technique for capturing the transition curvature and analysis of the write head characteristics," *J. Appl. Phys.*, vol. 87, no. 9, pp. 5004–5006, 2000.

[106] F. Liu, S. Li, Y. Liu, G. Gray, and A. Schultz, "Quantitative analysis of transition curvature by magnetic force microscopy," *J. Appl. Phys.*, vol. 91, no. 10, pp. 6842–6844, 2002.

[107] M. Plumer and J. van Ek, "Micromagnetic study of track edge and medium orientation effects in high areal density recording," *IEEE Trans. Magn.*, vol. 36, no. 5, pp. 2225–2231, 2000.

[108] J.-G. Zhu, Y. S. Luo, and J. R. Ding, "Magnetic force microscopy study of edge overwrite characteristics in thin-film media," *IEEE Trans. Magn.*, vol. 30, no. 6, pp. 4242–4244, 1994.

[109] Y. Luo, T. T. Lam, and J.-G. Zhu, "Density and phase dependence of edge erase band in MR/thin film head recording," *IEEE Trans. Magn.*, vol. 31, no. 6, pp. 3105–3107, 1995.

[110] S. Li *et al.*, "Erase band width evaluation by phase coherency," *J. Appl. Phys.*, vol. 91, no. 10, pp. 7089–7091, 2002.

[111] E. Y. Wu and J. V. Peske, "Edge effects in narrow track recording using symmetrical and asymmetric write pole geometries," *IEEE Trans. Magn.*, vol. 30, no. 6, pp. 4254–4256, 1994.

[112] S. X. Wang and P. R. Webb, "Modeling of submicron trackwidth inductive write head designs," *IEEE Trans. Magn.*, vol. 31, no. 6, pp. 2687–2689, 1995.

[113] Y. Guo, J. Chang, and K. Ju, "Low fringe-field and narrow-track MR heads," *IEEE Trans. Magn.*, vol. 33, no. 5, pp. 2827–2829, 1997.

[114] Y. Tanaka and T. K. Taguchi, "The effects of head configuration on write resolution for submicron track recording," *IEEE Trans. Magn.*, vol. 31, no. 6, pp. 2684–2686, 1995.

[115] R. Hoyt and H. Sussner, "Precise side writing measurements using a single recording head," *IEEE Trans. Magn.*, vol. 20, no. 5, pp. 909–911, 1984.

[116] L. Mei, D. Wachenschwanz, M. Alex, and N. H. Yeh, "Novel characterization and control of recorded track edges," *IEEE Trans. Magn.*, vol. 35, no. 5, pp. 2724–2726, 1999.

[117] F. Z. Wang, L. He, D. J. Mapps, W. W. Clegg, D. T. Wilton, and P. Robinson, "Interaction between track and linear densities," *IEEE Trans. Magn.*, vol. 35, no. 5, pp. 2238–2240, 1999.

[118] K. C. Lin and G. Thomas, "Effect of media properties on side erase bands," *IEEE Trans. Magn.*, vol. 26, no. 1, pp. 132–134, 1990.

[119] T. Itoh, H. Kobayashi, and T. Ozeki, "Dependence of side-erasing effect and core efficiency on side taper angle of high $B_s$ metal in gap head," *J. Appl. Phys.*, vol. 81, no. 8, pp. 4492–4494, 1997.

[120] N. H. Yeh, "Asymmetric crosstalk of magnetoresistive head," *IEEE Trans. Magn.*, vol. 18, no. 6, pp. 1155–1157, 1982.

[121] D. E. Heim, "On the track profile in magnetoresistive heads," *IEEE Trans. Magn.*, vol. 30, no. 4, pp. 1453–1464, 1994.

[122] Y. Shen *et al.*, "Comparative study of MR head designs with abutted vs overlaid permanent magnet bias," *IEEE Trans. Magn.*, vol. 32, no. 1, pp. 19–24, 1996.

[123] S. W. Yuan and H. N. Bertram, "Off-track spacing loss of shielded MR heads," *IEEE Trans. Magn.*, vol. 30, no. 3, pp. 1267–1273, 1994.

[124] K. Wiesen and B. Cross, "GMR head side-reading and bit aspect ratio," *IEEE Trans. Magn.*, vol. 39, no. 5, pp. 2609–2611, 2003.

[125] J. B. Albertini, H. Sibuet, P. Renaux, and P. Gaud, "A new solenoid magnetic integrated head for digital video recording," *IEEE Trans. Magn.*, vol. 33, no. 5, pp. 2836–2838, 1997.

[126] P. Gaud *et al.*, "Process for producing read and/or write heads for magnetic recording," U.S. Patent 5 250 150, 1992.

[127] S. X. Wang and A. M. Taratorin, *Magnetic Information Storage Technology.* Academic Press, 1999.

[128] L. T. Nguyen, "Sputtered thin films for high density tape recording," Ph.D. dissertation, University of Twente, 2004.

[129] A. Roesler and J.-G. Zhu, "Understanding the effect of the tape surface on the metal-particle tape medium noise," *J. Appl. Phys.*, vol. 91, no. 10, pp. 8745–8747, 2001.

[130] P. Luo, H. N. Bertram, B. Buchan, and Z. Jin, "Experimental study of signal-dependent noise in metal particle tape," *IEEE Trans. Magn.*, vol. 38, no. 4, pp. 1807–1813, 2002.

[131] P. Luo, Z. Jin, and H. N. Bertram, "PRML channel performance under the influence of medium noise in tape recording systems," *IEEE Trans. Magn.*, vol. 39, no. 2, pp. 1072–1080, 2003.

[132] T. Mercer, P. R. Bissell, P. Ardeleanu, L. Stoleriu, and A. Stancu, "Effects of magnetic layer thickness and of head-to-medium spacing on noise in advanced particulate recording media," *J. Appl. Phys.*, vol. 93, no. 10, pp. 6334–6343, 2003.

[133] H. Inaba, K. Ejiri, K. Masaki, and T. Kitahara, "Development of an advanced metal particulate tape," *IEEE Trans. Magn.*, vol. 34, no. 4, pp. 1666–1668, 1998.

[134] R. J. Veitch, A. Ilmer, W. Lenz, and V. Richter, "MP technology for a new generation of magnetic tapes," *J. Magn. Magn. Mater.*, vol. 193, no. 1-3, pp. 279–283, 1999.

[135] T. Suzuki and T. Tanaka, "Inter-particle interaction and thermal stability of ultra-fine Ba ferrite particles for high-density recording," *J. Magn. Magn. Mater.*, vol. 242, no. 1, pp. 328–330, 2002.

[136] A. Lisfi and J. C. Lodder, "Magnetic domains in Co thin films obliquely sputtered on a polymer substrate," *Phys. Rev. B*, vol. 63, no. 17, 2001.

[137] T. Ito, Y. Iwasaki, H. Tachikawa, Y. Murakami, and D. Shindo, "Microstructure of a Co-CoO obliquely evaporated magnetic tape," *J. Appl. Phys.*, vol. 91, no. 7, pp. 4468–4473, 2002.

[138] T. Kawashima, Y. Kanemaki, T. Sato, W. Okawa, and Y. Okazaki, "The digital-recording performance of obliquely oriented metal-evaporated tape in the reverse direction," *J. Appl. Phys.*, vol. 93, no. 10, pp. 7795–7797, 2003.

[139] T. Ishida, K. Tohma, H. Yoshida, and K. Shinohara, "More than 1 $Gb/in^2$ recording on obliquely oriented thin film tape," *IEEE Trans. Magn.*, vol. 36, no. 1, pp. 183–188, 2000.

[140] T. Ito *et al.*, "Growth mechanism and structure of obliquely evaporated Co-CoO tapes," *IEEE Trans. Magn.*, vol. 40, no. 4, pp. 2410–2412, 2004.

[141] H.-S. Lee, D. E. Laughlin, and J. A. Bain, "Recording properties of CoCrPt tape media sputter-deposited at room temperature on polymeric substrates," *J. Appl. Phys.*, vol. 93, no. 10, pp. 7783–7785, 2003.

[142] H.-S. Lee, L. Wang, J. A. Bain, and D. E. Laughlin, "Use of room-temperature bias sputtering to decrease intergranular coupling in magnetic media deposited on polymeric substrates," *IEEE Trans. Magn.*, vol. 39, no. 6, pp. 3616–3618, 2003.

[143] G. Collins, "The mechanical challenge of ultra-high track densities: how far can tape guide rollers go?" THIC Meeting, Boulder CO, June 2004. [Online]. Available: http://www.thic.org/Agenda0406.html

[144] K. B. Klaassen and J. C. van Peppen, "Exploring data rate limitations of channel front-ends for rigid disk drives," *IEEE Trans. Magn.*, vol. 37, no. 2, pp. 619–626, 2001.

[145] K. B. Klaassen and J. C. van Peppen, "Read/write electronics front-end systems for hard disk drives," *IEEE Trans. Magn.*, vol. 40, no. 1, pp. 263–268, 2004.

[146] K. Wiesen, R. M. Lansky, and C. Sobey, "Recording asymmetries at large skew angles," *IEEE Trans. Magn.*, vol. 29, no. 6, pp. 4002–4004, 1993.

[147] C. Tsang *et al.*, "Track width study of E-beam defined GMR read heads on longitudinal and perpendicular media," *IEEE Trans. Magn.*, vol. 40, no. 1, pp. 295–300, 2004.

[148] Y. Honda, N. Inaba, M. Suzuki, A. Kikugawa, and M. Futamoto, "Magnetization structures of tracks recorded on longitudinal thin film medium," *IEEE Trans. Magn.*, vol. 29, no. 6, pp. 3721–3723, 1993.

[149] Y. Martin and H. K. Wickramasinghe, "Magnetic imaging by "force microscopy" with 1000 Å resolution," *Appl. Phys. Lett.*, vol. 50, no. 20, pp. 1455–1457, 1987.

[150] T. Kawabe and J. H. Judy, "Micromagnetic structures of track-center and track-edge transitions recorded in isotropic longitudinal thin film media with a thin film head," *IEEE Trans. Magn.*, vol. 28, no. 5, pp. 2470–2472, 1992.

[151] E. N. Abarra, I. Okamoto, and T. Suzuki, "Magnetic force and Lorentz transmission electron microscopy analysis of bit transitions in longitudinal media," *J. Appl. Phys.*, vol. 85, no. 8, pp. 5015–5017, 1999.

[152] E. R. Katz, "Erase profiles of floppy disk heads," *IEEE Trans. Magn.*, vol. 20, no. 4, pp. 528–541, 1984.

[153] J. Akiyama, Y. Ohinata, T. Hikosaka, T. Taguchi, and Y. Tanaka, "Trilayer media for high track density longitudinal recording," *J. Appl. Phys.*, vol. 79, no. 8, pp. 5655–5657, 1996.

[154] B. Liu, S. B. Hu, T. S. Low, S. H. Soh, and J. Yip, "Skew angle and its effects on $Gb/in^2$ density magnetic recording," *IEEE Trans. Magn.*, vol. 32, no. 3, pp. 1743–1748, 1996.

[155] T. T. Lam, J.-G. Zhu, and H.-C. Tong, "Effect of head skew on edge erasure and transition noise at submicron recording track width," *IEEE Trans. Magn.*, vol. 33, no. 5, pp. 2719–2721, 1997.

[156] S. Lalbahadoersing, M. H. Siekman, J. P. J. Groenland, S. B. Luitjens, and J. C. Lodder, "Track edges in metal-evaporated tape and thin metal-particle tape," *J. Magn. Magn. Mater.*, vol. 219, no. 2, pp. 248–251, 2000.

[157] A. V. Lakshmikumaran, J. C. Cates, and G. A. Hungerford, "Recording performance and tribological evaluation of FIB defined tape recording heads," *IEEE Trans. Magn.*, vol. 36, no. 5, pp. 2718–2720, 2000.

[158] T. Pan, A. C. Kennedy, J. A. Bain, Y. Yip, and T. Schwarz, "Tape erase bands measured by MFM compared to MR head cross erase band responses," *IEEE Trans. Magn.*, vol. 32, no. 5, pp. 3407–3409, 1996.

[159] R. H. Dee and J. Cates, "Crosstrack profiles of thin film MR tape heads using the azimuth displacement method," *IEEE Trans. Magn.*, vol. 32, no. 5, pp. 3464–3466, 1996.

[160] K. D. McKinstry and R. Dee, "TMR window measurements with thin film write/MR readheads on metal particle tape including erase bands," *IEEE Trans. Magn.*, vol. 34, no. 4, pp. 1958–1960, 1998.

[161] K. D. McKinstry, M. L. Watson, and L. E. Daby, "Erase and write widths for narrow track high-density flexible storage media applications," *IEEE Trans. Magn.*, vol. 38, no. 5, pp. 1913–1915, 2002.

[162] S. Fukuda, T. Shirai, T. Ozue, T. Ikegami, and S. Kumagai, "Track profile of MR head and its performance in a helical scan tape system," *IEEE Trans. Magn.*, vol. 36, no. 5, pp. 2499–2501, 2000.

[163] M. Saito *et al.*, "Narrow track current-perpendicular-to-plane spin valve GMR heads," *IEEE Trans. Magn.*, vol. 40, no. 1, pp. 207–212, 2004.

[164] S. E. Lambert, I. L. Sanders, A. M. Patlach, and M. T. Krounbi, "Recording characteristics of submicron discrete magnetic tracks," *IEEE Trans. Magn.*, vol. 23, no. 5, pp. 3690–3692, 1987.

[165] S. E. Lambert and M. L. Williams, "Recording head characterization using 1 m wide discrete tracks," *IEEE Trans. Magn.*, vol. 24, no. 6, pp. 2832–2834, 1988.

[166] R. Fayling, T. Szczech, and E. Wollack, "A model for overwrite modulation in longitudinal recording," *IEEE Trans. Magn.*, vol. 20, no. 5, pp. 718–720, 1984.

[167] D. Palmer and J. V. Peske, "Spatial distribution of overwrite interference on film disks," *IEEE Trans. Magn.*, vol. 26, no. 5, pp. 2451–2453, 1990.

[168] G. H. Lin, Y. Zhao, and H. N. Bertram, "Overwrite in thin film disk recording systems," *IEEE Trans. Magn.*, vol. 29, no. 6, pp. 4215–4223, 1993.

[169] K. Ogawa, T. Miyauchi, and T. Ozue, "Micromagnetic study of side-writing phenomena using thin-film heads and Co-CoO metal-evaporated tape," *J. Appl. Phys.*, vol. 93, no. 10, pp. 7780–7782, 2003.

[170] J. van Ek, M. Plumer, H. Zhou, and H. N. Bertram, "Micromagnetic recording model of pole-tip saturation effects," *IEEE Trans. Magn.*, vol. 36, no. 6, pp. 3975–3983, 2000.

[171] M. Abe and Y. Tanaka, "Measuring magnetic field saturation and its site dependence in a recording head with a magnetic force microscope," *IEEE Trans. Magn.*, vol. 40, no. 3, pp. 1708–1711, 2004.

# Samenvatting

Dit proefschrift houdt zich bezig met het onderzoek van het recordingproces bij kleine spoorafstand, tot in het submicron-bereik, met aandacht voor zijschrijf- en wiseffecten. Deze maken dat het recordingproces aan de randen minder efficient is dan in het midden van de sporen. Dit resulteert in een effectieve verkleining van de schrijf-spoorbreedte die erger is bij hoge lineaire dichtheid, en de maximaal haalbare oppervlaktedichtheid begrenst. Het spoorrandgebied dat niet bijdraagt aan het bruikbare leessignaal is veelal bekend als zijwisband. In de huidige hoge dichtheids-tape drives worden wisbanden rond 0.5 $\mu$m gehaald, en deze zouden moeten worden verkleind tot onder de 0.2 $\mu$m om submicron-sporen te verwezelijken. In dit onderzoek zijn dergelijke kwesties uitgebreid bestudeerd hetgeen een verbeterd begrip van tape recording met smalle sporen oplevert. Zijlezen wordt ook behandeld. Dit onderwerp wordt echter niet als een zware kwestie beschouwd voor toekomstige tape-geheugensystemen.

Het eerste hoofdstuk geeft een overzicht van tape recording-technologie met korte geschiedenis, huidige status, en trends voor de toekomst. In de afgelopen tijd is een hogere groeisnelheid van de oppervlaktedichtheid gerealiseerd om rekening te houden met de sterkgroeiende vraag naar geheugencapaciteit. Belangrijke voortgang wordt aangekondigd als gevolg van het vergroten van de spoordichtheid, die ruwweg iedere vier jaar zou moeten verdubbelen. De kleinste spoorafstand in de nieuwste tape drives is ongeveer 3.6 $\mu$m, en spoorbreedtes met waarden onder 1 $\mu$m worden in minder dan tien jaar verwacht. Kortgeleden is getoond dat het lezen van submicron-sporen met hoge lineaire dichtheid mogelijk is met gebruikmaking van “giant magnetoweerstand” (GMR) leeskoppen, met breedtes van 0.45 $\mu$m en 0.80 $\mu$m. Echter, het schrijven van sporen met een spoorafstand onder de micrometer is tot op heden niet aangetoond. De belangrijkste beperkingen zijn daarbij gerelateerd aan spoor-randeffecten en spoorvolgfouten.

Hoofdstuk 2 is gewijd aan het introduceren van het digitale magnetische recordingproces. Het schrijfproces wordt beschreven met het "William-Comstock slope model", en het lezen wordt behandeld via het reciprociteitsprincipe. Het recordingproces in dikke media, dat nog representatief is voor de meeste tapes, wordt ook bediscussieerd. Tenslotte wordt recording met smalle sporen gepresenteerd, hetgeen het hoofdonderwerp van dit onderzoek vormt. Er wordt aandacht gegeven aan verschijnselen die plaatshebben aan de spoorranden ten gevolge van onvoldoende inperking van de schrijf- en leesvelden, hetgeen zijschrijven/-wissen en zijlezen veroorzaakt. Een overzicht van de moderne technologie van recording-tape en -koppen is opgenomen in hoofdstuk 3. Dunne-film schrijfkoppen en magnetoweerstand (MR) sensorelementen worden uitgebreid toegepast. "Metal particulate" (MP) en "metal evaporated" (ME) magnetische tapes ontwikkelen zich in de richting van dunnere magnetische lagen met $\delta < 100$ nm, en coërciviteit $H_c$ tot 200 kA/m en hoger. "Metal sputtered" (MS) tapes, met $\delta \approx 30$ nm en $H_c > 250$ kA/m, worden als kansrijke kandidaten beschouwd voor toekomstige ontwikkelingen. De recordingkoppen en -tapes die hier worden gebruikt voor het bestuderen van randeffecten worden ook geïntroduceerd. Er zijn geavanceerde "Helical Scan Silicon" (HSS) koppen met poolbreedtes van 1.3 $\mu$m tot 6.2 $\mu$m gebruikt, en tevens smalle "metal-in-gap" (MIG) ferrietkoppen. HSS koppen zijn gebaseerd op geavanceerde dunne filmtechnologie met "solenoid" spoel, geïntegreerde azimuthoek, korte spleetlengte, en goed uitgerichte polen. Er zijn MP en ME tapes onderzocht met diverse dikten van de recordinglaag tussen 50 nm tot 300 nm, en coërciviteit tussen 120 kA/m en 200 kA/m.

De recordingexperimenten zijn uitgevoerd op een "tape-drum tester" die is aangepast voor hoge stabiliteit en nauwkeurigheid, en die wordt beschreven in hoofdstuk 4. Een bestaande opstelling werd gemodificeerd en gedeeltelijk opnieuw ontworpen teneinde de prestaties aanmerkelijk te verbeteren. De stabiliteit van de snelheid, contact tussen kop en tape, de "cross-track" positionering, en de signaal-conditionering zijn in eerste instantie verbeterd. Dit werd bereikt door bepaalde componenten zoals de tape-drums opnieuw te bewerken, en door het ontwikkelen van nieuwe ontwerpen voor andere modules waaronder het kop-positioneringsplateau en de lees/schrijf-circuits. De verbeterde tester bleek bruikbare prestaties en bedieningsgemak te leveren voor het schrijven van smalle sporen dichtbij één micrometer. De nauwkeuringheid voor het positioneren in dwarsspoorrichting was onder 100 nm voor bewegingen over korte afstanden tot 10 $\mu$m.
Het is te verwachten dat uiterst superieure prestaties bereikbaar zijn door een geheel nieuwe tester te constueren volgens een geoptimaliseerd ontwerp. Dergelijke zaken zijn in dit werk geanalyseerd met het doel om een ultieme tape-drum tester te ontwikkelen die geschikt is voor spoorbreedten afnemend tot 200 nm. Dit vereist lage druk, alsmede stabiel kop/tape-kontakt en een positioneringsnauwkeurigheid in dwarsspoorrichting rond 20 nm voor bewegingen van ten-

minste 1 $\mu$m. Een piezo-elektrische tafel zou kunnen worden geïntegreerd in het koppositionerings-mechanisme teneinde de resolutie hiervan te vergroten, en actieve spoorvolging zou misschien moeten worden geïmplementeerd. Een oordeelkundige constructie is vereist voor de tape-drum terwijl een zeer preciese luchtlager zou worden gebruikt. Uitgebreide ontwerpkriteria en suggesties werden uitgewerkt die de belangrijke mechanische en elektronische componenten van de opstelling betreffen.

De nauwkeurigheid van de ge-upgrade tape-drum tester maakte het mogelijk om diverse methoden te implementeren om de randeffecten direct vanuit recordingexperimenten te bestuderen. Het was mogelijk om spoorprofielen adequaat te meten, waarvan het gebruik in het algemeen was voorbehouden aan hard disk-opstellingen als gevolg van de superieure precisie en stabiliteit hierbij. Verschillende methoden voor het onderzoeken van tape recording met smalle sporen en randeffecten van HSS- en MIG-koppen konden om deze reden worden gebruikt. Sommige technieken waren afgeleid van de praktijk met harde schijven, zoals "triple-track profiling", terwijl andere specifiek in dit onderzoek zijn ontwikkeld, zoals spectrummetingen van micro-sporen. "Track profiling" en magnetische afbeeldingstechnieken als magnetische krachtmicroscopie (MFM) worden bediscussieerd in hoofdstuk 5. Hoewel MFM een betere resolutie bereikt, is het een indirecte observatietechniek voor de magnetisatie in het medium, en de afbeeldingen moeten oordeelkundig worden geïnterpreteerd. Het is een bruikbaar instrument om spoorrandvervormingen te beoordelen, zoals faseverschuivingen van de overgangen. Echter, de wisbanden kunnen anders worden gereproduceerd door MFM dan dat ze door de leeskop worden gesignaleerd. De directe invloed van de spoorranden op het leeskopsignaal kan worden bestudeerd m.b.v. "track profile"-metingen en de evaluatie van de wisbanden is mogelijk met geschikte technieken. De implementatie hiervan vraagt in het bijzonder een preciese dwarsspoor-positionering van de kop.

Er is een "ongebalanceerde" overschrijfmethode ontwikkeld die geschikt is voor kwalitatieve studie van zijschrijven, en die beperkte "track profiling"-mogelijkheden vereist. Deze is gebaseerd op het schrijven van een origineel spoor met lange golflengte en hoge stroom, waardoor zijschrijven excessief optreedt. De randen hiervan zijn daarom moeilijk te wissen met practische stromen voor een overschrijfsignaal, en dienen als referentie om het zijschrijven en wissen hierbij te monitoren. De methode is erg gevoelig voor zijschrijfasymmetrie en is toegepast om een HSS kop uit een vroege serie te bestuderen. De magnetische polen hiervan waren zeer goed uitgericht aan één spleetrand, en slecht uitgericht aan de andere rand. De poolbreedte en spleetlengte waren respectievelijk 3.3 $\mu$m en 0.11 $\mu$m. De overschrijfpatronen zijn onderzocht aan de hand van dwarsspoor-profielen met drie typen ME- en MP-media die significante zijschrijf-asymmetrie laten zien. Bij de spleetrand met slechte pooluitlijning waren de schrijfvelden niet voldoende ingeperkt binnen het spleetgebied hetgeen in een sterk zijschrijven resulteerde. Bij de goed-uitgelijnde rand

waren zijschrijfeffecten nauwelijks waarneembaar. De methode is erg gevoelig gebleken in combinatie met dunne ME-media ($\delta = 50$ nm), waarbij het "on-track"-residue klein was en de randeffecten dominant. Randeffecten waren in dikkere MP-media ($\delta = 200$ nm en $\delta = 300$ nm) nog zichtbaar en deze leken bij hogere coërciviteit ($H_c = 195$ kA/m) minder te worden. De overschrijfpatronen die zijn geschreven in de ME-tape zijn ook afgebeeld door middel van MFM, en geanalyseerd met gebruik van fast Fourier transformaties (FFT). Er is goede overeenstemming gevonden tussen de spoorprofielen en de MFM-afbeeldingen, waarbij de laatst genoemden een hoger detailniveau opleverden.

"Triple-track profiling" metingen zijn in dit werk uitgebreid onderzocht op hun toepasbaarheid bij tape-recording met smalle sporen. Er is een nieuw model ontwikkeld om de "triple-track"-profielen te interpreteren, dat in hoofdstuk 6 wordt gepresenteerd. Het model is gebaseerd op het representeren van de leeskop als de som van een referentiebreedte die golflengte-onafhankelijk is, en twee effectieve zijlees-breedtes die golflengteafhankelijk zijn. Hierbij is het mogelijk om de wisbanden en de relatieve zijleesbreedtes af te zonderen. De methode is toegepast voor het bepalen van de zijbanden en de zijleesbreedtes van de HSS- en MIG-koppen met poolbreedtes tussen 3.5 $\mu$m en 6.2 $\mu$m. Bij een soortgelijke spleetlengte van 0.2 $\mu$m werd vastgesteld dat de wisbanden van een HSS-kop met perfect uitgelijnde polen enkele malen kleiner waren dan voor een MIG-kop. Zij waren respectievelijk rond 0.23 $\mu$m en 0.86 $\mu$m bij een schrijf-golflengte $\lambda = 0.6$ $\mu$m. Voor een HSS-kop met spleetlengte 0.11 $\mu$m waren de wisbanden circa 0.3 $\mu$m bij korte recording-golflengten van 0.25 $\mu$m. Echter, de uitlijning van zijn polen was aan één zijde niet perfect, hetgeen betekent dat de wisbanden zelfs kleiner waren dan bij de goed-uitgelijnde spleetrand. De metingen zijn uitgevoerd met drie ME- en MP-tapes met coërciviteit tussen 124 kA/m en 195 kA/m. Het vergroten van de recordingstroom boven de optimale waarde veroorzaakte een vergrote wisband, hetgeen vermoedelijk komt door de verzadiging van de pool-hoeken. De wisbanden bleken enigzins smaller te zijn in de dunne ME-media ($\delta = 50$ nm) met hoge coërciviteit van 164 kA/m. Uit wisprofielen en FFT-bewerkte MFM-afbeeldingen kon worden aangetoond dat de wisbanden aan de kopranden niet gelijk zijn. Aan de goed-uitgelijnde rand waren ze aanmerkelijk smaller, en wel 0.2 $\mu$m, zelfs bij een zeer korte golflengte van 0.2 $\mu$m (254 kfc/in). Dit zijn de kleinste wisbanden die tot op heden voor magnetiche recording zijn gerapporteerd. Daarom zijn een goede uitlijning, kleine spleetlengte en materialen met hoge verzadiging vereist om de wisbanden te minimaliseren en de vergrote spoordichtheid te ondersteunen.

In hoofdstuk 7 wordt getoond dat het onderzoek van microsporen een zinvolle methode is om de recordingeigenschappen van toekomstige tapesystemen met smalle sporen te voorspellen, en de kritische aspecten zoals zijschrijven aan de orde te stellen. Microsporen worden gecreëerd door de rand(en) van een volledig spoor gedeeltelijk te wissen, en ze kunnen worden gemaakt in het centrum van het spoor of aan de randen. Rand-microsporen worden sterk aangetast

door zijschrijven, terwijl centrale microsporen de "on-track"-eigenschappen tonen. Het analyseren van de frequentie- en stroom-respons van de microsporen is een krachtig instrument voor het karakteriseren van het zijschrijfgedrag van recording-koppen en -tapes. De methode blijkt diepgaand inzicht te geven in de zijschrijf-fenomenen en geeft de mogelijkheid om de invloed te bestuderen van de kop- en tape-parameters als functie van de schrijf-stroom en -frequentie. De verandering van de overgangen kan aan iedere spleetrand van de kop onafhankelijk worden onderzocht. Er zijn één HSS-kop met perfecte pooluitlijning en twee MIG-koppen geanalyseerd die spleetlengtes rond 0.2 $\mu$m hebben die dicht bij elkaar liggen. Verder had één MIG-kop polen die met "Focussed Ion Beam" (FIB) waren getrimd. De goed-uitgelijnde HSS- en MIG-koppen hadden vergelijkbare zijschrijfeigenschappen. De effectieve spoorbreedte-reductie van de rand-microsporen was onder de 0.5 $\mu$m met zeer korte golflengtes tot 0.25 $\mu$m. De resultaten waren aanmerkelijk slechter voor de MIG-kop met slecht-uitgelijnde polen, waarbij het frequentieverval van de rand-microsporen drastisch slechter was geworden. Er werd tevens een sterke asymmetrie van de rand-microtracks waargenomen, die afhing van de bewegingsrichting van de tape. Dit werd veroorzaakt door de asymmetrie van de vooroplopende ("trailing") polen en veroorzaakt door hun slechte uitlijning.

# List of Publications

- A. Hozoi, J. P. J. Groenland, J.-B. Albertini, and J. C. Lodder, "Novel profiling model and side effects of helical scan silicon heads," *IEEE Trans. Magn.*, vol. 38, no. 5, pp. 1916–1918, 2002.

- A. Hozoi, J. P. J. Groenland, J.-B. Albertini, and J. C. Lodder, "Analysis of Side Writing Asymmetry," *IEEE Trans. Magn.*, vol. 39, no. 5, pp. 2353–2355, 2003.

- A. Hozoi and J. C. Lodder, "Recording performances of perfectly aligned HSS heads," *IEEE Trans. Magn.*, vol. 40, no. 4, pp. 2422–2424, 2004.

- L. T. Nguyen, A. Hozoi, and J. C. Lodder, "NiAl seedlayer for obliquely sputtered thin film tape," *IEEE Trans. Magn.*, vol. 40, no. 4, pp. 2401–2403, 2004.

# Thanks

To Cock Lodder who followed with high interest and enthusiasm my research activity. His constant support, advice, and encouragement greatly contributed to the accomplishment of this thesis.
To Hans Groenland for supervising the project, correcting the manuscript, and translating the *Samenvatting*.
To Long Nguyen for the captivating discussions and for being a great friend. Long, I never had to present a more interesting work than the sputtered tapes you made!
To Ite-Jan Hoolsema, Martin Siekman, and Thijs Bolhuis who offered precious technical support and helped with the MFM and VSM measurements.
To Johnny Sanderink who always found time to do some FIB or SEM for me.
To all people at SMI for ensuring a pleasant and stimulating atmosphere. Their different experiences and cultural backgrounds make a rich environment that I enjoyed very much.
To the Dutch Technology Foundation (STW) for funding this project and to the User Committee members who got actively involved.
To Jean-Baptiste Albertini (CEA-LETI) for the intensive cooperation and the numerous HSS heads supplied.
To the researchers from the ME Media Division, Sony Corporation, for useful discussions and providing tape samples and recording heads.
To Bill Doyle (MINT, University of Alabama) for helpful advices during his stay at SMI, and to Tomohiro Okada (Hitachi GST) for teaching me about hard disk technology.

*Don't let it end like this. Tell them I said something.*

Pancho Villa (1878 – 1923),
Mexican bandit and revolutionary.
Last words.